

**The role of inflammatory mediators
in the development
of
insulin resistance
and hepatocellular carcinoma**

**Inaugural-Dissertation
zur
Erlangung des Doktorgrades
der Mathematisch-Naturwissenschaftlichen Fakultät
der Universität zu Köln**



**vorgelegt von
Peter Dirk Ströhle
aus Mutlangen**

Köln 2011

Berichtersteller/in: Prof. Dr. Jens C. Brüning
Priv. Doz. Dr. F. Thomas Wunderlich

Tag der mündlichen Prüfung: 25. Januar 2012

„Jedem tiefen Naturforscher muß eine Art religiösen Gefühls naheliegen, weil er sich nicht vorzustellen vermag, daß die ungemein feinen Zusammenhänge, die er erschaut, von ihm zum erstenmal gedacht werden.“

Albert Einstein (1879 – 1955)

„Liebe Familie und Freunde, ich schätze eure Geduld und Unterstützung, die ihr mir immer entgegengebracht habt. Damit habt ihr auch einen großen Teil zu dieser Arbeit beigetragen. Ihr seid unbezahlbar!“

Table of contents:

Table of contents:	I
Figure index:	V
Table index:	VII
Abbreviations:	VIII
1. Introduction:	1
1.1 Obesity	1
1.2 Energy homeostasis	2
1.2.1 The role of insulin signaling in energy homeostasis	2
1.2.2 The insulin signaling cascade	3
1.2.3 The role of hepatic gluconeogenesis in glucose homeostasis	5
1.3 Obesity-associated inflammation and insulin resistance	6
1.3.1 IL-6 and insulin resistance	7
1.3.2 TNF- α and insulin resistance	9
1.4 Cancer and hepatocellular carcinoma (HCC)	10
1.5 Linking inflammatory processes to HCC	11
1.5.1 Toll-like receptor (TLR) signaling in liver damage and HCC	11
1.5.2 MyD88 dependent TLR signaling	13
1.5.3 MAPK signaling and HCC	14
1.5.4 NF- κ B signaling and HCC	15
1.6 Objectives	16
2. Materials and Methods:	17
2.1 Chemicals and enzymes	17
2.2 Mouse experiments	21
2.2.1 Animal care	21
2.2.2 Generation of IL-6R α ^{L-KO} and MyD88 ^{L-KO} mice	22
2.2.3 Body weight and body composition	22
2.2.4 Collection of blood samples and determination of blood glucose levels	22
2.2.5 Glucose and insulin tolerance test	23

2.2.6 Indirect calorimetry, locomoter activity and daily food intake	23
2.2.7 Euglycemic-hyperinsulinemic clamp studies (EHCS)	24
2.2.7.1 Implantation of the catheter	24
2.2.7.2 Radioactive EHCS procedure	24
2.2.7.3 Determination of the glucose turnover rate (mg/[kg*min])	25
2.2.7.4 Calculation of the hepatic glucose production (HGP)	26
2.2.7.5 Determination of the <i>in vivo</i> glucose uptake in the tissues	26
2.2.8 Ablation of Kupffer cells (KCs)	26
2.2.9 Glucose-induced insulin secretion of isolated pancreatic islets	27
2.2.10 Diethylnitrosamine (DEN) treatment	27
2.2.10.1 Long-term treatment:	27
2.2.10.2 Short-term treatment:	28
2.2.11 Analysis of serum protein and cytokine concentrations	28
2.3 Molecular biology	29
2.3.1 Isolation of genomic DNA	29
2.3.2 Quantification of nucleic acids	29
2.3.3 Southern blot analysis	29
2.3.4 Polymerase chain reaction (PCR)	30
2.3.5 RNA extraction	31
2.3.6 Quantitative real-time PCR	32
2.4 Biochemistry	34
2.4.1 Protein extraction	34
2.4.2 Western blot analysis	35
2.4.3 Electrophoretic mobility shift assay (EMSA)	36
2.4.4 Enzyme-linked immunosorbent assay (ELISA)	36
2.4.5 Histological analysis and immunohistochemistry	37
2.4.5.1 Immunohistochemistry	37
2.5 Computer analysis	38
2.5.1 Densitometrical analysis	38
2.5.2 Quantitation of pancreatic islet mass	38
2.5.3 Statistical methods	38
3. Results	39
3.1 The effect of hepatic IL-6Rα signal transduction on glucose homeostasis	39
3.1.1 Generation of hepatocyte specific IL-6R α knock out mice	39

3.1.2 IL-6R α ^{L-KO} mice exhibit unaltered energy homeostasis	41
3.1.3 IL-6R α ^{L-KO} mice exhibit impaired glucose homeostasis and insulin sensitivity.....	44
3.1.4 IL-6R α ^{L-KO} mice exhibit counteracting actions on hepatic glucose metabolism.....	46
3.1.5 Mice lacking hepatic IL-6 signaling exhibit insulin resistance in skeletal muscle and WAT.....	50
3.1.6 Increased inflammatory tone in IL-6R α ^{L-KO} mice.....	52
3.1.7 Neutralization of TNF- α normalizes glucose homeostasis in IL-6R α ^{L-KO} mice.....	56
3.2 The effect of hepatic Myd88 signaltransduction on glucose homeostasis and HCC development.....	60
3.2.1 Generation of MyD88 ^{L-KO} mice	60
3.2.2 Unaltered adiposity in mice lacking hepatic MyD88 signaling	62
3.2.3 Glucose homeostasis and insulin sensitivity is unaltered in MyD88 ^{L-KO} mice.....	64
3.2.4 MyD88 ^{L-KO} mice exhibit reduced DEN-induced hepatocarcinogenesis	65
3.2.5 Reduced expression of macrophage markers in HCC of mice lacking hepatic MyD88 signaling	69
3.2.6 The mRNA expression of LIF in HCC is mediated by hepatic MyD88	71
3.2.7 Reduced NF- κ B activation in DEN-induced HCC of MyD88 ^{L-KO} mice	74
3.2.8 MyD88 ^{L-KO} mice exhibit reduced hepatic JNK activation in DEN-induced HCC	75
4. Discussion.....	80
4.1 The ALFP-Cre transgene mediates specific inactivation of the loxP-flanked IL-6R α or MyD88 alleles in hepatocytes.....	81
4.2 Hepatocyte specific disruption of the IL-6R α impairs glucose homeostasis and insulin sensitivity	82
4.3 Crosstalk between hepatocytes and Kupffer cells through hepatic IL-6 signaling controls the inflammatory tone	84
4.5 The role of hepatic MyD88 in energy homeostasis	86
4.6 Hepatocyte specific disruption of MyD88 reduces chemically induced HCC	87

5. Summary.....	90
6. Zusammenfassung	92
7. References.....	94
8. Acknowledgements	113
9. Erklärung	114
10. Curriculum Vitae	115

Figure index:

Fig. 1: Prevalence of obesity in adults from 2001 and 2010	1
Fig. 2: Insulin signal transduction	4
Fig. 3: The role of G6Pase and GK in the regulation of glucose homeostasis	5
Fig. 4: IL-6 signaling cascade	8
Fig. 5: Potential mechanisms for the inhibition of insulin signal transduction	9
Fig. 6: Cancer distribution and HCC incidence rates worldwide in 2011	10
Fig. 7: Toll-like receptors and their PAMP ligands	12
Fig. 8: Toll-like receptor signaling cascade	13
Fig. 9: Targeting strategy and confirmation of the IL-6R α ^{FL/FL} allele	40
Fig. 10: Liver specific ablation of the IL-6R α gene	41
Fig. 11: IL-6R α ^{L-KO} mice show unaltered adiposity	42
Fig. 12: Unchanged energy homeostasis in mice lacking hepatic IL-6R α signaling	43
Fig. 13: IL-6R α ^{L-KO} mice exhibit decreased glucose tolerance	44
Fig. 14: Impaired insulin sensitivity in IL-6R α ^{L-KO} mice	45
Fig. 15: Altered regulation of glucose homeostasis in IL-6R α ^{L-KO} mice	47
Fig. 16: Counteracting actions on hepatic glucose metabolism in IL-6R α ^{L-KO} mice	49
Fig. 17: Decreased insulin sensitivity in liver, skeletal muscle and WAT of IL-6R α ^{L-KO} mice ..	51
Fig. 18: Increased inflammation in livers of IL-6R α ^{L-KO} mice	53
Fig. 19: IL-6R α ^{L-KO} mice exhibit elevated inflammatory state in skeletal muscle	54
Fig. 20: IL-6R α ^{L-KO} mice exhibit enhanced systemic inflammation	55
Fig. 21: Ablation of TNF- α lead to normalized glucose homeostasis in IL-6R α ^{L-KO} mice	56
Fig. 22: Normalized glucose homeostasis in IL-6R α ^{L-KO} mice after depletion of Kupffer cells	57
Fig. 23: Alterations of glucose stimulated insulin secretion after depletion of Kupffer cells in IL-6R α ^{L-KO} mice	58
Fig. 24: Targeting strategy and ablation of MyD88 specific in the liver	61
Fig. 25: Similar bodyweight and body fat content between control and MyD88 ^{L-KO} mice	63
Fig. 26: Unaltered cholesterol and lipid metabolism in MyD88 ^{L-KO} mice	63
Fig. 27: Unaltered glucose homeostasis and insulin sensitivity in MyD88 ^{L-KO} mice	65
Fig. 28: Reduced DEN-induced liver damage in MyD88 ^{L-KO} mice	67
Fig. 29: Lower DEN-induced HCC incidence in MyD88 ^{L-KO} mice	68
Fig. 30: MyD88 ^{L-KO} mice show reduced macrophage marker expression in the liver	70
Fig. 31: Unaltered mRNA expression of chemokines between control and MyD88 ^{L-KO} mice ..	71
Fig. 32: Elevated mRNA expression of LIF in MyD88 ^{L-KO} mice compared to control mice	72
Fig. 33: Unaltered IL-6 signaling in MyD88 ^{L-KO} mice compared to control mice upon acute DEN treatment	73

Fig. 34: MyD88^{L-KO} mice exhibit reduced p65 activation upon DEN treatment..... 74

Fig. 35: Reduced JNK activation in HCC of MyD88^{L-KO} mice compared to control mice 76

Fig. 36: Unaltered MAPK signaling in MyD88^{L-KO} mice upon acute DEN treatment..... 77

Fig. 37: MyD88^{L-KO} mice exhibit decreased pro-apoptotic marker expression 78

Table index:

Table 1: Chemicals.....	17
Table 2: Enzymes.....	21
Table 3: List of oligonucleotides used for Southern probe generation	30
Table 4: List of oligonucleotides used for PCR	31
Table 5: List of Taqman gene expression assays	32
Table 6: List of primary antibodies used for Western blot analysis	35
Table 7: EMSA probes	36
Table 8: List of ELISA kits	37

Abbreviations:

°C	Degrees celsius
β-me	β-mercaptoethanol
2DG	2-Deoxy-D-[1- ¹⁴ C] glucose
2DG6P	2-Deoxy-D-[1- ¹⁴ C] glucose-6-phosphate
3'	Three prime end of DNA sequences
5'	Five prime end of DNA sequences
A	Adenosine
AKT	Protein kinase B
ALFP	Albumin promotor/ α -fetoprotein enhancer
ALT	Alanine transaminase
AMP	Adenosinmonophospat
AMPK	AMP-dependent kinase
AP-1	Activator protein 1
APS	Ammonium persulfate
ASR	Age-standardized incidence rates
AST	Aspartate transaminase
Ba(OH) ₂	Barium hydroxide
Bcl-2	B-cell lymphoma 2
BHI	BamHI
bp	Base pairs
BMI	Body mass index
BSA	Bovine serum albumine

C	Cytosine
c-Jun	Jun proto-oncogene
c-Rel	V-rel reticuloendotheliosis viral oncogene homolog (avian)
CaCl ₂	Calcium chloride
CBA	Cytometric bead array
CD-68	Cluster of differentiation 68
cDNA	Complementary DNA
Ci	Curie
CNS	Central nervous system
CO ₂	Carbon dioxide
cps	Counts per second
Cre	Site-specific recombinase from phage P1 (<u>causes recombination</u>)
ct	Threshold cycle value
CTP	Cytosine triphosphate
DAMPS	Damage-associated molecular patterns
DAPI	4',6-diamidino-2-phenylindole
DEN	Diethylnitrosamine
DMSO	Dimethylsulfoxide
DNA	Desoxyribonucleic acid
DNase	Desoxyribonuclease
dNTP	Desoxyribonucleotide-triphosphate
dpm	Disintegrations per minute
ds	Double-stranded
DTT	1,4-Dithio-DL-threitol

e.g.	<i>exempli gratia</i>
ECL	Enhanced chemiluminescence
EDTA	Ethylendiamine tetraacetate
EHCS	Euglycemic-hyperinsulinemic clamp studies
ELISA	Enzyme-linked immunosorbent assay
ERK	Extracellular signal-regulated kinase
EtBr	Ethidium bromide
EtOH	Ethanol
F4/80	EGF-like module containing, mucin-like, hormone receptor-like sequence 1
FACS	Fluorescence activated cell sorting
FCS	Fetal calf serum
g	Gram
G	Guanine
G6P	Glucose-6-phosphate
G6Pase	Glucose-6-phosphatase
GIR	Glucose infusion rate
GK	Glucokinase
Grb2	Growth factor receptor-bound-2 protein
GSIS	Glucose stimulated insulin secretion
GTP	Guanosine triphosphate
GTT	Glucose tolerance test
Gusb	Glucuronidase beta
h	Hour
H ₂ O	Water

HCC	Hepatocellular carcinoma
HCl	Hydrochloric acid
H&E	Hematoxylin/eosin
HEPES	N-2-hydroxyethylpiperazine-N'-2-ethansulfonic acid
HGP	Hepatic glucose production
HFD	High fat diet
HMGB1	High mobility group box 1
HPRT-1	Hypoxanthine guanine phosphoribosyl transferase-1
i.e.	<i>id est</i>
<i>i.p.</i>	Intraperitoneal
<i>i.v.</i>	Intravenous
I κ B	Inhibitor of κ B
IKK	I κ B kinase
IL-10	Interleukin 10
IL-1Ra	IL-1 receptor antagonist
IL-6	Interleukin 6
IL-6R α	Interleukin 6 receptor α
IR	Insulin receptor
IRAK	Interleukin-1 receptor-associated kinase
IRS	Insulin receptor substrate
ITGAM	Integrin- α -M
ITGAX	Integrin- α -X
ITT	Insulin tolerance test
JNK	C-Jun-N-terminal kinase

k	Kilo
kb	Kilobase
KC	Kupffer cell
KCl	Potassium chloride
KOH	Potassium hydroxide
l	Liter
LIF	Leukemia inhibitory factor
loxP	Recognition sequence for Cre (locus of crossing over phage P1)
LPS	Lipopolysaccharide
m	Milli
M	Mol
MAC-2	Galectin-3
MAPK	Mitogen-activated protein kinase
MCP-1	Monocyte chemo-attractant protein 1
MCP-3	Monocyte chemo-attractant protein 3
MgCl ₂	Magnesium chloride
min	Minute
MIP-1 α	Macrophage inflammatory protein 1 α
MIP-1 β	Macrophage inflammatory protein 1 β
MKK	MAPK kinase
MKKK	MAPK kinase kinase
MyD88	Myeloid differentiation primary response gene 88
mRNA	Messenger ribonucleic acid
NaCl	Sodium chloride

n	Nano
NaF	Sodium fluoride
NaOH	Sodium hydroxide
NCD	Normal chow diet
NF- κ B	Nuclear factor 'kappa-light-chain-enhancer' of activated B-cells
NMR	Nuclear magnetic resonance
O ₂	Oxygen
OD	Optical density
P	Phosphorylation
p	Pico
p38	Mitogen-activated protein kinase 14
p53	Tumor protein p53
PAGE	Polyacrylamid gel electrophoresis
PAMPS	Pathogen-associated patterns
PBS	Phosphate buffered saline
PCR	Polymerase chain reaction
PDK1	Phosphoinositide-dependent protein kinase 1
PEPCK	Phosphoenolpyruvate carboxykinase
PFA	Paraformaldehyde
PH	Pleckstrin homology
PI3K	Phosphatidylinositol 3 kinase
PIP ₂	Phosphatidylinositol-4,5-bisphosphate
PIP ₃	Phosphatidylinositol-3,4,5-trisphosphate
PKB	Protein kinase B

PMSF	Phenylmethylsulfonylfluoride
PTB	Phosphotyrosine binding
PVDF	Polyvinylidene fluoride
RI	EcoRI
RANTES	Regulated upon activation, normally T-expressed, and presumably secreted
Ras	Rat sarcoma
RD	Glucose disposal rate
RelA	V-rel reticuloendotheliosis viral oncogene homolog A
RelB	V-rel reticuloendotheliosis viral oncogene homolog B
RER	Respiratory exchange ratio
RIP1	Receptor interacting protein 1
RNA	Ribonucleic acid
RNase	Ribonuclease
ROS	Reactive oxygen species
rpm	Rounds per minute
RT	Room temperature
SAPK	Stress-activated protein kinases
SDS	Sodiumdodecylsulfate
sec	Second
SEM	Standard error of the mean
Ser	Serin
SH2	Src-homology 2
SHP2	SH2-domain-containing phosphatase
SOCS3	Suppressor of cytokine signalling 3

SOS	Son of sevenless homolog
Src	Sarcoma
ss	Single-stranded
SSC	Sodium chloride/ sodium citrate buffer
STAT-3	Signal transducer and activator of transcription 3
T	Thymine
TAE	Tris-acetic acid-EDTA buffer
Taq Pol	Polymerase from <i>Thermus aquaticus</i>
TBE	Tris/borate/EDTA buffer
TBK1	TANK-binding kinase 1
TBS	Tris buffered saline
TE	Tris-EDTA buffer
TEMED	Tetramethylethylenediamine
TG	Triglyceride
Thr	Threonine
TIR	Toll/interleukin-1 receptor
TIRAP	TIR domain-containing adapter protein
TLR	Toll-like receptor
TNF	Tumor necrosis factor
TNFRp55	Soluble TNF receptor p55
TRAF6	Tumor necrosis factor receptor-associated factor 6
TRAM	TRIF-related adapter molecule
TRIF	TIR domain-containing adapter-inducing IFN β
Tris	2-amino-2-(hydroxymethyl)-1,3-propanediol

TWEEN	Polyoxethylene-sorbitan-monolaureate
Tyr	Tyrosine
U	Unit
UV	Ultraviolet
V	Volt
v/v	Volume per volume
W	Watt
w/o	Without
w/v	Weight per volume
WHO	World Health Organization
wt	Wild-type
ZnSO ₄	Zinc sulfate
μ	Micro

1. Introduction:

1.1 Obesity

Obesity is defined as a condition of abnormal or excessive bodyfat accumulation that may have adverse effects on health. It is one of the biggest public health threats of the 21st century and its prevalence is steadily increasing worldwide (Fig. 1). In 2008, approximately 1.5 billion adults were overweight. Of these adults, over 200 million men and approximately 300 million women were obese. Following recordings of each country in the WHO European Region from 2008, over 50% of both men and women have a body mass index (BMI = weight in kilograms / size in meters²) higher than 25 and are thus considered overweight. Nearly 23% of these were obese indicated by a BMI above 30 (1).

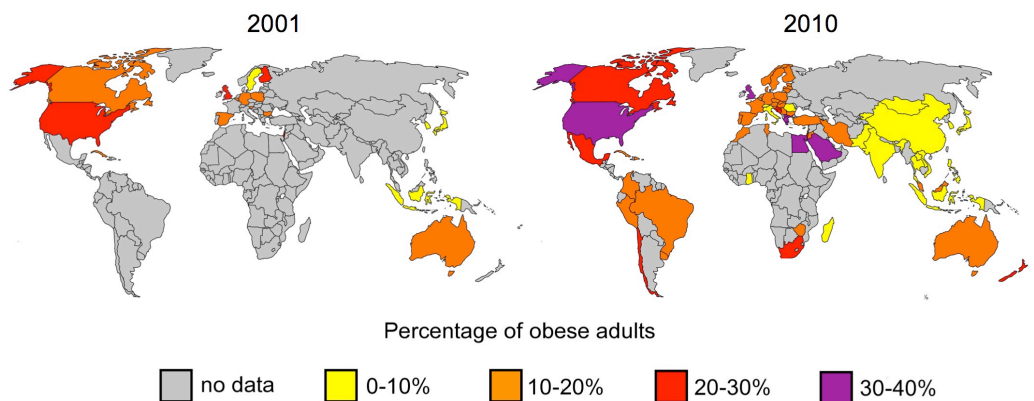


Fig. 1: Prevalence of obesity in adults from 2001 and 2010

The worldwide prevalence of obese adults (BMI >30) compared from 2001 and 2010. Datas were obtained from the WHO.

Obesity is known to increase the risk of developing various diseases, such as cardiovascular diseases, diabetes mellitus, atherosclerosis and certain types of cancer (2-5). As a consequence, approximately 0.7% to 2.8% of a country's total healthcare expenditures are associated with overweight and obesity and thus place a significant financial burden on the healthcare system (6, 7). Due to these facts, remarkable efforts have been conducted to understand the regulatory mechanisms of energy homeostasis, insulin action and body weight gain.

1.2 Energy homeostasis

The relationship between daily energy expenditure and bodyweight regulation was first demonstrated 50 years ago (8). To maintain stable body mass and body composition, the balance between energy intake and energy expenditure is essential and tightly regulated by physiological signals within the organism (9-14). These signals include fat mass gain during overabundance or increased calorie intake in case of depleted energy (9, 15). Malfunction of the regulatory system, either due to genetic predisposition or environmental factors or a combination of both, are presumably leading to the development of obesity (16-18). Importantly, almost unlimited access to high caloric food and the trend to reduced physical activity in industrialized countries results in a positive energy balance, ultimately leading to overweight and obesity.

In the last decade, numerous studies investigated the underlying regulatory mechanisms of energy homeostasis and identified the metabolic hormones insulin and leptin as two of the central regulators of body weight control, energy homeostasis and glucose metabolism (19, 20).

1.2.1 The role of insulin signaling in energy homeostasis

The peptide hormone insulin is secreted by β -cells, which are exclusively located on the pancreatic islets of Langerhans. Its active form is derived from cleavage of the inactive precursor proinsulin in the β -cells (21). As response to rising blood glucose levels, insulin is released into the circulation, and subsequently stimulates glucose uptake in peripheral tissues (22, 23). After being taken up into the cell, glucose is either directly metabolized to generate energy in the form of adenosine-5'-triphosphate (ATP) or, especially in liver and muscle, stored as glycogen. Furthermore, insulin is also involved in the control of different metabolic processes, such as the stimulation of amino acid uptake and glycolysis, as well as the inhibition of catabolic processes, such as

glycogenolysis, gluconeogenesis and hepatic glucose production (24, 25). The amino acid sequence of insulin is highly conserved among vertebrates and some other species, emphasizing the importance of this hormone and its pleiotropic effects (26).

1.2.2 The insulin signaling cascade

Upon release, insulin binds to its receptor and initiates an intracellular signaling cascade (Fig. 2) resulting in the regulation of various cellular functions (27). Like other receptors for protein hormones, the insulin receptor (IR) is a membrane-bound receptor and belongs to the family of receptor tyrosine kinases. The IR comprises two extracellular α - and two intracellular β -subunits, which are linked by disulfide bridges. Binding of insulin to the α -subunits induces a conformational change of the receptor, leading to the activation of the intrinsic tyrosine kinase activity of the β -subunits and thus to autophosphorylation of multiple tyrosine residues (28-30). Due to these phosphorylations, intracellular signaling molecules, such as the four closely related insulin receptor substrates (IRS 1-4) are recruited to the IR via the phospho-tyrosine binding (PTB) domain, resulting in their activation by tyrosine phosphorylation (31, 32). Additionally, most of the IRS proteins contain a N-terminal pleckstrin homology (PH) domain, allowing the localization of the IR and its downstream targets to the membrane by interactions with inositol phosphates in the cell membrane (33, 34). After activation and localization to the membrane, the IRS proteins serve as docking platforms for proteins containing a rous sarcoma virus (Src)-homology 2 (SH2) domain. Different signaling molecules, such as growth factor receptor-bound-2 protein (Grb2), the protein tyrosine phosphatase 2 (Shp2) and the regulatory subunit p85 of phosphatidylinositol 3 kinase (PI3K), contain a SH2 domain and interact with IRS proteins (35-38). Whereas Grb2 subsequently mediates activation of the mitogen activated protein kinase (MAPK) pathway, responsible for regulating cell growth and mitosis (39), PI3K activation mediates the majority of insulin's effects on

glucose and lipid metabolism (40-42). The PI3K primarily catalyzes the phosphorylation of phosphatidylinositol (4,5) biphosphate (PIP₂) to phosphatidylinositol (3,4,5) trisphosphate (PIP₃). PIP₃ in turn translocates the protein kinase B (PKB, also known as AKT), co-localized with the phosphoinositide-dependent protein kinase 1 (PDK1), to the cell membrane and leading to the activation of AKT (43, 44). AKT then regulates the activation of downstream targets (45).

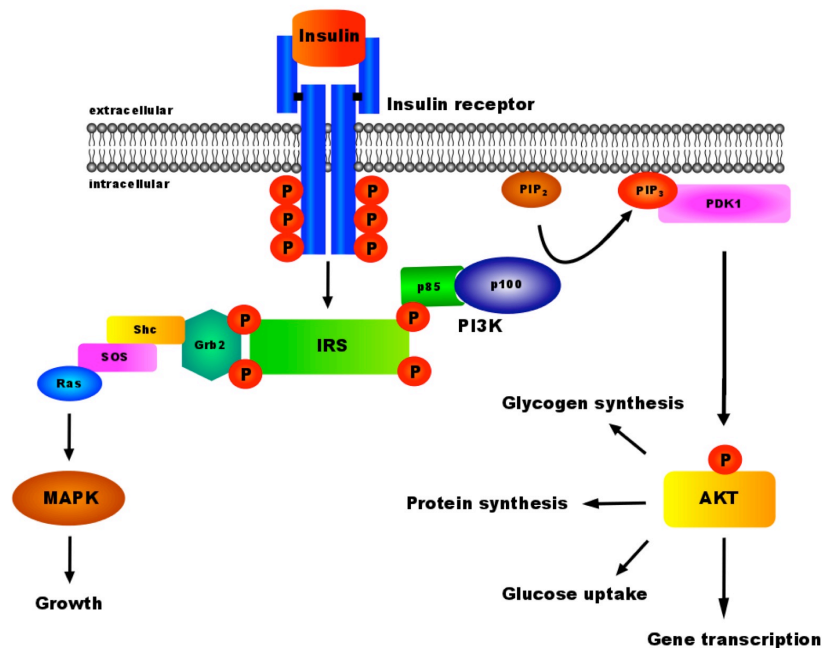


Fig. 2: Insulin signal transduction

Binding of insulin to the insulin receptor results in a conformational change of the receptor and autophosphorylation of the intracellular β -subunits. This leads to recruitment and activation of IRS proteins, which in turn serve as docking platforms for other SH2 domain containing proteins, e.g. Grb2 or PI3K. Activation of these proteins subsequently drives further downstream signaling pathways, such as MAPK or AKT, responsible for growth and glucose homeostasis.

Resistance to the metabolic effects of insulin represents one of the major consequences of excessive weight gain and obesity. It is characterized by a reduced ability of insulin to activate its downstream signaling cascade, thus leading to disturbed glucose clearance from the blood.

1.2.3 The role of hepatic gluconeogenesis in glucose homeostasis

One of the most strictly controlled processes in energy homeostasis is the maintenance of steady blood glucose levels. In response to a high blood glucose concentration, insulin is released and promotes hepatic glucose storage in form of glycogen. Conversely, if blood glucose levels drop, catabolic pathways promote the breakdown of glycogen to glucose and its subsequent release into the bloodstream. Since the generation of glucose from glycogen is rather short-lived, long-term energy supply, e.g. during long fasting periods, is highly dependent on hepatic gluconeogenesis (46-48). Therefore, hepatic gluconeogenesis is of central importance to maintain constant blood glucose levels (49). Notably, obesity-associated insulin resistance and subsequent hyperglycemia is thought to arise, at least partially, from a deregulation of hepatic glucose production due to the reduced ability of insulin to inhibit gluconeogenesis (50-53).

During gluconeogenesis, glucose is generated from non-carbohydrate substrates in a cascade of enzymatic reactions. Rate-limiting enzymes, such as glucose-6-phosphatase (G6Pase) and phosphoenolpyruvate carboxykinase (PEPCK), control important nodes of this pathway and therefore can adjust its activity in response to hormonal stimuli, e.g. insulin or glucagon (Fig. 3) (54, 55).

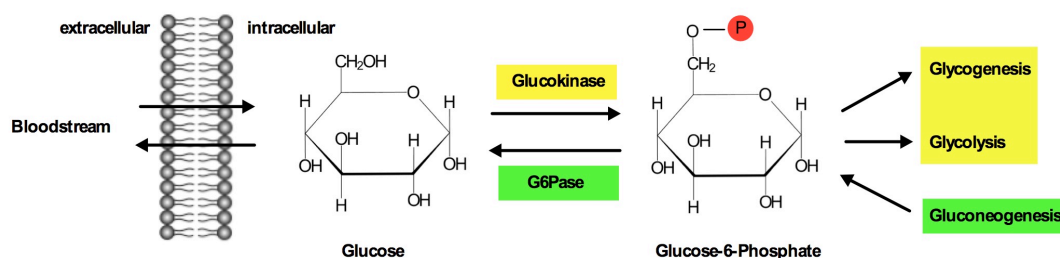


Fig. 3: The role of G6Pase and GK in the regulation of glucose homeostasis

Insulin is released in response to high blood glucose level, which stimulates glucose uptake in peripheral tissues. There, glucokinase catalyzes the phosphorylation of glucose into G6P, which is used for glycogenesis or glycolysis. On the other hand, gluconeogenesis generates glucose from non-carbohydrate substrates by synthesis of G6P. As a rate-limiting enzyme, G6Pase is required for the conversion of glucose-6-phosphate into glucose, which is then released into the bloodstream.

G6Pase is required for the conversion of glucose-6-phosphate (G6P) into glucose, and its inactivation or inhibition leads to poor fasting tolerance, accumulation of glycogen in the liver and ultimately to metabolic disorders (56). In contrast, the insulin-regulated glucokinase (GK) acts antagonistically to G6Pase by catalyzing the phosphorylation of glucose to produce G6P, thus preventing glucose to be released from the cell (Fig. 3) (57-59). After phosphorylation to G6P, glucose is able to enter the glycolysis or glycogenesis.

In summary, hepatic glucose output is regulated by the rates of hepatic glucose production (HGP) and hepatic glucose utilization. Thus, glycogenolysis, gluconeogenesis, and glucose cycling between glucose and G6P are important mechanisms in regulating glucose homeostasis.

1.3 Obesity-associated inflammation and insulin resistance

The concept of chronic, low level inflammation in response to obesity was first shown by markedly increased expression of the pro-inflammatory cytokine tumor necrosis factor α (TNF- α) in adipose tissue of obese rodents. Administration of a recombinant soluble TNF- α receptor (TNFR) immunoglobulin neutralized TNF- α in these rodents and ameliorates insulin sensitivity (60). Thus, the first link between an increase in pro-inflammatory cytokines and insulin resistance was established. Follow-up studies confirmed this observation in humans, where adipose tissue also increasingly expressed TNF- α upon obesity, which was decreased after weight loss, together with a restoration of insulin sensitivity (61-64). Additional work demonstrated that obesity is associated with a state of chronic, low-grade inflammation not only locally in adipose tissue, but also systemically, indicated by elevated plasma concentrations of other inflammation-associated factors despite TNF- α , such as interleukin-6 (IL-6) and interleukin-10 (IL-10) (65-68). During the development of obesity, immune cells, e.g. macrophages, infiltrate tissues, such as white adipose tissue (WAT) and lead to increased secretion of TNF- α .

and IL-6 (69, 70). Furthermore, chronic inflammation in WAT, liver and skeletal muscle plays a crucial role in the development of obesity-induced insulin resistance (69, 71, 72). In the liver, Kupffer cells (KC) represent the population of resident macrophages, which are derived from circulating monocytes and line the sinusoid walls of the liver (73, 74). They are thought to be the main source of hepatic TNF- α , although other local types of cells are also able to produce this pro-inflammatory cytokine.

1.3.1 IL-6 and insulin resistance

IL-6 is a pleiotropic cytokine that not only affects the immune system, but also drives many physiological events in various tissues. Binding of IL-6 to its receptor complex, comprising of IL-6R α and gp130, leads to the phosphorylation of the Janus kinase (JAK) and subsequent phosphorylation of the receptor complex. This phosphorylation interacts with proteins harbouring a SH2 domain. Signal transducer and activator of transcription (STAT) and tyrosine-protein phosphatase non-receptor type 11 (SHP-2) contain SH2 domains and are capable of binding to the receptors, resulting in the phosphorylation of specific tyrosine residues by JAK. Activated STATs form dimers and activate transcription of their target genes, such as suppressor of cytokine signaling 3 (SOCS-3) (75). An alternative IL-6 signaling branch results in the phosphorylation of SHP-2 that leads to rat sarcoma (ras)-mediated activation of mitogen-activated protein kinase (MAPK) signaling (Fig. 4) (76).

Currently, the function of IL-6 as mediator of obesity-induced insulin resistance is controversially discussed (77). Due to the observation that IL-6, along with the pro-inflammatory cytokine TNF- α , is often elevated in serum during obesity or in patients with metabolic diseases, it has been suggested that IL-6 signaling promotes insulin resistance (78, 79). Consistently, IL-6 treatment induces cellular insulin resistance in hepatocytes and injection of IL-6 triggers expression of suppressor of cytokine signaling 3 (SOCS-3),

which can potentially inhibit insulin action (80, 81). Moreover, IL-6 infusion during euglycemic-hyperinsulinemic clamp studies markedly blunts insulin response, reflected by a lower glucose infusion rate, indicating that IL-6 indeed causes insulin resistance (82).

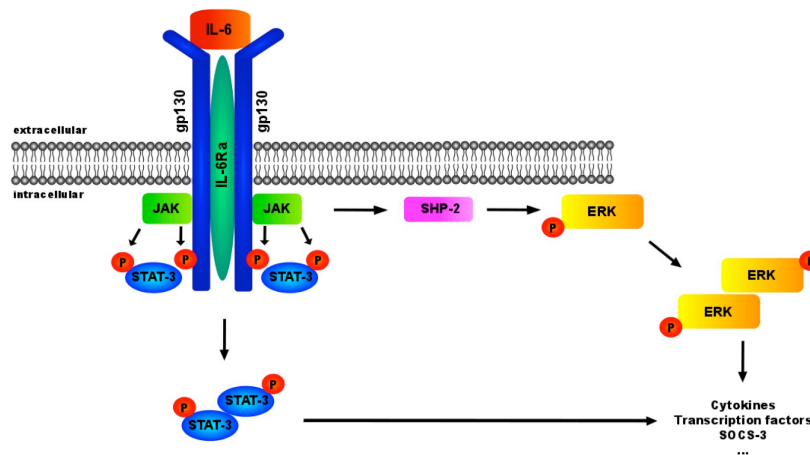


Fig. 4: IL-6 signaling cascade

Binding of IL-6 to its receptor complex, comprising of IL-6R α and gp130, leads to the phosphorylation of JAK and subsequent phosphorylation of the receptor complex. Recruitment of STAT-3 or SHP-2 to the receptor leads to their activation by phosphorylation through JAK. Active STAT-3 forms dimers, whereas SHP-2 leads first to the activation of ERK, which in turn dimerizes. These dimers then translocate into the nucleus and activate the transcription of target genes.

Whereas these studies suggest a harmful role of IL-6 action in the development of obesity-associated insulin resistance, other reports could demonstrate a positive effect of IL-6 on glucose metabolism. Acute treatment with IL-6 increases insulin-stimulated glucose disposal rate in healthy humans, without affecting endogenous glucose production, by an AMP-dependent kinase (AMPK) mediated mechanism (83). Additional findings reveal that IL-6 injection increases systemic insulin sensitivity and improves glucose tolerance (84). A connection between insulin action in the central nervous system (CNS) and hepatic IL-6 release was also shown. Following activation of signal transducer and activator of transcription (STAT-3) in hepatocytes (Fig. 4) leads to inhibition of G6Pase and PEPCK expression (85).

1.3.2 *TNF- α* and insulin resistance

The role of $TNF-\alpha$ in developing obesity-associated insulin resistance is object of many observations and an increased expression of $TNF-\alpha$ in skeletal muscle from insulin-resistant humans has also been noted (86). Additionally, prolonged infusion of $TNF-\alpha$ impairs insulin-mediated glucose disposal and insulin-stimulated suppression of total hepatic glucose output, whereas HGP and glucose utilization were elevated (87).

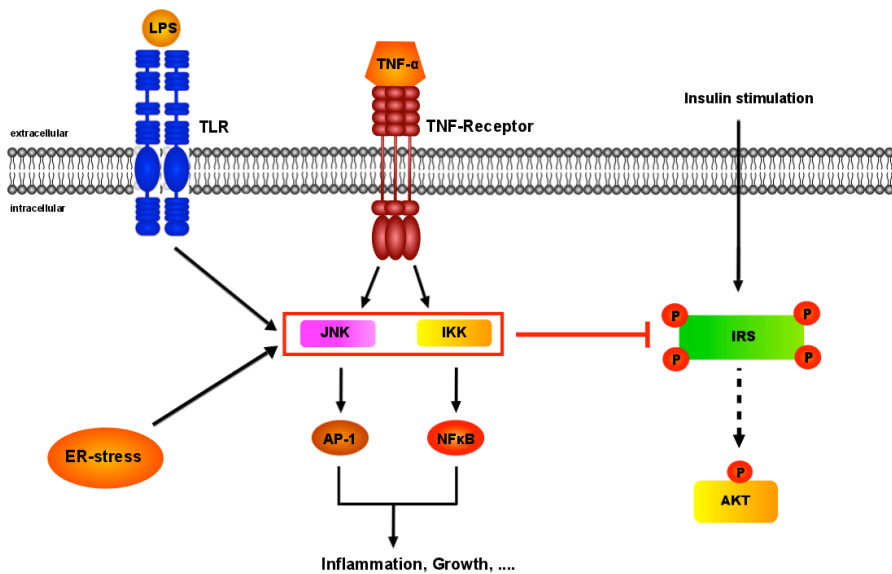


Fig. 5: Potential mechanisms for the inhibition of insulin signal transduction

Activation of cell surface receptors, which induce serine kinases, such as c-Jun N-terminal kinase (JNK) and inhibitor of $NF-\kappa B$ kinase (IKK) complex, mediate inhibitory serine (S307) phosphorylation events on insulin receptor substrates (IRS) and thereby blocking insulin action. Furthermore, endoplasmatic reticulum (ER) stress and intermediates of fatty acid metabolism may activate stress kinases.

It was also shown that inhibition of $TNF-\alpha$ improves hepatic and peripheral insulin sensitivity *in vivo* (88). Finally, activation of $TNF-\alpha$ downstream kinases (Fig. 5), such as inhibitor of nuclear factor κB ($NF-\kappa B$) kinases (IKK) and c-Jun amino-terminal kinases (JNK), reveal impaired insulin signal transduction in peripheral tissues (71, 89-91).

1.4 Cancer and hepatocellular carcinoma (HCC)

Cancer is a generic term for a large group of diseases that can occur in almost all parts of the body. It is characterized by an uncontrolled cell growth that leads to tumor formation and invasion of these cells into nearby tissues (92). The surrounding tissue is often destroyed by the cancer growth and invasion. Influenced by an increasing and aging population, the World Health Organization (WHO) estimates that the global cancer-related mortality rate will increase from 7.9 million (2007) to 11.5 million (2030) incidents per year. The WHO also suggests that the majority of all cancer cases occurs in low- and middle-income countries, such as Asia and South America. Nevertheless, in most industrialized countries, cancer is the second most frequent cause of death after cardiovascular diseases (93).

Hepatocellular carcinoma (HCC) represents approximately 85%-90% of primary liver cancers (94), with an average mortality of 95% within 5 years. Since it often remains unnoticed in the early stages, HCC is usually advanced when the patients exhibit clinical symptoms. Due to this fact, it represents the third largest cause of cancer deaths worldwide, particularly in Africa and Eastern Asia (Fig. 6). However, the incidence of HCC in Western countries cannot be ignored, as it is rising constantly (95).

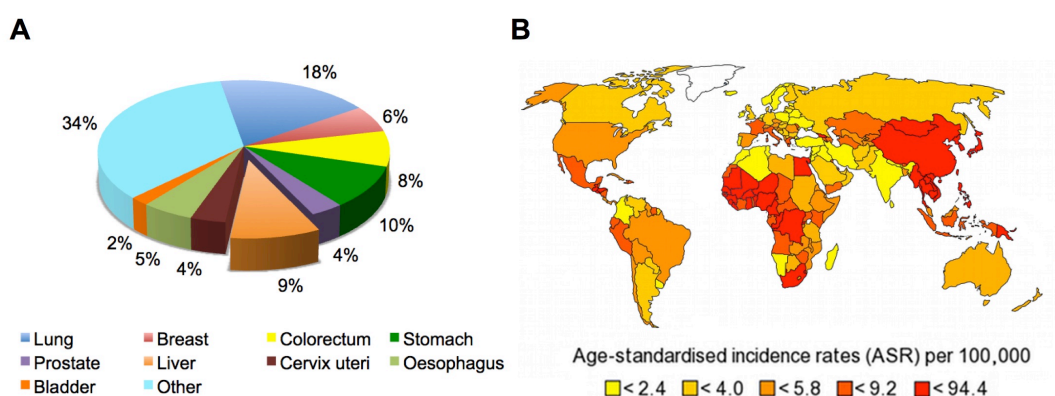


Fig. 6: Cancer distribution and HCC incidence rates worldwide in 2011

(A) Worldwide distribution of different cancer forms of both genders in percentage of total cancer numbers from 2011. (B) Distribution of HCC incidence in 2011 (ASR per 100,000). Data from (A) and (B) are documented by the WHO globocan project.

A variety of genetic predispositions, such as mutations in tumor suppressor genes, are linked to HCC, as well as cirrhosis which is caused by chronic hepatitis infections, alcohol abuse or metabolic disorders, e.g. due to obesity (96-102). Strikingly, male individuals have a 4 times higher risk to develop liver cancer than women.

1.5 Linking inflammatory processes to HCC

The observation that leukocytes are highly abundant in neoplastic tissue was the first indicator for a connection between inflammation and cancer (103). Over the last decades, several reports raised the hypothesis of inflammation-mediated oncogenesis (104). HCC represents a classic case of inflammation-associated cancer, since it is promoted by chronic hepatic inflammation due to hepatic injury (105, 106). A response mechanism to this chronic inflammation is the compensatory proliferation of hepatocytes, which may ultimately lead to HCC (107).

1.5.1 Toll-like receptor (TLR) signaling in liver damage and HCC

The toll-like receptor (TLR) signaling pathway represents a classic signaling cascade in innate immune cells and its activation is thought to be linked to the development of HCC as result of chronic liver diseases (108). Exogenous ligands, such as microbial components, known as pathogen-associated molecular patterns (PAMPS), specifically activate their corresponding TLR (Fig. 7) (109). Furthermore, endogenous TLR ligands, so called damage-associated molecular patterns (DAMPS), are able to trigger TLR signaling (110). The majority of these ligands, such as high mobility group box 1 (HMGB1), heat shock proteins and free fatty acids, are predominantly released from dying cells (111-113).

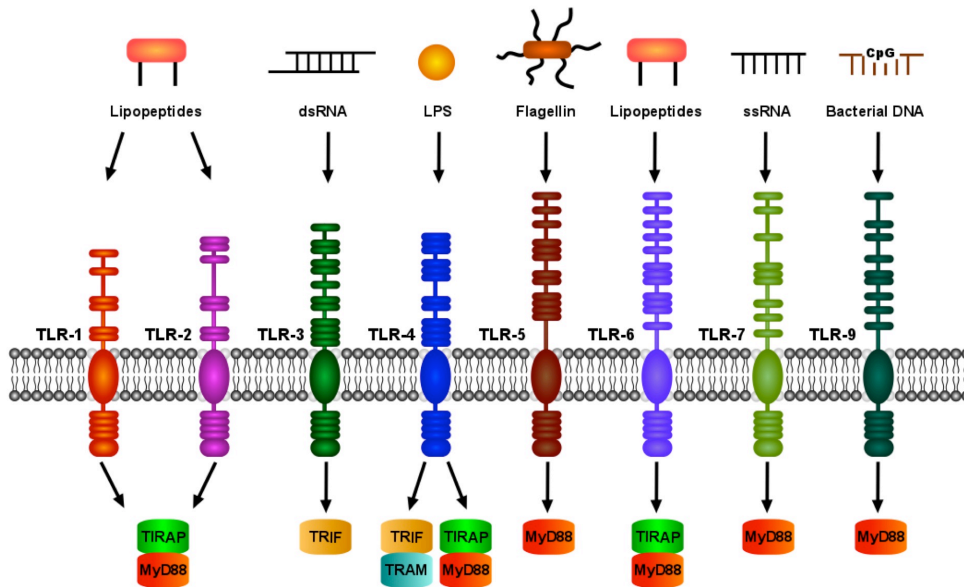


Fig. 7: Toll-like receptors and their PAMP ligands

The family of mammalian TLRs, their microbial component ligands and the used adaptor proteins for activation and proper signal transduction.

TLRs are highly dependent on specific adaptor molecules and kinases, such as myeloid differentiation primary response gene 88 (MyD88), TIR domain-containing adapter protein (TIRAP), TIR domain-containing adapter inducing interferon- β (TRIF) and TIR domain-containing adapter protein (TRAM) (Fig. 7) (114-116). These adaptor molecules activate downstream targets upon binding of DAMPS or PAMPS to their corresponding TLRs, which ultimately triggers the transcription of cytokines or chemokines, among others (117).

Mice deficient in MyD88 are highly resistant to chemically induced HCC (e.g. by administration of diethylnitrosamine (DEN)), indicating a strong connection between TLR signaling and hepatocarcinogenesis (118). Presumably, DEN induces cell death in hepatocytes, which in turn activates KCs via TLRs and induces expression of pro-inflammatory cytokines, eventually enhancing the development of HCC (119). Although KCs are the initial cells responding to PAMPS in the liver, recent studies provide evidence for an active TLR signaling cascade in hepatic nonimmune cells, e.g. hepatocytes (120, 121). However, MyD88 deficient cells are still able to activate JNK and NF- κ B in

response to the TLR-4 ligand lipopolysaccharide (LPS), indicating signal activation in a MyD88 independent manner (Fig. 8) (122).

1.5.2 MyD88 dependent TLR signaling

MyD88 is a central adaptor protein, used by almost all TLRs for intracellular signaling (Fig. 7). Upon activation of TLRs by specific stimuli, toll/interleukin-1 receptor (TIR) domain containing adaptors, such as MyD88 and TIR domain-containing adapter protein (TIRAP), interact with the TIR domain of TLRs. This association recruits members of the interleukin-1 receptor-associated kinase (IRAK) family, followed by their phosphorylation and dissociation from MyD88. Active IRAKs then associate with tumor necrosis factor receptor-associated factor 6 (TRAF6), leading to the activation of two distinct signaling pathways and finally to the activation of JNK and NF- κ B (Fig. 8) (117).

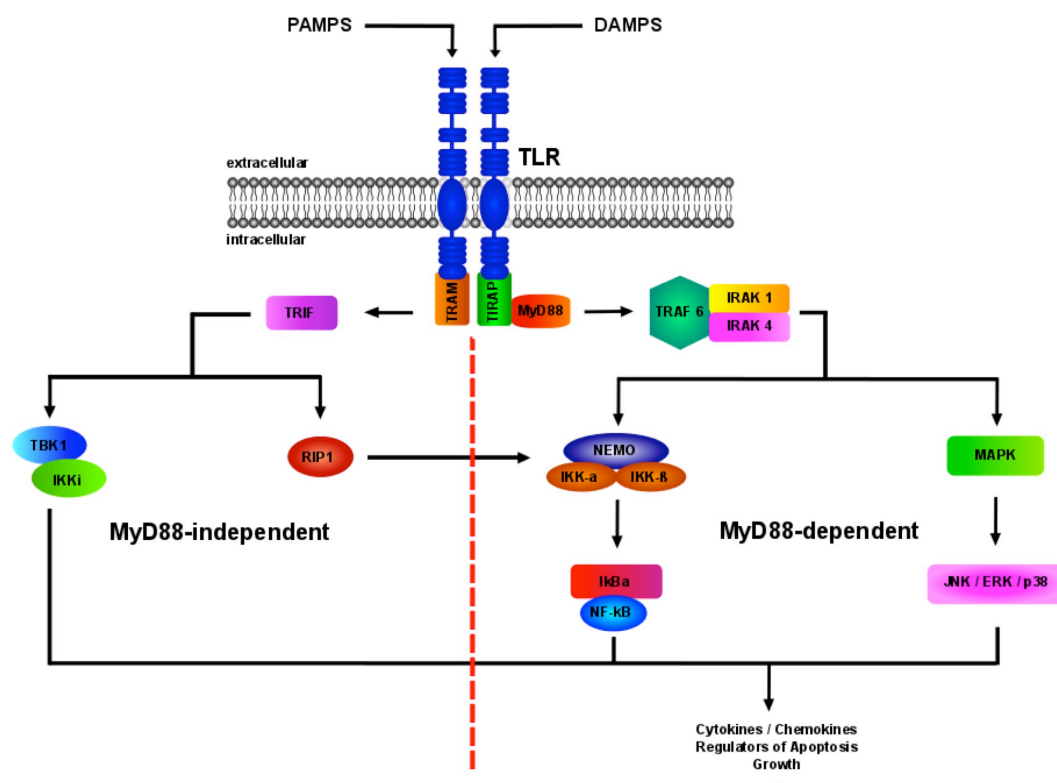


Fig. 8: Toll-like receptor signaling cascade

The intracellular TLR-signaling cascade in a MyD88 dependent (right) and independent (left) manner.

1.5.3 MAPK signaling and HCC

The mammalian family of mitogen-activated protein kinases (MAPKs) consists of extracellular signal-regulated kinase (ERK), p38, and JNK, and each of these exists in several isoforms. For intact MAPK signaling, the induction of at least three kinases is necessary to establish the sequential activation pathway, the MAPK kinase kinase (MKKK), MAPK kinase (MKK), and MAPK itself. Generally, these signaling components are expressed in all cell types and transduce signaling upon stimulation with cytokines, growth factors and stress signals (123). Moreover, the MAPK signaling pathways are often deregulated in various types of cancers, including HCC (124).

ERK1 and ERK2 are highly homologous and display overlapping regulatory mechanisms (125). They are activated by a wide variety of receptors, particularly receptor tyrosine kinases. Alterations of the ERK pathway are contributed to the development of HCC, especially elevated levels of active ERK were observed in hepatocellular carcinomas (126).

The p38 subfamily consists of four different isoforms (p38 α , p38 β , p38 γ and p38 σ) and their activation is mediated by the upstream kinases MKK3, MKK4, and MKK6 (127-131). Published studies about p38 MAPK mostly refer to p38 α , which is involved in inflammation induced apoptosis as well as various types of stresses (132-134). An important role in suppression of HCC tumorigenesis has also been demonstrated. Mice lacking hepatic p38 α exhibit enhanced HCC development, triggered by accumulation of reactive oxygen species (ROS), which leads to enhanced liver injury (135).

JNK proteins are encoded by three genes: JNK1, JNK2 and JNK3. JNK1 and JNK2 are ubiquitously expressed, whereas JNK3 is mainly found in brain, heart and testis (136, 137). Their regulation is mediated by the upstream MAPK kinases, MKK4 and MKK7, which are activated upon stimulation with stress signals and pro-inflammatory stimuli (138, 139). During HCC development, the JNK pathway was assigned a pro-oncogenic role. Increased

JNK1 activity was observed in human HCC and mice lacking JNK1 exhibit reduced liver carcinogenesis (140, 141). Additionally, the downstream target c-Jun promotes chemically induced liver cancer through suppression of the p53 pathway (142).

1.5.4 NF- κ B signaling and HCC

The mammalian family of NF- κ B transcription factors consists of five members (RelA, RelB, c-Rel, NF- κ B1, and NF- κ B2), which are assembled by dimerization (143). Among the inflammatory signaling pathways that are associated with cancer development, the transcription factor NF- κ B is of central importance in the promotion of tumor development (144), since it is involved in the regulation of immune responses, inflammation and cell survival (145). Various pro-inflammatory stimuli are able to activate NF- κ B, mainly via activation of IKK. IKK in turn phosphorylates I κ B proteins, which keep NF- κ B in an inactive state, leading to the degradation of I κ B (146). The most prominent I κ B protein is I κ B α . Since NF- κ B is a major activator of anti-apoptotic gene expression, it is thought to play a key role in tumorigenesis (147, 148). Evidence for the involvement in mouse carcinogenesis *in vivo* was shown by the promotion of inflammation-induced cancer by NF- κ B (149-151). In contrast, other published studies showed that inactivation of hepatic NF- κ B increases HCC incidence, indicating a suppressive role in tumor development (152, 153).

1.6 Objectives

Obesity-associated insulin resistance as well as hepatocellular carcinoma are steadily increasing diseases worldwide and both are somehow related with inflammation. Additionally, epidemiological studies have shown that obesity is a risk factor for hepatocellular carcinoma, indicating related mechanisms in the development of both diseases. Understanding the underlying mechanisms involved in the development of obesity and hepatocellular carcinoma is a first step to find therapeutical approaches to treat these diseases. The liver, affected in both, is known to play a key role and is subject of many studies. The aim of this study was to analyse inflammatory pathways in the development of obesity-associated insulin resistance and chemically induced hepatocellular carcinoma *in vivo*. Therefore, mice with conditional disruption of either the IL-6R α or the TLR adaptor protein MyD88 in hepatocytes were generated. Mice lacking hepatic IL-6 signaling served for the analysis of energy homeostasis, glucose metabolism and insulin signaling. For the analysis of hepatic inflammatory processes in the development of chemically induced hepatocellular carcinoma, mice lacking MyD88 in the liver were used.

2. Materials and Methods:

2.1 Chemicals and enzymes

Size markers for agarose gel electrophoresis (Gene Ruler DNA ladder mix) and for SDS-PAGE (Prestained protein ladder Mix) were got from Fermentas (St. Leon-Rot, Germany). For polymerase chain reactions, RedTaq polymerase (Sigma-Aldrich, Seelze, Germany) or DreamTaq (Fermentas, St. Leon-Rot, Germany) were used. Chemicals and enzymes used in this work are listed in table 1 and 2, respectively. All solutions were prepared with double distilled water.

Table 1: Chemicals

Chemical	Distributor
α ^[32P] -dCTPs	Amersham, Freiburg, Germany
β -Mercaptoethanol (β -ME)	AppliChem, Darmstadt, Germany
γ ^[32P] -dATP	Amersham, Freiburg, Germany
ϵ -Aminocaproic acid	Sigma-Aldrich, Seelze, Germany
0.9% Saline (sterile)	Delta Select, Pfullingen, Germany
2,2,2-Tribromoethanol (Avertin [®])	Sigma-Aldrich, Seelze, Germany
2-Deoxy-D-[1- ¹⁴ C]-Glucose	Amersham, Freiburg, Germany
Acetic acid	Merck, Darmstadt, Germany
Acrylamide	Roth, Karlsruhe, Germany
Agarose	Peqlab, Erlangen, Germany
Ammonium acetate	Merck, Darmstadt, Germany
Ammoniumpersulfat (APS)	Sigma-Aldrich, Seelze, Germany
Aprotinin	Sigma-Aldrich, Seelze, Germany

Biotin	Bode Chemie, Hamburg, Germany
Complex-Vectastain Elite	Fluka, Sigma-Aldrich, Seelze, Germany
Bacillo [®]	Sigma-Aldrich, Seelze, Germany
Barium hydroxide (Ba(OH) ₂)	Sigma-Aldrich, Seelze, Germany
Benzamidine	Merck, Darmstadt, Germany
Bovine serum albumin (BSA)	Merck, Darmstadt, Germany
Bradford reagent	Bio-Rad, München, Germany
Bromphenol blue	Merck, Darmstadt, Germany
Calcium chloride (CaCl ₂)	AppliChem, Darmstadt, Germany
Chloroform	Sigma-Aldrich, Seelze, Germany
Count off [™]	NEN [®] Research Products, Boston, USA
D-[3- ³ H]-Glucose	Amersham, Freiburg, Germany
Desoxy-ribonucleotid-triphosphates (dNTPs)	Amersham, Freiburg, Germany
Dextrane sulfate	Sigma-Aldrich, Seelze, Germany
Dimethylsulfoxide (DMSO)	Merck, Darmstadt, Germany
Di-sodiumhydrogenphosphate	Merck, Darmstadt, Germany
Dithiothreitol (DTT)	Boehringer, Mannheim, Germany
Enhanced chemiluminescence (ECL) Kit	Perbio Science, Bonn, Germany
Ethanol, absolute	AppliChem, Darmstadt, Germany
Ethidium bromide	Sigma-Aldrich, Seelze, Germany
Ethylendiamine tetraacetate (EDTA)	AppliChem, Darmstadt, Germany
Fetal calf serum (FCS)	Gibco BRL, Eggenstein, Germany
Forene [®] (isoflurane)	Abbot GmbH, Wiesbaden, Germany
Glucose (20%)	DeltaSelect, Pfullingen, Germany

Glutamine	Invitrogen, Karlsruhe, Germany
Glycerol	Serva, Heidelberg, Germany
Glycine	Applichem, Darmstadt, Germany
HEPES	Applichem, Darmstadt, Germany
Hydrochloric acid (37%) (HCl)	KMF Laborchemie, Lohmar, Germany
Hydrogen peroxide	Sigma-Aldrich, Seelze, Germany
Insulin	Novo Nordisk, Bagsværd, Denmark
Isopropanol (2-propanol)	Roth, Karlsruhe, Germany
Magnesium chloride	Merck, Darmstadt, Germany
Methanol	Roth, Karlsruhe, Germany
N-Nitrosodiethylamine (DEN)	Sigma-Aldrich, Seelze, Germany
Nitrogen (liquid)	Linde, Pullach, Germany
NP-40	Merck, Darmstadt, Germany
Octenisept [®]	Schülke & Mayr, Norderstedt, Germany
Paraformaldehyde (PFA)	Fluka, Sigma-Aldrich, Seelze, Germany
Penicillin/Streptomycin solution	Gibco BRL, Eggenstein, Germany
Phenol-chloroform-isoamyl alcohol	AppliChem, Darmstadt, Germany
Phenylmethylsulfonylfluoride (PMSF)	Sigma-Aldrich, Seelze, Germany
Phosphate buffered saline (PBS)	Gibco BRL, Eggenstein, Germany
Poly (dl-dC)	Amersham Pharmacia Biotec, Uppsala, Sweden
Potassium chloride	Merck, Darmstadt, Germany
Potassium hydroxide	Merck, Darmstadt, Germany
Protease inhibitor cocktail	Roche, Mannheim, Germany
RPMI 1640 medium	Gibco BRL, Eggenstein, Germany

Ready Safe™, liquid scintillation cocktail	Beckman Coulter, Fullerton, USA
Sodium acetate	AppliChem, Darmstadt, Germany
Sodium chloride (NaCl)	AppliChem, Darmstadt, Germany
Sodium citrate	Merck, Darmstadt, Germany
Sodium dodecyl sulfate (SDS)	AppliChem, Darmstadt, Germany
Sodium fluoride (NaF)	Merck, Darmstadt, Germany
Sodium heparin (Liquemin®)	Roche, Grenzach-Wyhlen, Switzerland
Sodium hydroxide (NaOH)	AppliChem, Darmstadt, Germany
Sodium orthovanadate	Sigma-Aldrich, Seelze, Germany
Tetramethylethylenediamine (TEMED)	Sigma-Aldrich, Seelze, Germany
Tissue freezing medium	Jung, Heidelberg, Germany
Tramadolhydrochlorid (Tramal®)	Grünenthal, Aachen, Germany
TriFast™	Peqlab, Erlangen, Germany
Trishydroxymethylaminomethane (Tris)	AppliChem, Darmstadt, Germany
Triton X-100	Appllichem, Darmstadt, Germany
Tween 20	Appllichem, Darmstadt, Germany
Vectashield® mountin medium with DAPI	Appllichem, Darmstadt, Germany
Western blocking reagent	Vector, Burlingame, USA
Xylene cyanol	Sigma-Aldrich, Seelze, Germany
Zinc sulfate (ZnSO ₄)	Roche, Mannheim, Germany

Table 2: Enzymes

Enzyme	Distributor
BglI	NEB, Schwalbach, Germany
DNase, RNase-free	Promega, Madison, WI, USA
EuroScript reverse transcriptase	Eurogentec, Seraing, Belgium
Proteinase K	Roche, Mannheim, Germany
RNAseI	Fermentas, St. Leon-Rot, Germany
T4 polynucleotide kinase	NEB, Schwalbach, Germany

2.2 Mouse experiments

General animal handling was performed as described by Hogan (154) and Silver (155).

2.2.1 Animal care

Care and procedures of all animals was approved by local government authorities (Bezirksregierung Köln, Cologne, Germany) and reviewed by the animal care committee of the University of Cologne in accordance with National Institutes of Health guidelines. Animals were kept in groups of 3 to 5 animals (depending on weight) or individually (depending on the experiment). Mice were housed at 22°C – 24°C using a 12 h light / 12 h dark cycle with lights on at 7 AM. Animals were fed regular chow food (NCD; Teklad Global Rodent 2018; Harlan) containing 53.5% carbohydrates, 18.5% protein, and 5.5% fat (12% of calories from fat) and had *ad libitum* access to water at all times. Food was only withdrawn if required for an experiment. Mice were sacrificed at the end of the study period by lethal CO₂ anaesthesia, the relevant organs were dissected, snap-frozen and stored at -80°C until further preparation.

2.2.2 Generation of IL-6R α ^{L-KO} and MyD88^{L-KO} mice

For the generation of IL-6R α ^{L-KO} and MyD88^{L-KO} mice, albumin promoter/ α -fetoprotein enhancer (ALFP)-Cre^{+/-} mice were mated with either MyD88^{FL/FL} or IL-6R α ^{FL/FL} mice (generated and kindly provided by PD Dr. F. Thomas Wunderlich from the laboratory of Prof. Dr. Jens C. Brüning in the Institute for Genetics, University of Cologne, Germany) and double heterozygous mice were further intercrossed to yield hepatocyte specific IL-6R α or MyD88 knockout mice (IL-6R α ^{L-KO} and MyD88^{L-KO}).

The breeding colonies were maintained by mating either MyD88^{FL/FL} or IL-6R α ^{FL/FL} mice with ALFP-Cre^{+/-} MyD88^{FL/FL} or ALFP-Cre^{+/-} IL-6R α ^{FL/FL} mice, respectively. All mice had been backcrossed for 10 generations on a C57BL/6 background before used for experiments and the background was unchanged throughout all experiments. Littermates were used for analysis at all times and were genotyped by PCR using genomic DNA isolated from tail tips.

2.2.3 Body weight and body composition

Body weight was measured once a week and body composition was measured *in vivo* by nuclear magnetic resonance using the minispec mq 7.5 (Bruker Optik, Ettlingen, Germany) at the end of the study period.

2.2.4 Collection of blood samples and determination of blood glucose levels

The collection of blood samples was performed according to guidelines (154, 155) in the morning to avoid variations by the circadian rhythm. The blood cells and platelets were separated from serum by centrifugation of the blood samples for 30 min at 4°C. The obtained serum was stored at -20°C.

The determination of blood glucose levels was performed from whole venous blood using an automatic glucose monitor (GlucoMen® GlycÓ; A. Menarini Diagnostics).

2.2.5 Glucose and insulin tolerance test

Glucose tolerance tests (GTT) were performed on animals after a fasting period of 16 h over night. Insulin tolerance tests (ITT) were performed on random fed mice. The animals received an *i.p.* injection of either 2 g/kg body weight of glucose or 0.75 U/kg body weight of human regular insulin, respectively. Glucose levels were determined in blood collected from the tail tip immediately before and 15, 30 and 60 min after the injection of insulin, with an additional measurement after 120 min for the GTT.

2.2.6 Indirect calorimetry, locomoter activity and daily food intake

The measurements for indirect calorimetry, locomoter activity and daily food intake over 48 h were performed in 7.1-l chambers of the PhenoMaster System (TSE systems, Bad Homburg, Germany) at room temperature (22 - 24°C). For the adaptation, the mice were placed in the chambers for 48 h before the experiment. The food and water were provided *ad libitum* in appropriate devices and daily food intake was measured through the PhenoMaster System as well as VO_2 and VCO_2 by indirect calorimetry. To monitor the locomotor activity, an infrared light-beam frame was used.

2.2.7 Euglycemic-hyperinsulinemic clamp studies (EHCS)

2.2.7.1 Implantation of the catheter

Male mice at the age of 10 weeks were anesthetized by an intraperitoneal injection of 240 mg/kg avertin and adequacy of the anesthesia was ensured by the loss of pedal reflexes. After the loss of pedal reflexes, a Micro-Renathane catheter (Micro-Renathane, MRE 025; Braintree Scientific Inc., Braintree, Massachusetts, USA) was inserted into the right internal jugular vein and advanced to the level of the superior *vena cava*. After the irrigation with 0.9% saline solution, the catheter was filled with heparin solution, sealed at its distal end and left in a subcutaneous pocket at the back of the neck. The cutaneous incisions were closed with a 4-0 silk suture and the free end of the catheter was attached to the suture in the neck in such a fashion as to allow the retrieval of the catheter on the day of the experiment. After the implantation of the catheter the mice received an intraperitoneal injection of 1 ml saline solution (0.9%) containing 15 µg/g body weight of tramadol and were placed on a heating pad in order to facilitate recovery.

2.2.7.2 Radioactive EHCS procedure

After 6 days of recovery, only mice that had lost less than 10% of their preoperative weight were studied and included in the experimental groups. Each animal was fasted for 16 h and placed into restrainers for the whole duration of the clamp experiment. After an infusion of a 5 µCi D-[3-³H] glucose tracer bolus solution at the beginning of the experiment, a tracer solution (0.05 µCi/min) was infused continuously for the whole experiment. At the end of the basal period (40 min), a blood sample (60 µl) was collected to determine the basal parameters and a 40 µU/g insulin bolus solution was infused, followed by the infusion of a 4 µU/g/min insulin solution containing 0.1% BSA at a fixed rate. To minimize blood loss, red blood cells were

collected by centrifugation and reinfused after being resuspended in 0.9% saline solution. The blood glucose levels were analyzed every 10 min with a B-Glucose Analyser (Hemocue, Wetzikon, Switzerland). To prevent counterregulatory response to hypoglycemia, a 20% glucose solution was infused to maintain the physiological blood glucose level (120 - 145 mg/dl). Approximately 60 min before the steady state period, a 10 μ Ci bolus of 2-Deoxy-D-[1- 14 C] glucose was infused to later determine the glucose disposal rate in the tissues. After the glucose bolus, blood samples (15 μ l) were collected at the timepoints 0, 5, 15, 25, 35, 55 min after bolus infusion. Once the glucose measurements were constant for at least 30 min at a fixed glucose infusion rate, the steady state phase was achieved. During the steady state period, blood samples (50 μ l) were collected at every 10 min for the measurement of steady state parameters. At the end of the experiment, mice were sacrificed by a lethal dose of isofluran and brain, liver, WAT and skeletal muscle were dissected and stored at -80°C .

*2.2.7.3 Determination of the glucose turnover rate (mg/[kg*min])*

To determine the glucose turnover rate, the D-[3- ^3H] glucose radioactivity in the plasma was assessed. Therefore, the plasma samples of basal and steady state period were deproteinized with 0.3 M $\text{Ba}(\text{OH})_2$ and 0.3 M ZnSO_4 followed by the evaporation of $^3\text{H}_2\text{O}$, using a liquid scintillation counter (Beckmann, Krefeld, Germany).

To calculate the glucose turnover rate, the infusion rate of tracer solution (dpm/min) was divided by the glucose specific activity (dpm/mg) in the plasma. The result was then corrected for body weight of the animals.

2.2.7.4 Calculation of the hepatic glucose production (HGP)

Hepatic glucose production was calculated as the difference between the rate of glucose appearance and the infusion rate of glucose.

2.2.7.5 Determination of the in vivo glucose uptake in the tissues

For the determination of the *in vivo* glucose uptake in WAT, brain and skeletal muscle, the tissues were homogenized and 2-Deoxy-D-[1-¹⁴C] glucose (2DG) was separated from 2-Deoxy-D-[1-¹⁴C] glucose-6-phosphate (2DG6P) by using ion exchange chromatography columns (Poly-Prep® Prefilled Chromatography Columns, AG®1-X8 formate resin, 200 - 400 mesh dry; Bio Rad Laboratories). The 2-Deoxy-D-[1-¹⁴C] glucose radioactivity in the plasma was directly measured in the liquid scintillation counter (Beckmann, Krefeld, Germany). The calculation of the *in vivo* glucose uptake (nmol/[g*min]) of the tissues is based on the accumulation of 2DG6P in the respective tissue and the disappearance rate of 2DG from the plasma and was calculated as described previously (156).

2.2.8 Ablation of Kupffer cells (KCs)

To efficiently ablate the Kupffer cells in the liver, the mice received a single 1 ml intraperitoneal injection of clodronate liposomes (157) 2 days before the experiment. To confirm the ablation of the KCs, a MAC-2/Galectin-3 antibody (#CL8942AP; Cedarlane Laboratories Ltd, Burlington, ON, Canada) staining was performed.

2.2.9 Glucose-induced insulin secretion of isolated pancreatic islets

To assess the glucose-induced insulin secretion of isolated pancreatic islets, the pancreatic islets were isolated as described previously (158) by a collagenase technique. Then, the islets were maintained overnight in RPMI 1640 culture medium supplemented with 10% FCS, 2 mM glutamine, 100 µg/ml streptomycin and 100 units of penicillin at 37°C in a humidified atmosphere (5% CO₂ in the air). Afterwards, the islets were preincubated in HEPES buffer (pH 7.4) containing 125 mM NaCl, 5.9 mM KCl, 1.2 mM MgCl₂, 1.28 mM CaCl₂, 3 mM glucose and 1 mg/ml BSA for 30 min at 37°C. Batches of 6 to 9 islets were subsequently incubated with either 3 mM or 11 mM glucose for 30 min at 37°C. To stop the incubation, batches were chilled on ice and samples were taken for the analysis of insulin by the TPX plate reader (ArcDia International Oy Ltd, Turku, Finland) (159). The resting islets were collected for the quantification of dsDNA in the islets using the Pico-Green dsDNA quantification reagent kit (Invitrogen, Karlsruhe, Germany).

2.2.10 Diethylnitrosamine (DEN) treatment

The chemical diethylnitrosamine (DEN) causes DNA alkylation, leading to mismatches during replication. This results in DNA mutations and ultimately to the development of hepatocellular carcinoma (HCC) (160).

2.2.10.1 Long-term treatment:

Mice at 15 days of age were injected with 25 mg/kg DEN into the peritoneal cavity and sacrificed after 32 weeks. Blood samples were collected at week 12 and week 24 for further analysis. After dissection of the WAT, skeletal muscle and liver, HCC were counted and tissues were stored at -80°C.

2.2.10.2 Short-term treatment:

Animals at the age of 12 weeks received an *i.p.* injection of 100 mg/kg DEN and sacrificed after indicated timepoints. Afterwards, blood samples were collected and liver, skeletal muscle and WAT were dissected and stored at -80°C.

2.2.11 Analysis of serum protein and cytokine concentrations

Serum levels of AST, ALT, cholesterol and TG were determined in the diagnostic laboratory of the University Hospital Cologne using a standard protocol. The determination of IL-6, IL-10 and TNF- α levels in the sera was conducted using a cytometric bead array (CBA) (#552364, BD Biosciences) with a FACS Calibur (BD Biosciences) according to the manufacture's protocol.

2.3 Molecular biology

2.3.1 Isolation of genomic DNA

To isolate genomic DNA, mouse tail biopsies or tissues were taken and digested in 600 μ l tail lysis buffer (100 mM Tris pH 8.5, 5 mM EDTA, 0.2% (w/v) SDS, 0.2 M NaCl, 500 mg/ml Proteinase K) in a thermomixer (Eppendorf, Hamburg, Germany) at 56°C over night. The DNA was subsequently precipitated by adding an equivalent volume of 2-propanol (100%). After centrifugation and a wash step with 70% EtOH, the DNA pellet was dried and re-dissolved in 50-100 μ l TE-buffer (10 mM Tris/HCl [pH=8], 1 mM EDTA) containing 50 μ g/ml RNaseI.

2.3.2 Quantification of nucleic acids

The concentration of DNA and RNA was determined by measuring the sample absorption at 260 nm with a NanoDrop ND-1000 UV-Vis spectrophotometer (Peqlab, Erlangen, Germany). An optical density at 260 nm (OD_{260}) of 1 corresponds to approximately 50 μ g/ml of double stranded DNA and to 38 μ g/ml of RNA. The absorption at 280 nm (OD_{280}) was used for protein content in the samples. As an index of DNA/RNA purity the ratio of OD_{260}/OD_{280} was used. A ratio of 2 refers to pure DNA or RNA and lower values display protein contaminations of the probes.

2.3.3 Southern blot analysis

10-15 μ g of genomic DNA were digested overnight at 37°C, using BglI. Separation of DNA was performed electrophoretically on an 0.8% (w/v) agarose gel at 30 V with subsequent transfer on a HybondTM-N+ nylon membrane (Amersham, Braunschweig, Germany) by an alkaline capillary transfer (161). The followed crosslink of the DNA to the membrane was

performed by baking the membrane at 80°C for 20 min. Meanwhile the α -^[32P]-dCTP labeled probe was amplified by PCR using the Ladderman™ DNA Labeling Kit (TaKaRa; Cambrex Bio Science, Verviers, Belgium) with customized primers (Table 3). The Membranes were then equilibrated in 2 x SSC and prehybridized at 65°C for 4 h in hybridization solution (1 M NaCl, 1% (w/v) SDS, 10% (w/v) dextran sulfate, 50 mM Tris-HCl (pH 7.5), 250 µg/ml sonicated salmon sperm DNA). Afterwards, the radioactively labeled probe was added to the prehybridization solution for hybridization of the probe to its corresponding sequence on the nylon membrane (overnight at 68°C in a rotating cylinder). Unspecifically bound probe was removed by washing the membrane at 68°C for 10 – 20 min, until 20 – 80 cps were reached (monitored by a Geiger Müller Counter). The initial wash was performed with 2 x SSC / 0.1% (w/v) SDS, followed by 1 x SSC / 0.1% (w/v) SDS, if needed. The membrane was then sealed in a plastic bag and exposed to an X-ray film (Kodak XAR-5 or BioMAX MS; Eastman Kodak) at -80°C in an appropriate cassette. Films were developed in an automatic developer (Agfa, Köln, Germany).

Table 3: List of oligonucleotides used for Southern probe generation

Probe name	Primer name	Sequence (5'-3')
probe B	IL-6R_S_Probe_fwd	TTG TAG TCT CCA CCC ACA AGC C
	IL-6R_S_Probe_rev	AGC GAG CAA CCT CAG ACT CAG A

2.3.4 Polymerase chain reaction (PCR)

To genotype mice for the presence of loxP flanked exons or Cre transgenes, the PCR (162, 163) method was used, either performed in a Thermocycler iCycler PCR machine (BioRad, München, Germany) or in a Peltier Therman Cycler PTC-200 (MJ Research, Waltham, USA). The total reaction volume of each PCR was 25 µl, containing a minimum of 50 ng DNA template, 25 pmol of each customized oligo (Table 4), 25 µM dNTP mix, 1 x polymerase buffer

and 1 U of polymerase. A standard PCR program started with 5 min of denaturation at 95°C, followed by 35 - 40 cycles, consisting of denaturation at 95°C for 45 sec, annealing at the oligonucleotide-specific temperature for 30 sec and elongation for 30 sec at 72°C. A final elongation step at 72°C for 7 min was added at the end.

Table 4: List of oligonucleotides used for PCR

Name	Sequence	T _{Annealing} [°C]	Orientation
5GK12	CCG CGG GCG ATC GCC TAG G	55°C	sense
5IL6Ex3	CCA GAG GAG CCC AAG CTC TC	55°C	antisense
3IL6A	TAG GGC CCA GTT CCT TTA T	55°C	antisense
MyD88 1	GGG AAT AAT GGC AGT CCT CTC CCA G	55°C	sense
MyD88 2	GGA TCA TCT CCT GCA CAA ACT CG	55°C	antisense
MyD88 Del	CAG TCT CAT CTT CCC CTC TGC C	55°C	antisense

2.3.5 RNA extraction

To isolate total RNA, snap-frozen tissues were thawed and homogenized in 1 ml TriFast reagent using a polytron homogenizer. After a 5 min incubation step at RT, the homogenate was centrifuged for 10 min at 4°C and the supernatant was transferred into a new vial. A following phenol-chloroform extraction and precipitation with isopropanol were performed according to the manufacturers instruction of the TriFast reagent. The treatment with RNase-free DNase was necessary, when exon-spanning probes were not available. The RNA concentration was analyzed using a NanoDrop ND-1000 UV-Vis spectrophotometer (Pepqab, Erlangen, Germany) and diluted to an final concentration of 400 ng/µl.

2.3.6 Quantitative real-time PCR

For the quantitative real-time PCR analysis, 4 µg of each RNA sample was reversely transcribed using the Eurogentec RT Kit (Eurogentec, Cologne, Germany) according to manufacturer's instructions. The resulted cDNA was subsequently amplified using TaqMan® Universal PCR-Master Mix, NO AmpErase UNG with the specific TaqManR Assay on demand kits (Applied Biosystems, Foster City, USA) (Table 5). The quantitative RT-PCR was performed on an ABI-PRISM 7700 Sequence Detector (Applied Biosystems, Foster City, USA) and were linear over 4 orders of magnitude.

Table 5: List of Taqman gene expression assays

Gene name	Order name	Order number
Bcl-2-associated X protein (Bax)	Bax	Mm00432050_m1
B-cell lymphoma 2 (Bcl-2)	Bcl2	Mm00477631_m1
Bcl-2-like protein 11 (Bim)	Bcl2l11	Mm00437795_m1
Cluster of differentiation 68 (CD-68)	CD68	Mm03047340_m1
DNA damage-inducible transcript 3 (CHOP)	Ddit3	Mm00492097_m1
Egf-like module containing, mucin-like, hormone receptor-like 1 (F4/80)	Emr1	Mm00802530_m1
Glucose-6-phosphatase (G6Pase)	G6pc	Mm00839363_m1
Glucokinase (GK)	Gck	Mm00439129_m1
Interleukin 10 (IL-10)	Il10	Mm00439616_m1
Interleukin 6 (IL-6)	Il6	Mm00446190_m1
Interleukin 6 receptor, alpha (IL-6R α)	il6ra	Mm00439649_m1
Integrin alpha M (Itgam)	Itgam	Mm00434455_m1
Integrin alpha X (Itgax)	Itgax	Mm00498698_m1
Leukemia inhibitory factor (LIF)	Lif	Mm00434761_m1

Lectin, galactose binding, soluble 3 (MAC-2)	Lgals3	Mm00802901_m1
Chemokine (C-C motif) ligand 2 (MCP-1)	CCL2	Mm00441242_m1
Chemokine (C-C motif) ligand 7 (MCP-3)	CCL7	Mm00443113_m1
Chemokine (C-C motif) ligand 3 (MIP-1 α)	CCL3	Mm00441258_m1
Chemokine (C-C motif) ligand 4 (MIP-1 β)	CCL4	Mm00443111_m1
Myeloid differentiation primary response gene 88 (MyD88)	Myd88	Mm01351743_g1
Chemokine (C-C motif) ligand 5 (RANTES)	CCL5	Mm01302428_m1
Tumor necrosis factor alpha (TNF- α)	TNFalpha	Mm00443258_m1
Tumor necrosis factor receptor 1 (TNFR1)	Tnfrsf1b	Mm00441889_m1

The relative expression of genes was adjusted for total RNA content by glucuronidase β (GUSB) and hypoxanthine guanine phosphoribosyl transferase 1 (HPRT-1) mRNA quantitative real-time PCR. Calculations were performed by a comparative method ($2^{-(\Delta\Delta CT)}$). In brief, the amplification plot is the plot of fluorescence versus PCR number. The threshold cycle value (ct) is the fractional PCR cycle number at which the fluorescent signal reached the detection threshold. Therefore, the input cDNA copy number and ct are inversely related. Data were analyzed with the Sequence Detector System (SDS) software version 2.1 (ABI) and ct value was automatically converted to fold change RQ value ($(RQ) = 2^{-(\Delta\Delta CT)}$). The RQ values from each gene were then used to compare the gene expression across all groups.

2.4 Biochemistry

2.4.1 Protein extraction

For generation of tissue protein lysates, snap-frozen tissues were homogenized in 1 ml tissue lysis buffer (50 mM HEPES (pH 7.4), 1% (v/v) Triton X-100, 0.1 M NaF, 10 mM EDTA, 50 mM NaCl, 10 mM sodium orthovanadate, 0,1% (w/v) SDS, 10 µg/ml aprotinin, 2 mM benzamidine, 2 mM phenylmethylsulfonyl fluoride (PMSF)), using a polytron homogenizer (IKA Werke, Staufen, Germany). The tissue extracts were then centrifuged 1 h at 4°C to separate supernatant from cell debris and the protein concentration of the cleared supernatant was determined using a Bradford assay. A final concentration of 10 µg/µl in 1 x SDS loading buffer (62,5 mM Tris-HCl (pH 6.8), 2% (w/v) SDS, 10% (w/v) glycerol, 50 mM DTT, and 0.01% (v/v) bromophenol blue) was then used for the following Western blot analysis. Before loading of samples onto a Western blot gel, protein solutions were boiled at 95°C for 5 min in order to denature proteins.

To generate nuclear protein extracts from liver, the liver tissue was carefully homogenised in hypotonic solution (10 mM HEPES [pH 7.6], 10 mM KCl, 2 mM MgCl₂, 0.1 mM EDTA, supplemented with complete mini protease inhibitor cocktail tablets) and incubated on ice for 10 min. NP-40 was added to 1% (v/v), incubated for 5 min at 4°C and subsequent centrifugation (13000 rpm) for 1 min at 4°C. After removing the cytoplasmic fraction, the nuclear pellet was washed in hypotonic buffer and resuspended in high salt buffer (20 mM HEPES [pH 7.9], 420 mM NaCl, 1.5 mM MgCl₂, 0.5 mM DTT, 0.2 mM EDTA, 10% (v/v) glycerol, completed with protease inhibitor cocktail). After additional incubation for 30 min on ice and centrifugation at 4°C for at least 1 h, the nuclear protein fraction was transferred into a new vial, diluted to 4 µg/µl and stored at -80°C. If needed, the nuclear extracts were thawed on ice and used for the experiment.

2.4.2 Western blot analysis

The protein samples were separated on 10 – 15% (v/v) SDS polyacrylamide gels and blotted onto PVDF membranes (Bio-Rad, München, Germany). The membranes were then blocked with 10% (v/v) blocking reagent for 2 h at RT. Subsequently, primary antibodies (Table 6) diluted in 5% (v/v) blocking reagent were applied overnight at 4°C. After 5 x washing with 1 x TBS / 0.1% (v/v) Tween 20 for 5 min each, the respective secondary antibody was applied for 1 h at RT, followed by additional 5 x washing. The membranes were then incubated for 1 min in Pierce ECL Western Blocking Substrate and exposed to chemiluminescence films (Amersham, Braunschweig, Germany). Films were developed in an automatic developer (Kodak, Germany).

Table 6: List of primary antibodies used for Western blot analysis

Name	Order number	Distributor	Dilution
AKT	#4685	Cell signaling (Danvers, MA, USA)	1:1000
Beta actin	ab8227	Abcam (Cambridge, UK)	1:5000
Calnexin	208880	Calbiochem (Darmstadt, Germany)	1:5000
ERK1/2	#9102	Cell signaling (Danvers, MA, USA)	1:1000
G6Pase	sc-25840	Santa Cruz (Heidelberg, Germany)	1:500
I κ B α	#4812	Cell signaling (Danvers, MA, USA)	1:1000
MyD88	Ab2064	Abcam (Cambridge, UK)	1:1000
p38	#9212	Cell signaling (Danvers, MA, USA)	1:1000
p65	sc-372	Santa Cruz (Heidelberg, Germany)	1:1000
Phospho-AKT (Ser473)	#4060	Cell signaling (Danvers, MA, USA)	1:1000
Phospho-p65 (Ser536)	#3033	Cell signaling (Danvers, MA, USA)	1:1000
Phospho-ERK1/2 (Thr202/Tyr204)	#4377	Cell signaling (Danvers, MA, USA)	1:1000
Phospho-I κ B α (Ser32)	#2859	Cell signaling (Danvers, MA, USA)	1:1000

Phospho-p38 (Thr180/Tyr182)	#9215	Cell signaling (Danvers, MA, USA)	1:1000
Phospho-SAPK/JNK (Thr183/Tyr185)	#4668	Cell signaling (Danvers, MA, USA)	1:1000
Phospho-STAT-3 (Tyr705)	#9145	Cell signaling (Danvers, MA, USA)	1:1000
SAPK/JNK	#9258	Cell signaling (Danvers, MA, USA)	1:1000

2.4.3 Electrophoretic mobility shift assay (EMSA)

For the EMSA, 100 ng of EMSA probe DNA (Table 7) was radioactively end-labelled in a 25 µl reaction mix containing 2.5 µCi γ -³²P-dATP and 25 U T4 polynucleotide kinase. After 10 min incubation at 37°C the probe was purified from nonincorporated nucleotides with MicroSpin™ G-20 columns (GE Healthcare, Munich, Germany) according to manufacturer's guidelines. The binding reaction was performed by incubating 4 µg of nuclear protein extracts with 0.5 ng of ³²P-labelled probe and 2 µg poly(dI-dC) for 30 min at RT and stopped by adding 2 µl of tracking dye (0.25% bromphenol blue, 0.25% xylene cyanol and 30% Glycerol). The following electrophoresis was performed as previously described (164).

Table 7: EMSA probes

Name	Order number	Sequence	Distributor
SP-1	#sc-2502	ATT CGA TCG GGG CGG GGC GAG C	Santa Cruz (Heidelberg, Germany)
STAT-3	#sc-2571	GAT CCT TCT GGG AAT TCC TAG ATC	Santa Cruz (Heidelberg, Germany)

2.4.4 Enzyme-linked immunosorbent assay (ELISA)

To determine the concentrations of sIL-6R α , leptin and insulin in the serum, the specific ELISA Kits (Table 8) were used according to the manufacturer's guidelines. The measurements were done on a Precision Microplate Reader (Emax; Molecular Devices GmbH).

Table 8: List of ELISA kits

Name	Order number	Distributor
Mouse IL-6 sR ELISA	#DY1830	R&D systems (Wiesbaden, Germany)
Mouse leptin ELISA	#90030	Crystal Chem. (Downers Grove, IL, USA)
Rat/Mouse insulin ELISA	#INSKR020	Crystal Chem. (Downers Grove, IL, USA)

2.4.5 Histological analysis and immunohistochemistry

2.4.5.1 Immunohistochemistry

For immunohistochemistry, the tissues were embedded in tissue freezing medium directly after dissection. If needed, the tissues were sectioned on a cryostat and stained as indicated. The cryostat sections of liver and pancreatic tissue were stained with hematoxylin and eosin (H&E) for general histology and to visualize morphological changes. The Kupffer cells were stained on cryostat sections of liver tissue using MAC-2/Galectin-3 antibody (#CL8942AP; Cedarlane Laboratories Ltd, Burlington, ON, Canada). For the acquisition of digital images, the stained sections were viewed under a Zeiss Axioskop equipped with a Zeiss AxioCam using the Spot Advanced 3.0.3 software (Carl Zeiss MicroImaging GmbH, Oberkochen).

2.5 Computer analysis

2.5.1 Densitometrical analysis

Protein content of Western blots was analyzed densitometrically by measuring the pixel density per mm² using either ImageJ (National Institutes of Health, Bethesda, USA) or Quantity one software (Biorad). After subtracting the background and normalizing to an internal loading control, the relative density of control animals were set to 100% and compared to the relative density of indicated animals.

2.5.2 Quantitation of pancreatic islet mass

Quantitation of average pancreatic islet mass was determined on serial sections of pancreata stained with H&E. For the acquisition of digital images, the stained sections were viewed under a Zeiss Axioskop equipped with a Zeiss AxioCam using the Spot Advanced 3.0.3 software (Carl Zeiss MicroImaging GmbH, Oberkochen). The Quantification of pancreatic islet size was performed using AxioVision 4.2 (Carl Zeiss MicroImaging GmbH, Oberkochen, Germany).

2.5.3 Statistical methods

All data sets were analyzed by using a two-tailed unpaired student's t test for statistical significance. All *p* values below 0.05 were considered as statistical significant. All displayed values are means ± SEM. * *p* = 0.05; ** *p* = 0.01; *** *p* = 0.001 versus controls.

3. Results

3.1 The effect of hepatic IL-6R α signal transduction on glucose homeostasis

Obesity is a state of chronic, low-grade inflammation, characterized by elevated plasma concentrations of inflammation-associated factors, such as interleukin-6 (IL-6) and interleukin-1 β (IL-1 β), which in turn may contribute to the development of insulin resistance (65-68). The function of IL-6 signaling in the context of promoting insulin resistance under obesity is controversially discussed (77).

3.1.1 Generation of hepatocyte specific IL-6R α knock out mice

To address the role of inflammatory signaling downstream of the IL-6R α in hepatocytes on insulin action and glucose homeostasis *in vivo*, we generated mice lacking the IL-6R α selectively in hepatocytes (IL-6R α ^{L-KO}). Therefore we crossed mice expressing the Cre recombinase under the control of the ALFP-promotor (165) with mice harbouring the loxP-flanked IL-6R α gene (Fig. 9 A) and further intercrossing of siblings yielded IL-6R α ^{L-KO} mice. The littermates lacking expression of Cre recombinase (IL-6R α ^{FL/FL}) served as controls throughout the experiments.

To determine the specificity and efficiency of the deletion of loxP-flanked exons 2 and 3 of the IL-6R α gene, we performed Southern blot analysis on genomic DNA isolated from liver, WAT, skeletal muscle and tails of IL-6R α ^{L-KO} and control mice. While the 9kb loxP-flanked band was detectable in all analyzed tissues of both groups, only the liver of IL-6R α ^{L-KO} showed the 6.3kb deleted allele of the IL-6R α gene. This analysis revealed that the expression of the Cre recombinase under the control of the ALFP-promotor efficiently excised the loxP-flanked exons 2 and 3 of the IL-6R α gene exclusively in the liver of IL-6R α ^{L-KO} mice (Fig. 9 B).

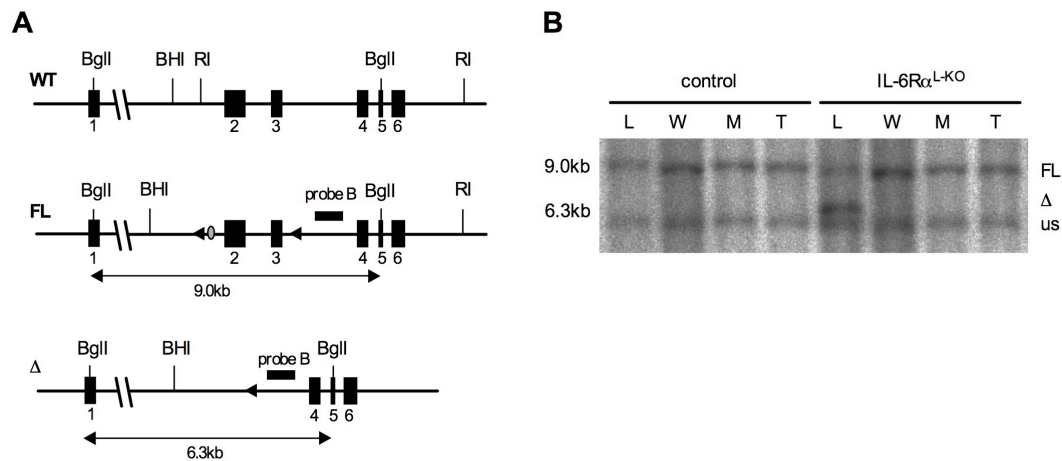


Fig. 9: Targeting strategy and confirmation of the IL-6R α ^{FL/FL} allele

(A) Targeting strategy for the generation of the conditional IL-6R α allele. Upper lane shows the wildtype (WT) IL-6R α gene comprising exons 2, 3, 4, 5, and 6. The loxP-flanked exons 2 and 3 of the IL-6R α allele (FL) are shown in the middle lane and the Cre loxP mediated excision of these exons is shown at the bottom (Δ). (B) Southern blot analysis of the FL and Δ allele on BglII-digested DNA from liver (L), WAT (W), skeletal muscle (M) and tail (T) of control and IL-6R α ^{L-KO} mice using probe B.

Additionally, we performed quantitative RT-PCR for IL-6R α mRNA expression using mRNA isolated from liver tissues. As shown in Figure 10 A, the expression of IL-6R α mRNA was completely blunted in IL-6R α ^{L-KO} mice compared to control animals, implying an efficient reduction of IL-6R α mRNA in hepatocytes.

Besides the classical IL-6 signaling that is restricted to those cell types expressing the membrane bound form of the IL-6R α , another mechanism termed IL-6 trans-signaling exists that uses a soluble form of the IL-6R α to ensure IL-6 signaling in cells, which do not express the membrane bound form of the IL-6R α (166). To ascertain whether the loss of IL-6R α expression in the liver results in decreased levels of circulating sIL-6R α , serum levels for sIL-6R α from IL-6R α ^{L-KO} and control mice were determined by ELISA (Fig. 10 B). As the levels of circulating sIL-6R α were similar, the results indicated that the specific inactivation of the IL-6R α in hepatocytes does not affect the amount of circulating sIL-6R α concentrations.

Moreover, the lack of hepatic IL-6R α expression was unable to affect liver weight as well as histomorphological liver structure, shown by H&E staining of liver sections (Fig. 10 D and E).

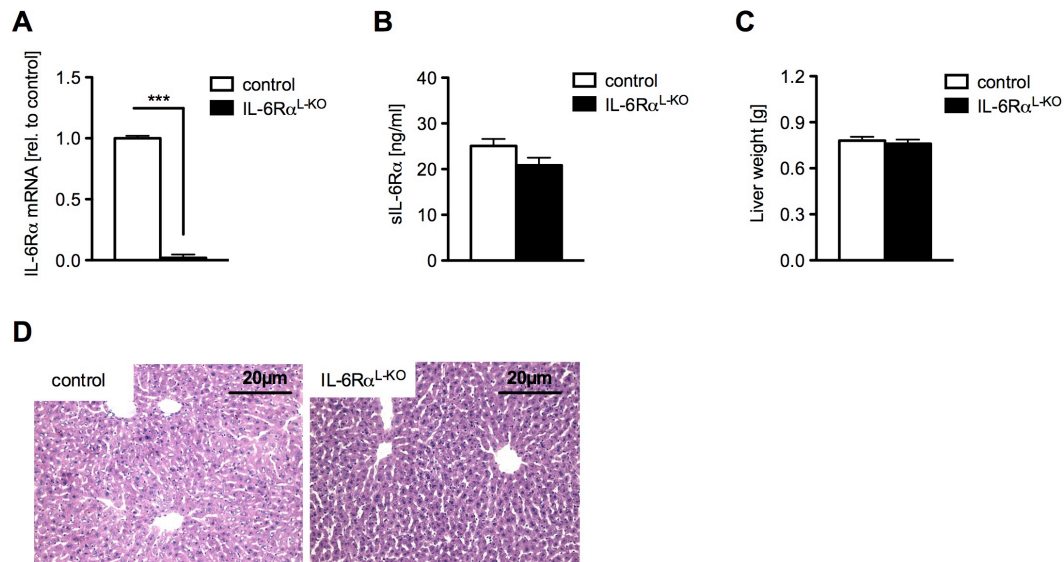


Fig. 10: Liver specific ablation of the IL-6R α gene

(A) Relative mRNA expression in livers of IL-6R α ^{L-KO} and control mice measured by quantitative RT-PCR (n=6/genotype). (B) Amount of circulating sIL-6R α concentrations in the blood serum of 8 weeks old mice, measured by ELISA (n=10/genotype). (C) Liver weight of IL-6R α ^{L-KO} and control mice at week 20 (n=8-10/genotype). (D) Histomorphological liver structure, analyzed by H&E staining of liver sections from IL-6R α ^{L-KO} and control mice. Data are displayed as means \pm SEM. *** p \leq 0.001 versus controls

Taken together, these experiments demonstrate that the IL-6R α ^{L-KO} mouse lacks the IL-6R α specific in hepatocytes without affecting liver morphology and can be used as a reliable tool to analyze the hepatocyte specific role of the IL-6 signaling in glucose homeostasis.

3.1.2 IL-6R α ^{L-KO} mice exhibit unaltered energy homeostasis

The role of IL-6 signaling in energy homeostasis, obesity and insulin resistance is not clear yet and remains controversially debated. Some studies could show, that conventional ablation of IL-6 signaling in mice leads to mature onset obesity (167). Nevertheless, the responsible tissue, which contributes to the development of obesity, remained unidentified.

To investigate the role of hepatic IL-6 signaling on energy homeostasis, we analyzed body weight, epigonadal fat pad mass and body fat content in IL-6R α ^{L-KO} and control mice (Fig. 11). The weight gain in response to normal chow diet (NCD) feeding from week 3 to week 19 of age (Fig. 11 A), as well as at week 20 of age (Fig. 11 B), was unaltered between IL-6R α ^{L-KO} and control mice. Consistently with the unaltered weight gain, epigonadal fat pad mass and body fat was indistinguishable between IL-6R α ^{L-KO} and control mice (Fig. 11 C).

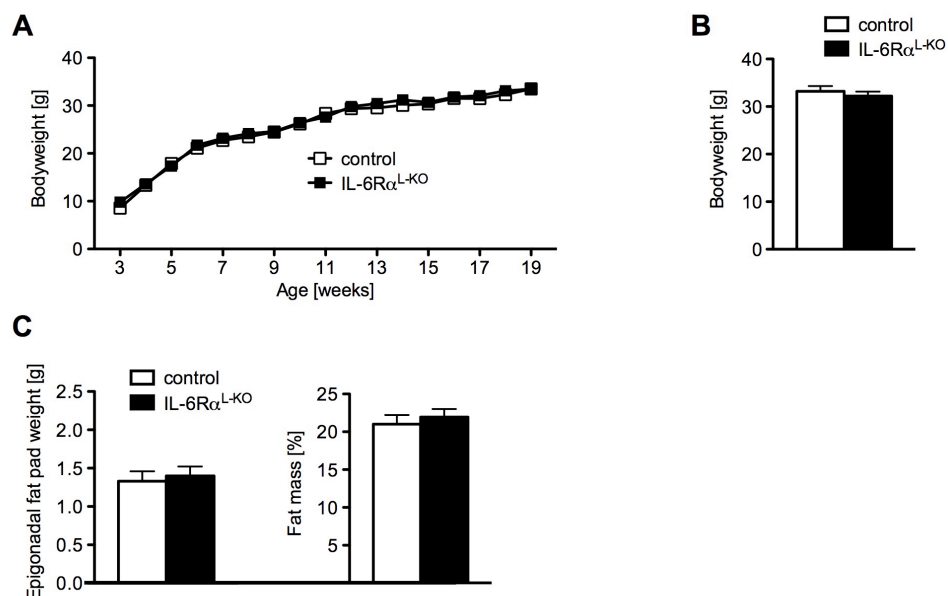


Fig. 11: IL-6R α ^{L-KO} mice show unaltered adiposity

(A) Average bodyweight was monitored from week 3 to week 19 of IL-6R α ^{L-KO} and control mice (n=12-16/genotype). (B) Average bodyweight at week 20 from both groups (n=12-16/genotype). (C) Epigonadal fat pad mass and total body fat content of IL-6R α ^{L-KO} and control mice at week 20. Body fat content was determined by using nuclear magnetic resonance (n=12-16/genotype). Displayed values are means \pm SEM.

Moreover, the circulating leptin levels were comparable between both groups indicating similar adiposity in the two groups of mice (Fig. 12 A). Similar adiposity was accompanied with equal food consumption of IL-6R α ^{L-KO} and control mice (Fig. 12 B). Additionally, energy expenditure was determined by indirect calorimetry using the PhenoMaster system. However, the analysis revealed no obvious alterations in O₂ consumption and CO₂ production between the groups (Fig. 12 C and D).

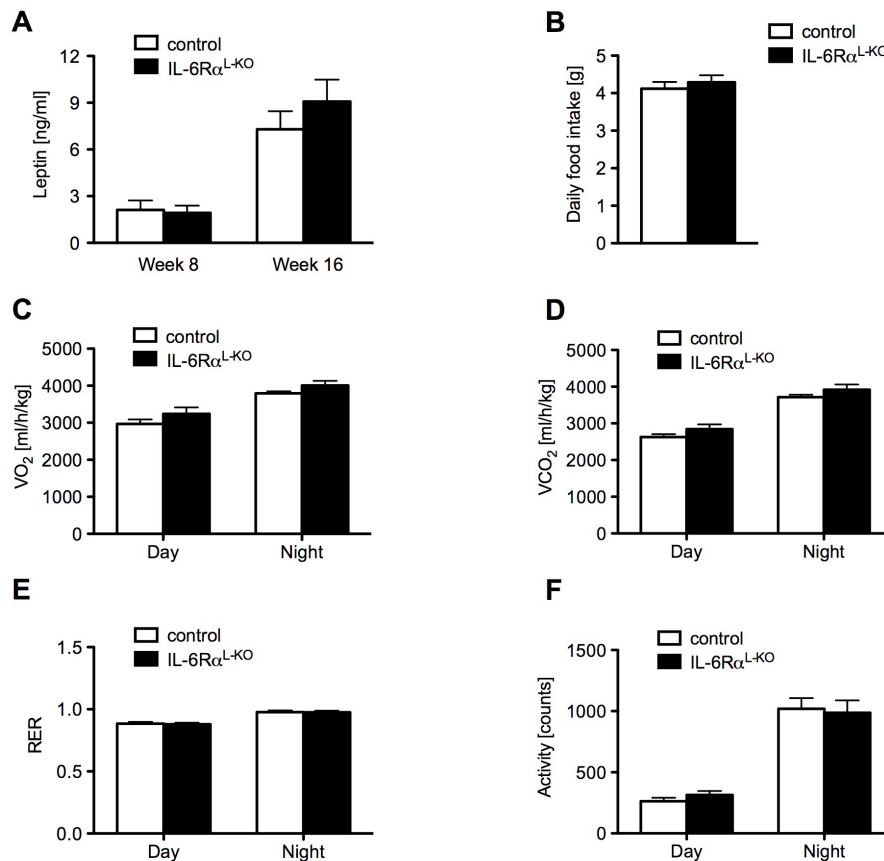


Fig. 12: Unchanged energy homeostasis in mice lacking hepatic IL-6R α signaling

(A) Amount of circulating leptin concentrations in the blood serum of 8 and 16 weeks old mice, measured by ELISA ($n=10$ /genotype). (B) Average daily food intake over 48 h of 10 weeks old IL-6R α ^{L-KO} and control mice ($n=7-9$ /genotype). (C-F) Daily and nightly (C) O₂ consumption, (D) CO₂ production, (E) respiratory exchange ratio and (F) locomotor activity of IL-6R α ^{L-KO} and control mice at 10 weeks of age. VO₂, VCO₂ and locomotor activity were determined in chambers of the PhenoMaster System by indirect calorimetry ($n=7-9$ /genotype). Displayed values are means \pm SEM.

In addition, the respiratory exchange ratio (RER), an indicator for the preferred metabolic source of energy, lipids or carbohydrates, remained unaltered between IL-6R α ^{L-KO} and control mice, indicating that both genotypes utilized the same substrates for oxidative metabolism (Fig. 12 E). To determine whether the deletion of IL-6R α in hepatocytes impacts on locomotor activity, basal locomotor activity of IL-6R α ^{L-KO} and control mice was determined. At week 10 of age, no obvious difference in locomotor activity was observed in IL-6R α ^{L-KO} mice compared to control mice (Fig. 12 F).

In summary, the lack of hepatic IL-6R α signaling, does not affect weight gain, adiposity and energy homeostasis.

3.1.3 IL-6R α ^{L-KO} mice exhibit impaired glucose homeostasis and insulin sensitivity

Given the observation that systemic IL-6 concentrations are elevated in obesity and in patients suffering from type-2-diabetes (168), it was generally assumed that IL-6 somehow contributes to the development of insulin resistance and impaired glucose homeostasis (169). Additionally it has been shown that IL-6 inhibits insulin signaling *ex vivo* in mouse derived hepatocytes by inhibiting IRS-1 phosphorylation, mediated by induction of the IL-6 target gene SOCS-3 (81). To study the role of hepatic IL-6 signaling in glucose homeostasis, we first assessed the glucose metabolism in IL-6R α ^{L-KO} and control mice. Therefore we measured blood glucose concentrations under fasted and random fed conditions. Normal chow diet feeding of control and IL-6R α ^{L-KO} mice exhibited normal blood glucose levels under fasting and random feeding conditions (Fig. 13 A). Furthermore, we investigated the glucose homeostasis by performing a glucose tolerance test (GTT) with both groups (Fig. 13 B). Although basal blood glucose concentrations were unaltered, the IL-6R α ^{L-KO} mice exhibited a significantly impaired tolerance to glucose during the GTT compared to control mice.

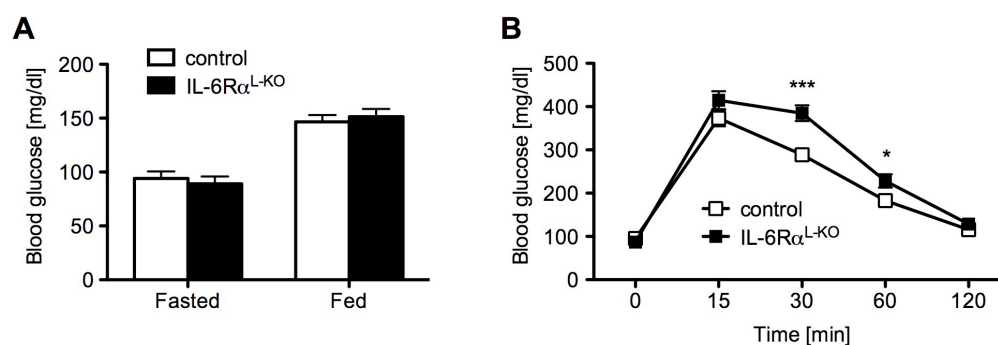


Fig. 13: IL-6R α ^{L-KO} mice exhibit decreased glucose tolerance

(A) Monitored blood glucose levels under fasted and random fed conditions of IL-6R α ^{L-KO} and control mice at 8 weeks of age (n=10-14/genotype). **(B)** Glucose tolerance test (GTT) monitored over 120 min of 11 weeks old IL-6R α ^{L-KO} and control mice (n=10-13/genotype). Displayed values are means \pm SEM. * p \leq 0.05; *** p \leq 0.001 versus controls

To differentiate whether this impaired glucose tolerance develops as a consequence of decreased glucose induced insulin secretion from β -cells upon glucose stimulation, we first determined the insulin release under glucose challenge as measured by the circulating levels of insulin during the GTT (Fig. 14 A).

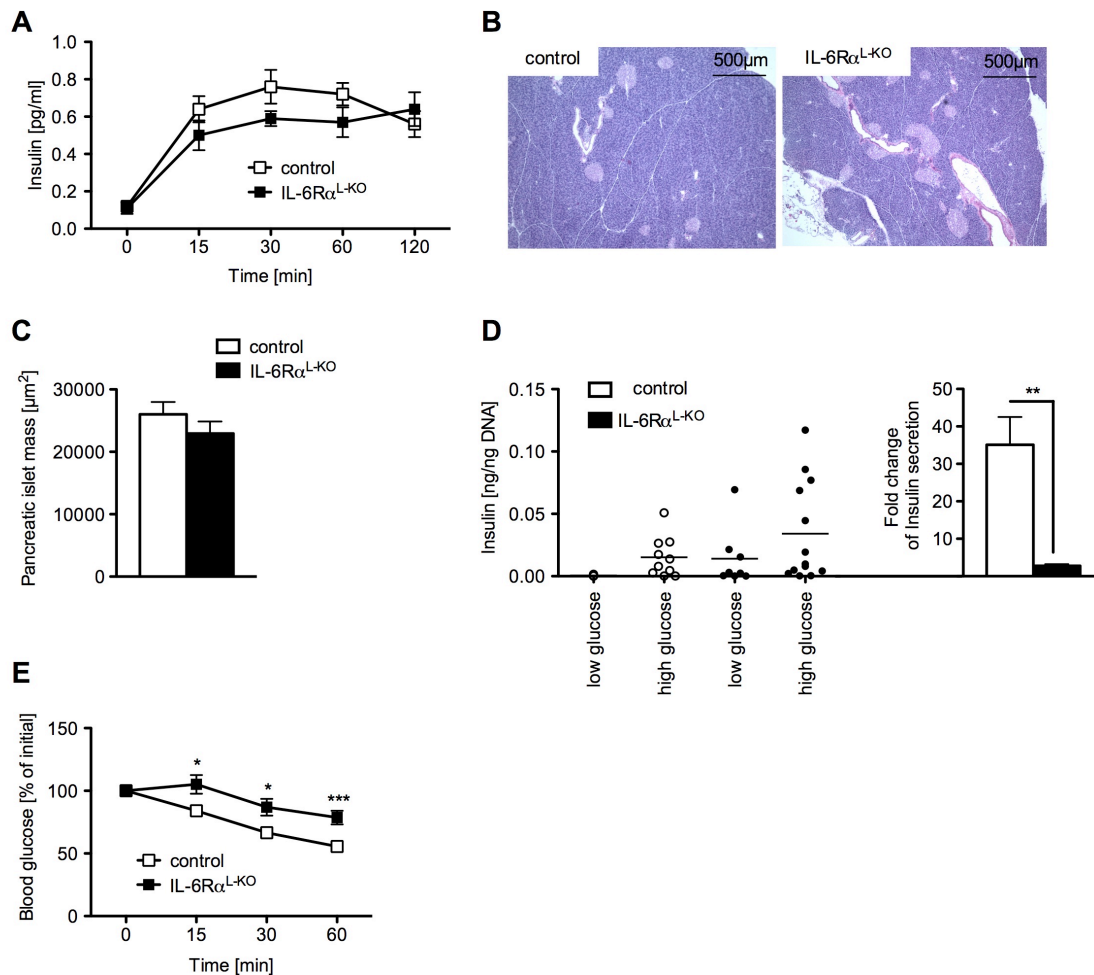


Fig. 14: Impaired insulin sensitivity in IL-6R α ^{L-KO} mice

(A) Measured insulin concentration in sera of IL-6R α ^{L-KO} and control mice during the glucose tolerance test by ELISA (n=9-13/genotype). **(B)** Histomorphological structure of pancreata, analyzed by H&E staining of pancreas sections from IL-6R α ^{L-KO} and control mice. **(C)** Average pancreatic islets mass, determined by analyzing H&E stained pancreas sections (n=8/genotype). **(D)** Scatter plot of glucose-stimulated insulin secretion (ng/ng DNA) of isolated islets from IL-6R α ^{L-KO} and control mice. Incubation of 6-9 islets at low (3 mM) or high glucose (11 mM) for 30 min was performed with different groups of batches. For measurements of low glucose, 6-8 batches (n=3-5/genotype) and for high glucose, 10-13 batches (n=5/genotype) were used. The fold change of insulin secretion after stimulation with high glucose is shown on the right. **(E)** Insulin tolerance test displayed over 60 min of 12 weeks old IL-6R α ^{L-KO} and control mice (n=10-13/genotype). Displayed values are means \pm SEM. * $p \leq 0.05$; ** $p \leq 0.01$; *** $p \leq 0.001$ versus controls

Additionally, pancreatic islet mass, β -cell function and the ability of insulin to lower blood glucose via insulin tolerance test (ITT) were investigated. Although the glucose stimulated insulin secretion during the GTT (Fig. 14 A) and the pancreatic islet mass (Fig. 14 B and C) were not significantly altered between control and IL-6R α ^{L-KO} mice, the IL-6R α ^{L-KO} mice exhibited compromised β -cell function and impaired insulin tolerance in ITTs. The β -cell function was determined *in vitro* in primary pancreatic islets, isolated from IL-6R α ^{L-KO} and control mice, by analyzing their ability of secreting insulin in response to glucose stimulation (Fig. 14 D). While isolated pancreatic islets of IL-6R α ^{L-KO} mice exhibit higher insulin secretion in response to low-glucose concentrations compared to islets of control mice, the ability to promote insulin secretion at high glucose concentrations was significantly decreased in islets of IL-6R α ^{L-KO} mice. Furthermore, consistent with the decreased tolerance to glucose during the GTT, the ability of insulin to lower blood glucose during the ITT was also significantly reduced (Fig. 14 E).

In summary, these experiments clearly demonstrated, that the lack of hepatic IL-6 signaling not only impairs the ability of β -cells to promote insulin secretion at high glucose concentrations, but also translates into the development of systemic insulin resistance and glucose intolerance.

3.1.4 IL-6R α ^{L-KO} mice exhibit counteracting actions on hepatic glucose metabolism

To determine the contribution of different insulin responsive tissues (e.g. liver, skeletal muscle and WAT), in altering insulin sensitivity and glucose homeostasis and thereby leading to the development of systemic insulin resistance, we performed euglycemic-hyperinsulinemic clamp studies in IL-6R α ^{L-KO} and control mice. In response to a constant infusion of insulin, resulting in hyperinsulinemia *in vivo* during the course of this study, a variable dose of glucose was infused to maintain euglycemia. Consistent with the impaired insulin sensitivity observed during the ITT, a decreased

responsiveness to insulin was also observed during this study. To achieve the comparable euglycemic state during the steady state phase of the experiment in both groups (Fig. 15 A), IL-6R α ^{L-KO} mice exhibited significantly reduced glucose infusion rate compared to control mice (Fig. 15 B). Consistent with these findings, the whole body glucose disposal rate was significantly reduced in IL-6R α ^{L-KO} compared to control mice during the steady state phase (Fig. 15 C). Since insulin maintains glucose homeostasis under conditions of high caloric intake by inhibiting hepatic glucose production (HGP), we investigated the HGP in IL-6R α ^{L-KO} and control mice during the euglycemic-hyperinsulinemic clamps. Although under the basal state the HGP remained elevated but unaltered between the two groups of animals, the ability of insulin to inhibit HGP was comparable between both groups during the steady state phase of the clamp study (Fig. 15 D).

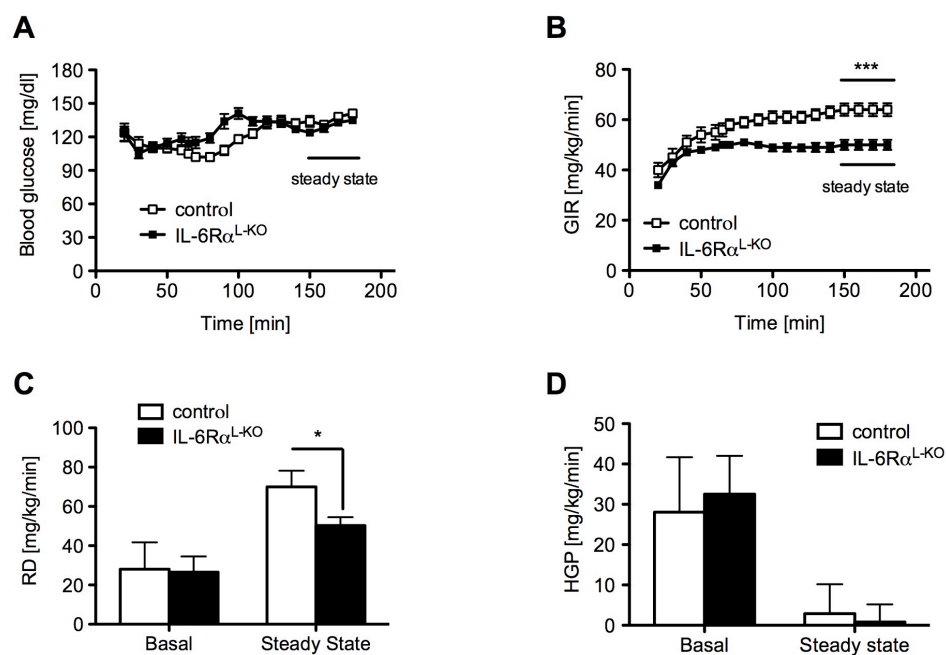


Fig. 15: Altered regulation of glucose homeostasis in IL-6R α ^{L-KO} mice

(A) Monitored blood glucose levels over 230 min during euglycemic-hyperinsulinemic clamp studies of IL-6R α ^{L-KO} and control mice (n=12/genotype). (B) Respective glucose infusion rate to maintain euglycemia during the euglycemic-hyperinsulinemic clamp study of IL-6R α ^{L-KO} and control mice (n=12/genotype). (C) Calculated glucose disposal rate during the basal and steady state phase of the clamp study (n=12/genotype). (D) Calculated HGP during the basal and steady state phase of the clamp study (n=12/genotype). Displayed values are means \pm SEM. * $p \leq 0.05$; *** $p \leq 0.001$ versus controls

To maintain stable and constant glucose homeostasis via HGP, two key metabolic pathways, gluconeogenesis and glycogenesis, play an essential role. Gluconeogenic key enzymes, e.g. G6Pase, had been reported to depend on hepatic IL-6 signaling (85). Therefore we determined hepatic G6Pase mRNA expression by quantitative RT-PCR and G6Pase protein level in the liver from control and IL-6R α ^{L-KO} mice by Western blot analysis during basal and steady state phase of the euglycemic-hyperinsulinemic clamp studies.

In consistency with the significant suppression of HGP during the steady state phase compared to the basal phase in both groups of animals, relative mRNA expression of G6Pase was also significantly reduced. Interestingly, the relative G6Pase mRNA expression during the steady state phase was significantly higher in IL-6R α ^{L-KO} mice compared to control mice (Fig. 16 A). In line with this observation, the protein level of G6Pase was also increased in the liver of IL-6R α ^{L-KO} mice compared to control mice during the steady state phase (Fig. 16 B). To sum up, these findings reveal a functional role of hepatic IL-6 signaling in the insulin-mediated suppression of G6Pase and thereby indicate the presence of a partial insulin resistance in the liver of IL-6R α ^{L-KO} mice.

A key enzyme in the process of glycogenesis and glycolysis is the phosphorylation of glucose by the glucokinase (GK). Thereby glucose is converted to glucose-6-phosphate, which then enters the glycogenesis or the glycolysis pathway. To investigate whether hepatic IL-6 signaling plays a role in regulating glycogen synthesis through glucokinase in the liver, we decided to determine the mRNA expression of GK in the liver of control and IL-6R α ^{L-KO} mice by quantitative RT-PCR. Although insulin increased the mRNA expression of GK during the steady state phase compared to basal state in control mice, this elevation was significantly enhanced in IL-6R α ^{L-KO} mice compared to control mice (Fig. 16 C). To further address the effect of increased GK mRNA expression and decreased G6Pase suppression in IL-6R α ^{L-KO} mice on glycogen storage in the liver, we analyzed the hepatic

glycogen content of both groups. Thus, glycogen was extracted and measured from livers of mice after a 16h fasting period as well as at the end of the steady state phase during the euglycemic-hyperinsulinemic clamp study.

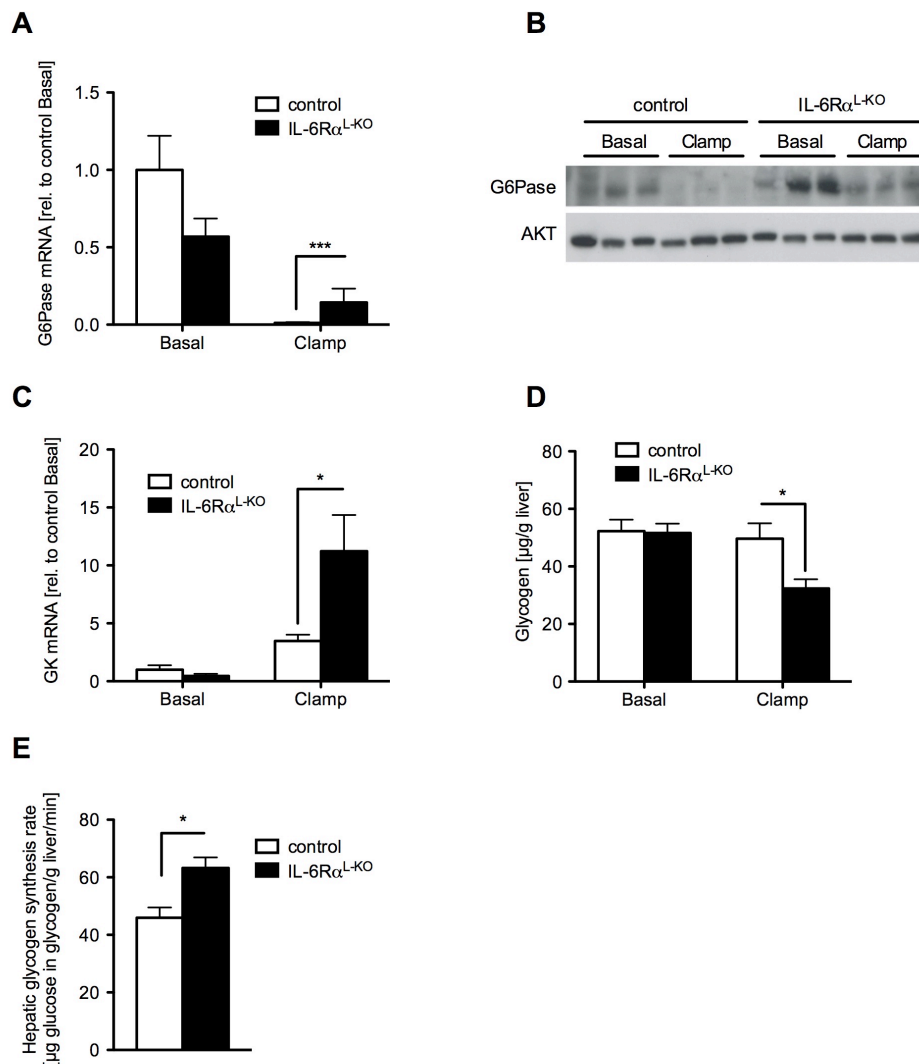


Fig. 16: Counteracting actions on hepatic glucose metabolism in IL-6R α ^{L-KO} mice

(A) Relative mRNA expression in livers of IL-6R α ^{L-KO} and control mice during basal and steady state phase of the clamp study (n=6/genotype). **(B)** Western blot analysis of liver lysates from indicated mice at both conditions by using G6Pase and AKT antibody. **(C)** Relative expression of GK mRNA in livers of both groups during basal and steady state phase (n=6/genotype). **(D)** Hepatic glycogen content, measured by using colorimetric glucose determination after enzymatic breakdown of glycogen into glucose (n=12/genotype). **(E)** Hepatic glycogen synthesis rate of IL-6R α ^{L-KO} and control mice was examined by ³H-glucose incorporation into glycogen at the end steady state phase of the clamp study (n=12/genotype). Displayed values are means \pm SEM. * p \leq 0.05; *** p \leq 0.001 versus controls.

While the glycogen content seemed unaffected between both conditions in control mice, the amount of glycogen during the steady state phase in mice lacking the hepatic IL-6R α was significantly reduced (Fig. 16 D). To investigate whether this was an effect of reduced hepatic glycogen synthesis, we additionally determined the hepatic glycogen synthesis rate of IL-6R α ^{L-KO} and control mice during the steady state phase. To this end, we measured the ³H-glucose incorporation into glycogen. Importantly, this analysis indicated a significant elevated glycogen synthesis rate in IL-6R α ^{L-KO} mice compared to control mice (Fig. 16 E). Thus, these data indicate impairment in the insulin-induced suppression of glycogenolysis in IL-6R α ^{L-KO} mice.

Collectively, these findings support the assumption, that hepatic IL-6 signaling has counteracting actions on glucose metabolism in the liver; on one hand by suppressing G6Pase, which is required for gluconeogenesis and on the other hand by increasing GK, which is required for glycogen synthesis. Nevertheless, the disruption of hepatic IL-6 signaling has no dramatic effect on glucose homeostasis in the liver and seemed largely balanced.

3.1.5 Mice lacking hepatic IL-6 signaling exhibit insulin resistance in skeletal muscle and WAT

One of the major molecular components of the activated insulin signaling is the phosphorylation of AKT at Ser 473, resulting in AKT activation, thereby mediating insulin's effects on glucose homeostasis further downstream. To get an insight in the alterations of glucose homeostasis and to further support the assumption of hepatic insulin resistance in IL-6R α ^{L-KO} mice, we analyzed the ability of insulin to stimulate AKT phosphorylation at Ser residue 473. Therefore we compared the protein levels of phosphorylated AKT in livers of IL-6R α ^{L-KO} and control mice by Western blot analysis during the basal state as well as the steady state phase of the euglycemic-hyperinsulinemic clamp study. In agreement with the assumption of a partial hepatic insulin resistance, the insulin stimulated AKT phosphorylation during the steady state

phase was significantly reduced in IL-6R α ^{L-KO} mice compared to control mice (Fig. 17 A and B).

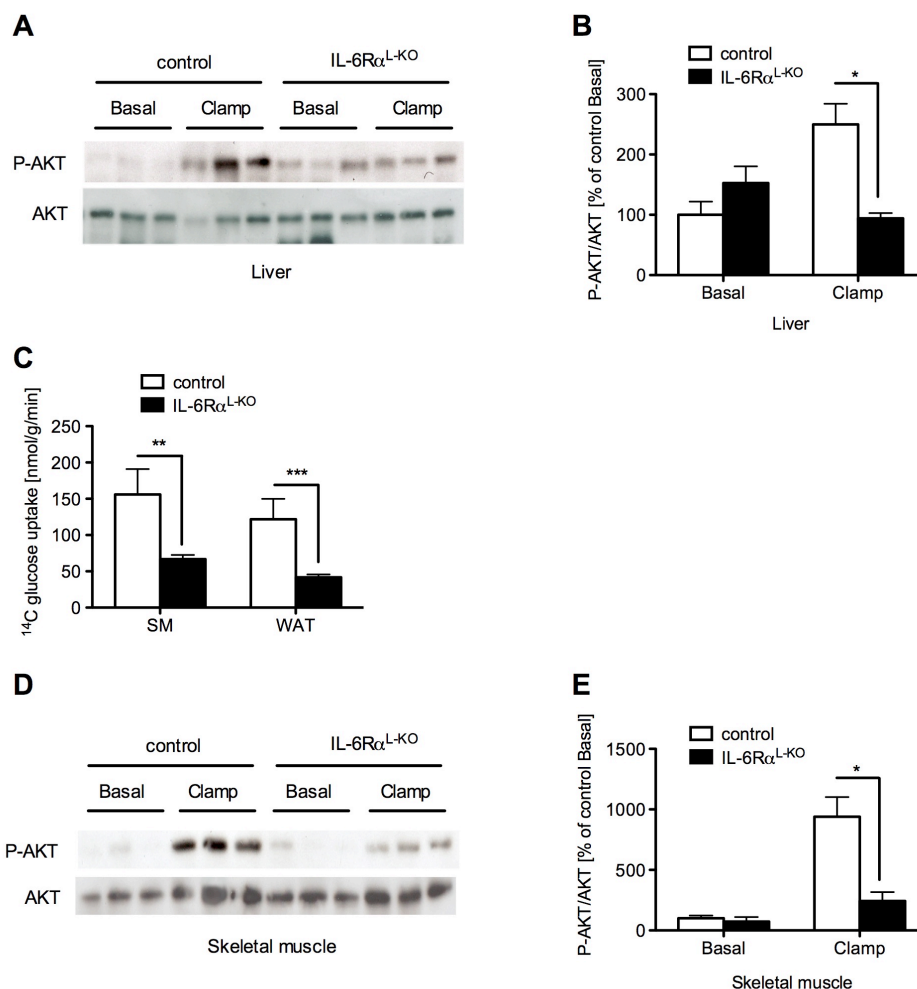


Fig. 17: Decreased insulin sensitivity in liver, skeletal muscle and WAT of IL-6R α ^{L-KO} mice

(A) Representative Western blot analysis of insulin-stimulated AKT phosphorylation in liver from indicated mice at basal and steady state condition by using P-AKT and AKT antibody. **(B)** Results of Western blot analysis from (A) by quantification of AKT phosphorylation relative to AKT (n=6/genotype). **(C)** Tissue specific ¹⁴C glucose uptake during euglycemic hyperinsulinemic clamp study of IL-6R α ^{L-KO} and control mice (n= 12/genotype). **(D)** Western blot analysis of skeletal muscle from indicated mice at basal and steady state condition by using P-AKT and AKT antibody. **(E)** Quantification of Western blot analysis from (D) under both conditions (n=6/genotype). Shown data are means \pm SEM. * p \leq 0.05; ** p \leq 0.01; *** p \leq 0.001 versus controls.

Other key insulin sensitive tissues, such as skeletal muscle and WAT are susceptible to develop local insulin resistance in the presence of increased caloric intake (170).

To elucidate the tissue specificity of insulin action and its contribution to the insulin resistance in IL-6R α ^{L-KO} mice, we additionally analyzed skeletal muscle and WAT for their insulin responsiveness. Strikingly, the insulin stimulated ¹⁴C-glucose uptake during the euglycemic-hyperinsulinemic clamp was significantly reduced in skeletal muscle and WAT of IL-6R α ^{L-KO} mice compared to control mice (Fig. 17 C), indicating the development of systemic insulin resistance in IL-6R α ^{L-KO} mice compared to control mice. Consistent with these data, the ability of insulin to stimulate AKT phosphorylation in skeletal muscle was significantly reduced in IL-6R α ^{L-KO} mice compared to control mice (Fig. 17 D and E).

Thus, the loss of hepatic IL-6 signaling has a moderate effect on the development of insulin resistance in the liver, but results in a pronounced impairment of insulin action in skeletal muscle and WAT.

3.1.6 Increased inflammatory tone in IL-6R α ^{L-KO} mice

Previous studies have revealed that an increased inflammatory tone, characterized by increased expression of inflammatory mediators, such as TNF- α and IL-6, correlates with the development of insulin resistance under obese conditions (60). To define the molecular basis of insulin resistance, both in liver and in skeletal muscle of IL-6R α ^{L-KO} mice, we next investigated the inflammatory tone in liver, skeletal muscle and WAT isolated from control and IL-6R α ^{L-KO} mice. Thus, the expression of key inflammatory cytokines IL-6, TNF- α , and the anti-inflammatory cytokine IL-10, were analyzed in liver and skeletal muscle isolated from control and IL-6R α ^{L-KO} mice at the basal and steady state phases of the euglycemic-hyperinsulinemic clamp study. While basal hepatic mRNA expression of IL-6, TNF- α , and IL-10 were comparable between both groups, the insulin-induced mRNA expression of IL-6, TNF- α , and IL-10 during the steady state phase of these genes was significantly increased in IL-6R α ^{L-KO} mice compared to control mice (Fig. 18 A). Additionally, the phosphorylation of inhibitor of NF- κ B (I κ B α) at Ser 32, which

is triggered by TNF- α stimulation, was clearly enhanced in livers of the IL-6R α ^{L-KO} mice compared to control mice during the steady state phase (Fig. 18 B and C). Nevertheless, phosphorylation of STAT-3 at Tyr residue 705, which is mediated by stimulation with IL-6, was induced to a similar extent in livers of both groups (Fig. 18 B and C), indicated overlapping mechanisms of STAT-3 activation in the absence of IL-6R α , presumably through IL-10 in response to *in vivo* insulin stimulation (Fig. 18 A).

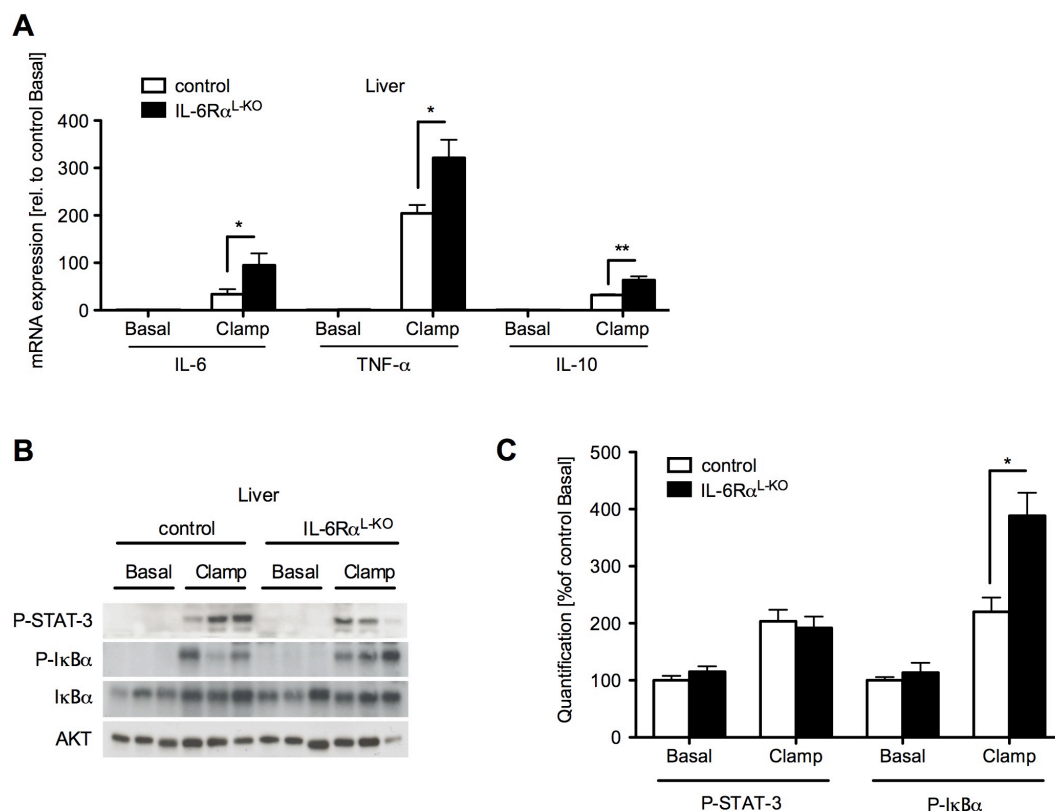


Fig. 18: Increased inflammation in livers of IL-6R α ^{L-KO} mice

(A) Relative mRNA expression in livers of IL-6R α ^{L-KO} and control mice during basal and steady state phase of the clamp study (n=6/genotype). (B) Representative Western blot analysis of STAT-3 and I κ B α activation in liver during basal and steady state condition by using the respective antibodies. (C) Quantification of Western blot analysis from (B) to determine STAT-3 and I κ B α activation relative to AKT and I κ B α under both conditions (n=6/genotype). Data represented as means \pm SEM. * p \leq 0.05; ** p \leq 0.01 versus controls.

Moreover, the mRNA expression of the inflammatory cytokines IL-6, TNF- α , and the anti-inflammatory cytokine IL-10, was also significantly enhanced in skeletal muscle of IL-6R α ^{L-KO} mice compared to control mice (Fig. 19 A). In consistency, increased TNF- α and IL-6 expression translates into the increased activation of I κ B α in skeletal muscle of IL-6R α ^{L-KO} mice compared

to control mice during the steady state phase of the clamp (Fig. 19 B and C). The activation of STAT-3, as determined by Tyr 705 phosphorylation, was similar in skeletal muscle of both genotypes (Fig. 19 B and C).

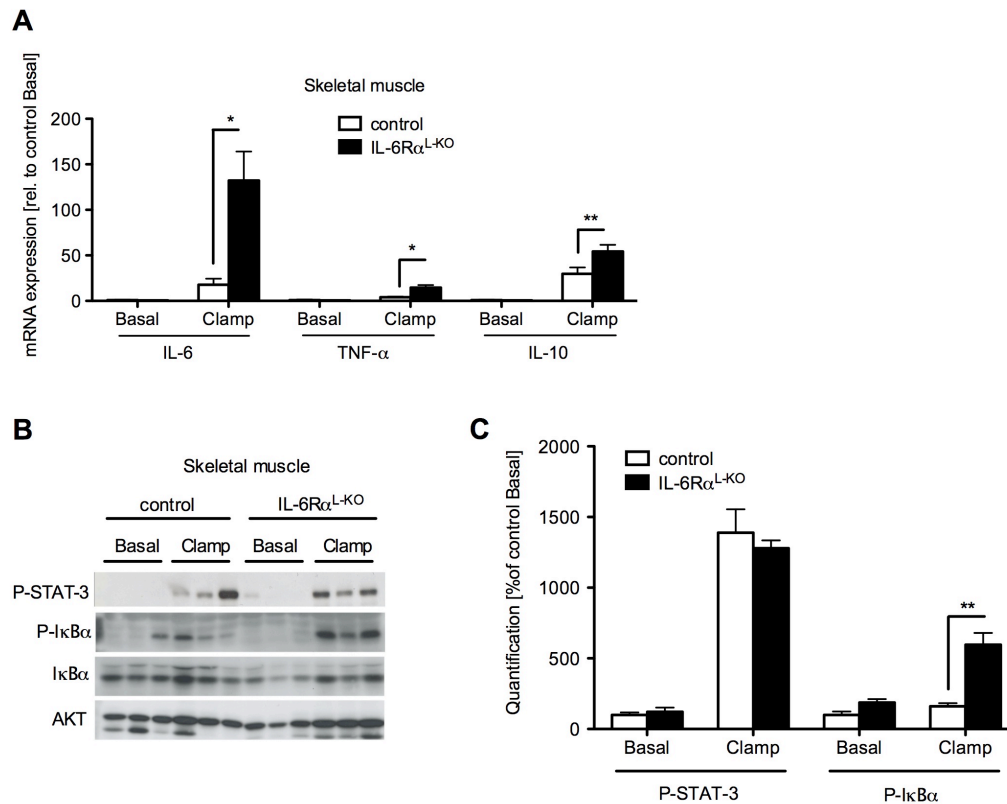


Fig. 19: IL-6R α ^{L-KO} mice exhibit elevated inflammatory state in skeletal muscle

(A) Relative mRNA expression of inflammatory genes in skeletal muscle of IL-6R α ^{L-KO} and control mice during basal and steady state phase of the clamp study (n=6/genotype). (B) Representative Western blot of STAT-3 and I κ B α phosphorylation in skeletal muscle during basal and steady state condition by using P-STAT-3, AKT, I κ B α and P-I κ B α antibodies. (C) Quantification of Western blot analysis from (B) to determine STAT-3 and I κ B α activation relative to AKT and I κ B α under both conditions (n=6/genotype). Displayed values are means \pm SEM. * p \leq 0.05; ** p \leq 0.01 versus controls.

Furthermore, the insulin-induced mRNA expression of IL-6, TNF- α and IL-10 was also significantly increased in WAT during the steady state phase compared to basal conditions in control and IL-6R α ^{L-KO} mice (Fig. 20 A). However, genotype specific differences were not observable.

To finally address whether the increased inflammatory cytokine expression in the respective tissues also translates into alterations of circulating cytokine concentrations, we determined the circulating levels of IL-6, TNF- α and IL-10

in serum, isolated from both genotypes, by cytokine bead array (CBA) (Fig. 20 B). Under basal state serum levels of IL-6, TNF- α and IL-10 were found to be unaltered in both the genotypes. Although under steady state of the clamp, the serum concentrations of IL-6 and TNF- α were significantly elevated in both genotypes compared to basal state, this elevation was significantly more pronounced in IL-6R α ^{L-KO} mice compared to control mice.

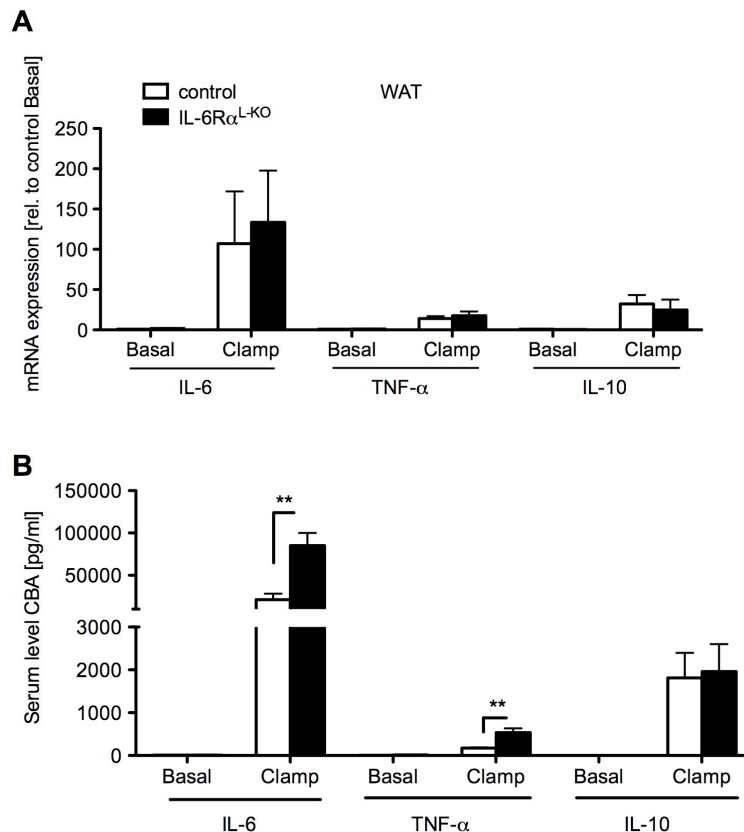


Fig. 20: IL-6R α ^{L-KO} mice exhibit enhanced systemic inflammation

(A) Expression of IL-6, TNF- α and IL-10 mRNA in WAT of IL-6R α ^{L-KO} and control mice measured by quantitative RT-PCR (n=6/genotype). (B) Measured concentrations of IL-6, TNF- α and IL-10 in the sera of indicated mice under basal and steady state phase. Concentrations were detected using cytometric bead array (n=10/genotype). Data represented as means \pm SEM. * $p \leq 0.05$; ** $p \leq 0.01$ versus controls.

Thus, consistent with the increased mRNA expression of IL-10 in the steady state compared to the basal state during the clamp, circulating IL-10 levels were elevated in the steady state compared to the basal state. However IL-10 levels were comparable between the control and IL-6R α ^{L-KO} mice in the steady state phase.

These data clearly indicate a role of hepatic IL-6 signaling in limiting liver and skeletal muscle inflammation by restricting the mRNA expression of the key inflammatory cytokines IL-6 and TNF- α and thereby, potentially protects from the development of local and systemic insulin resistance.

3.1.7 Neutralization of TNF- α normalizes glucose homeostasis in IL-6R α ^{L-KO} mice

To define the contribution of increased circulating TNF- α levels in mice lacking hepatic IL-6 signaling in the development of systemic insulin resistance and impaired glucose tolerance, the anti-TNF- α antiserum, that was previously described for its ability to diminish TNF- α signaling in mice (171), was administered *i.p.* to both genotypes. While the impaired glucose tolerance was similar in mice lacking hepatic IL-6 signaling before the administration (pre-treatment) of the anti-TNF- α antiserum (Fig. 14 A and Fig. 21 A), the administration of anti-TNF- α antiserum resulted in normalization of glucose homeostasis in IL-6R α ^{L-KO} mice during GTT (Fig. 21 B), without affecting glucose clearance in control mice. Taken together, these experiments clearly demonstrate that selectively elevated TNF- α levels lead to the impaired glucose tolerance in IL-6R α ^{L-KO} mice.

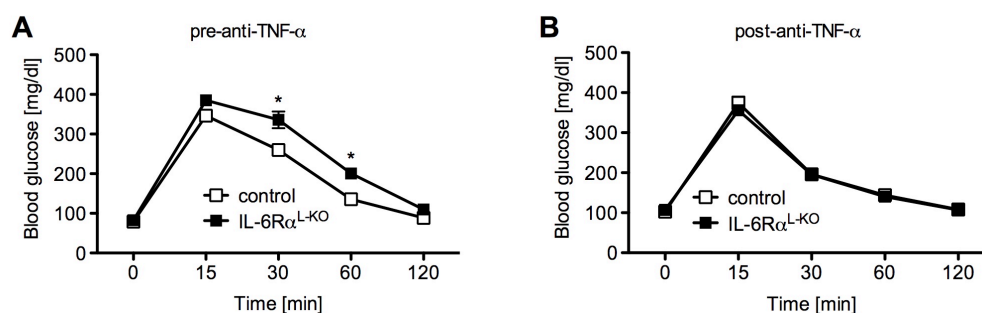


Fig. 21: Ablation of TNF- α lead to normalized glucose homeostasis in IL-6R α ^{L-KO} mice

(A) Glucose tolerance test (GTT) monitored over 120 min of 9 weeks old IL-6R α ^{L-KO} and control mice before treatment with an anti-TNF- α antibody (n=10/genotype). (B) GTT of the same animals as in (A) after a 100 μ l injection into the peritoneal cavity of an anti-TNF- α antiserum 1 h prior to the experiment (n=10/genotype). GTT was performed at week 10. Results represent means \pm SEM. * p \leq 0.05 versus controls.

Several studies have shown that IL-6 acts as negative feedback regulator of inflammatory signaling pathways in macrophages by decreasing expression of TNF- α (172).

To investigate the involvement of liver resident macrophages, the Kupffer cells (KCs), in the development of systemic insulin resistance and impaired glucose homeostasis in IL-6R α ^{L-KO} mice, we performed glucose tolerance tests in IL-6R α ^{L-KO} and control mice after depletion of liver resident macrophages. The efficient depletion of Kupffer cells with clodronate liposomes was previously described (157) and further confirmed by staining of liver sections with the macrophage glycoprotein marker MAC-2 (Fig. 22 A and B).

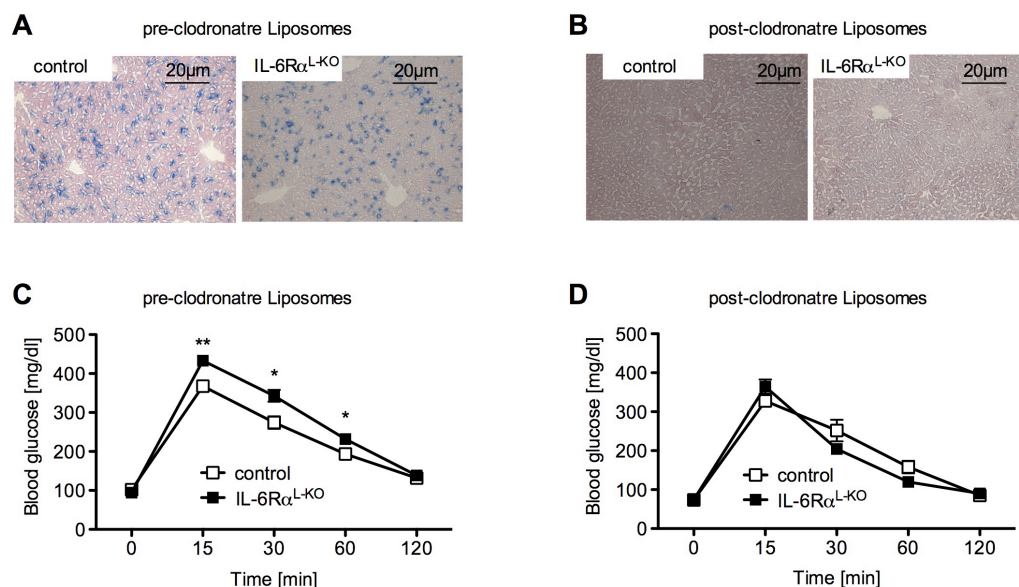


Fig. 22: Normalized glucose homeostasis in IL-6R α ^{L-KO} mice after depletion of Kupffer cells

(A) Cryostat sections of livers from IL-6R α ^{L-KO} and control mice stained with MAC-2 for visualization of liver resident macrophages. (B) Representative MAC-2 stainings of liver sections from IL-6R α ^{L-KO} and control mice after 1 ml *i.p.* injection of clodronate liposomes 2 days before the experiment. (C) Glucose tolerance test monitored over 120 min of IL-6R α ^{L-KO} and control mice at 11 weeks of age (n=10/genotype). (D) Glucose tolerance test of same animals as in (C) after injection of clodronate liposomes 2 days before the experiment (n=10/genotype). GTT were performed after a week regeneration period. Data represent means \pm SEM. * p \leq 0.05; ** p \leq 0.01 versus controls.

Consistent with our previous findings (Fig. 14 A and Fig. 21 A), we observed impaired glucose tolerance in mice lacking hepatic IL-6 signaling before the administration of clodronate liposomes (Fig. 22 C). Strikingly, the depletion of KCs normalizes glucose homeostasis of IL-6R α ^{L-KO} mice to a similar level as in control mice during the GTT (Fig. 22 C and D). These results clearly indicate that the insulin-induced activation of KCs contributes to the development of impaired glucose tolerance in IL-6R α ^{L-KO} mice.

In order to determine whether the treatment with clodronate liposomes affected the glucose stimulated insulin secretion, we next examined glucose stimulated insulin secretion (GSIS) *in vivo* of untreated and clodronate liposomes treated mice. The depletion of liver resident macrophages had no effect on insulin levels in control mice, but leads to an increased GSIS in IL-6R α ^{L-KO} mice compared to untreated mice (Fig. 23 A and B).

Thus, these data indicate that the increased inflammatory state of IL-6R α ^{L-KO} mice not only leads to the development of peripheral insulin resistance but also inhibits a compensatory elevation of glucose stimulated insulin secretion.

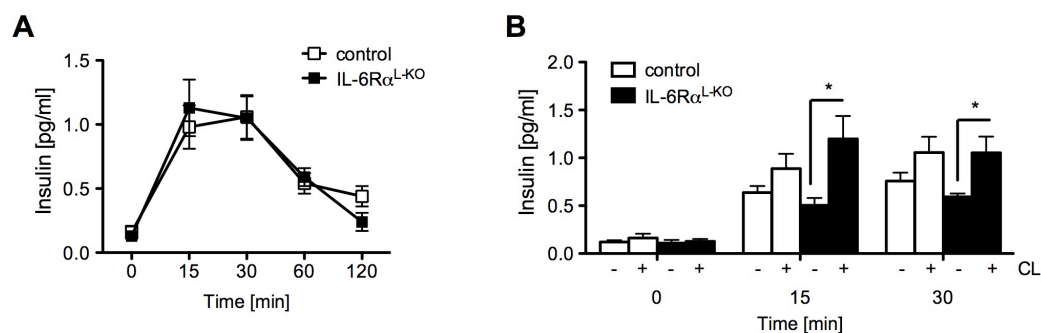


Fig. 23: Alterations of glucose stimulated insulin secretion after depletion of Kupffer cells in IL-6R α ^{L-KO} mice

(A) Insulin levels during the GTT from Fig. 22 D, measured by ELISA (n=10/genotype). **(B)** Comparison of serum insulin concentrations of untreated (Fig. 14 A) or clodronate liposome (CL) treated (Fig. 22 A) IL-6R α ^{L-KO} and control mice. Insulin levels were compared at 0, 15, and 30min after the glucose injection (n=9-13/genotype and treatment). Displayed values are means \pm SEM. * p \leq 0.05 versus controls.

Taken together, the present results reveal a novel role of hepatic IL-6 mediating crosstalk between liver parenchymal cells, i.e. hepatocytes, and liver resident macrophages to limit inflammation in the liver. The experiments clearly show, that the lack of IL-6 signaling in hepatocytes results in increased expression of TNF- α in Kupffer cells. The resulting systemic elevated level of TNF- α from Kupffer cells leads to the development of systemic insulin resistance in skeletal muscle and WAT as well as inhibiting glucose stimulated insulin secretion in pancreatic β -cells.

3.2 The effect of hepatic Myd88 signaltransduction on glucose homeostasis and HCC development

Multiple lines of evidence indicate that also the innate immune response pathway is involved in the development of obesity-associated diabetes (173). Recent studies have linked innate immune response to the development of obesity, impaired energy homeostasis and obesity-associated insulin resistance (174, 175). Excess accumulation of fatty acids is a characteristic of metabolic disease and Toll-like receptor 4 (TLR4) is known to play a critical role in the activation of innate immune responses by the recognition of lipopolysaccharide. Several studies show that mice lacking TLR4 signaling are protected from the development of obesity and insulin resistance (113, 176). Additionally, recent observations suggest an unexpected role for MyD88 in preventing diabetes (177) and an important role of MyD88 in DEN-induced liver tumor development (118). Since obesity and cancer development are intimately connected, we decided to inactivate MyD88 specifically in hepatocytes to get insights into the molecular mechanisms underlying these diseases.

3.2.1 Generation of MyD88^{L-KO} mice

To investigate the role of Toll-like receptor signaling in energy homeostasis and hepatocellular carcinoma (HCC) development, we generated mice lacking the major adaptor protein of TLR signaling, myeloid differentiation primary response gene 88 (MyD88), specifically in hepatocytes. Therefore we crossed mice in which exons 3 to 5 of the MyD88 gene were flanked by loxP sites (MyD88^{FL/FL} mice (178)), with mice expressing the Cre recombinase under the control of the ALFP promoter (ALFP-Cre mice) (165). The resulting double-heterozygous ALFP-Cre^{+/-} MyD88^{FL/+} mice were further intercrossed to yield hepatocyte specific MyD88 knockout mice (MyD88^{L-KO} mice). Littermates lacking the ALFP-Cre recombinase (MyD88^{FL/FL} mice) were used as controls throughout the study (Fig. 24 A).

To verify the efficient and specific deletion of the loxP-flanked MyD88 allele exclusively in hepatocytes, we performed quantitative RT-PCR analysis of mRNA isolated from liver tissue of control and MyD88^{L-KO} mice. The mRNA expression of hepatic MyD88 was significantly reduced in MyD88^{L-KO} mice compared to control mice (Fig. 24 B).

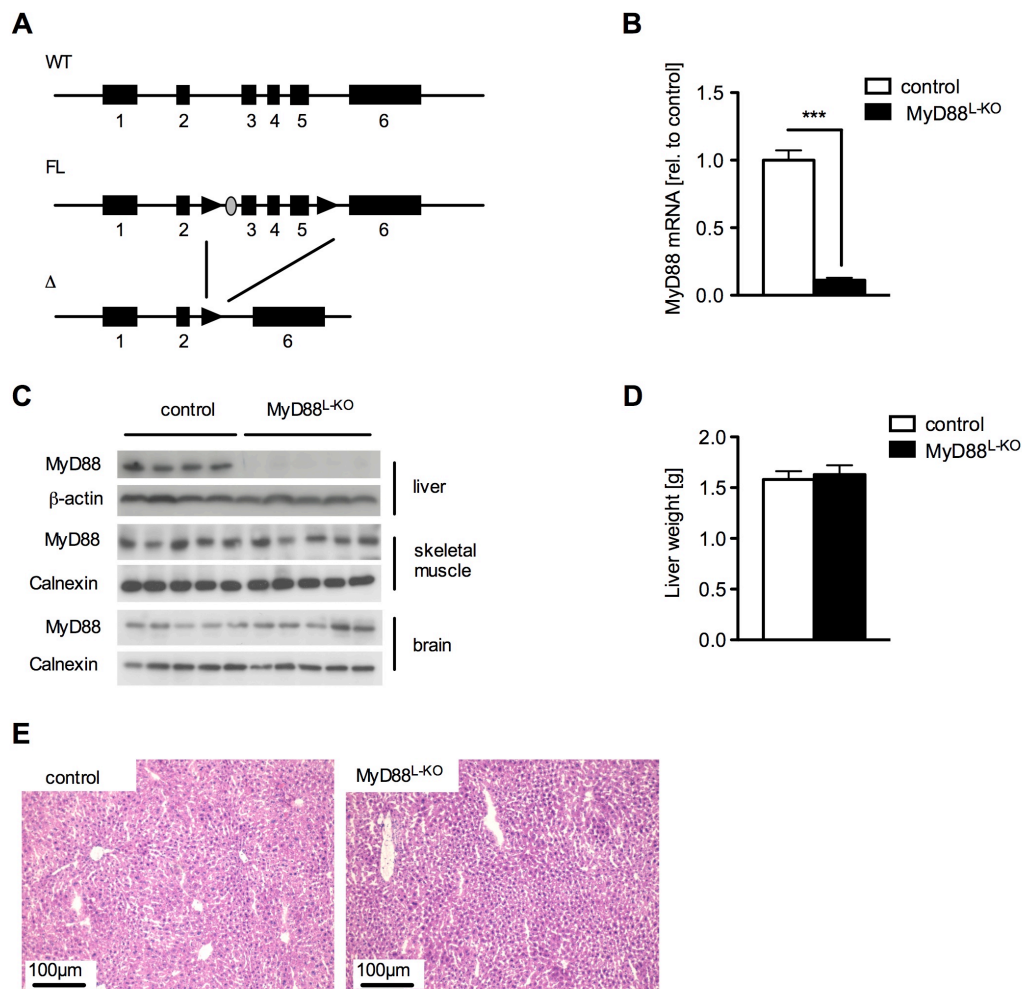


Fig. 24: Targeting strategy and ablation of MyD88 specific in the liver

(A) Map of the wildtype (WT), the exons 3 to 5 loxP-flanked (FL) and the deleted (Δ) allele of MyD88. The deleted allele is shown after Cre loxP-mediated recombination. **(B)** Relative mRNA expression of MyD88 in livers of MyD88^{L-KO} and control mice measured by quantitative RT-PCR (n=5-7/genotype). **(C)** Western blot analysis of protein lysates from MyD88^{L-KO} and control mice for determination of MyD88 levels in the respective tissues. Protein content was determined by using MyD88 as well as Calnexin and β -actin antibodies for loading controls. **(D)** Liver weight of MyD88^{L-KO} and control mice at week 20 (n=9-12/genotype). **(E)** Cryostat sections of livers from MyD88^{L-KO} and control mice stained with H&E to analyze overall liver morphology. Data displayed are means \pm SEM. *** p \leq 0.001 versus controls.

Furthermore, Western blot analysis of liver, skeletal muscle and brain revealed selective deletion of MyD88 in liver of the MyD88^{L-KO} mice, whereas the protein levels of MyD88 were unaltered in skeletal muscle and brain (Fig. 24 C). Moreover, the lack of hepatic MyD88 expression had no effect on liver weight as well as the integrity of the liver structure as determined by H&E staining of liver sections (Fig. 24 D and E).

In summary, these experiments demonstrate an efficient and specific disruption of MyD88 in hepatocytes of MyD88^{L-KO} mice without affecting liver morphology.

3.2.2 Unaltered adiposity in mice lacking hepatic MyD88 signaling

Recent studies revealed that obesity is characterized as a chronic low-grade inflammation, which in turn is causally linked to the development of insulin resistance (19, 179). Also, recent studies have suggested and linked innate immune responses to the development of obesity, impaired energy homeostasis and obesity-associated insulin resistance (174, 175).

To determine whether hepatic MyD88 signaling affects adiposity, we analyzed body weight, epigonadal fat pad mass and body fat content in MyD88^{L-KO} mice compared to control mice (Fig. 25). Although, control mice showed a consistent increase in body weight gain at older ages, no genotype-dependent differences in body weight gain were observed between control and MyD88^{L-KO} mice (Fig. 25 A). Similarly, epigonadfal fat pad mass (Fig. 25 B) and total body fat content (Fig. 25 C) were unaltered between both genotypes.

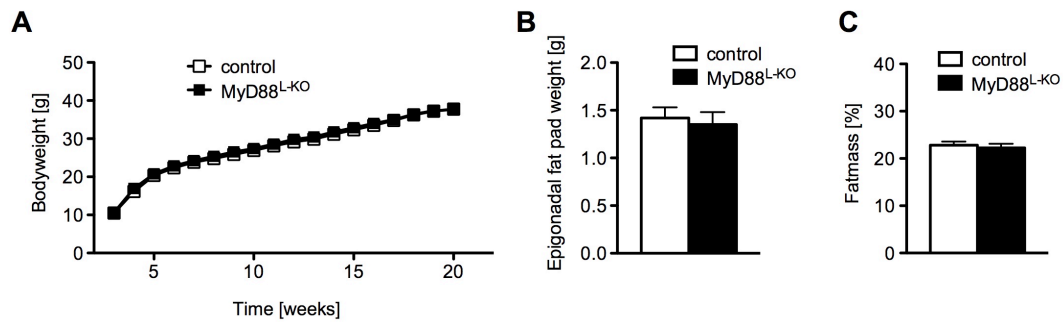


Fig. 25: Similar bodyweight and body fat content between control and MyD88^{L-KO} mice

(A) Average bodyweight from week 3 to week 20 of MyD88^{L-KO} and control mice (n=16-18/genotype). (B) Measured epigonadal fat pad mass of indicated mice (n=16-18/genotype). (C) Total body fat content of both groups determined using nuclear magnetic resonance (n=16-18/genotype). Displayed values are means ± SEM.

Usually, elevated plasma levels of triglycerides (TGs) as well as cholesterol are observed in obesity and are linked to the development of insulin resistance (3, 180, 181). To transport lipids, such as TGs and cholesterol, within the hydrophilic bloodstream, lipoproteins are used. The high-density lipoprotein (HDL) is one of the five major groups of lipoproteins and it is well known that obesity is frequently associated with low levels of serum HDL-cholesterol (182).

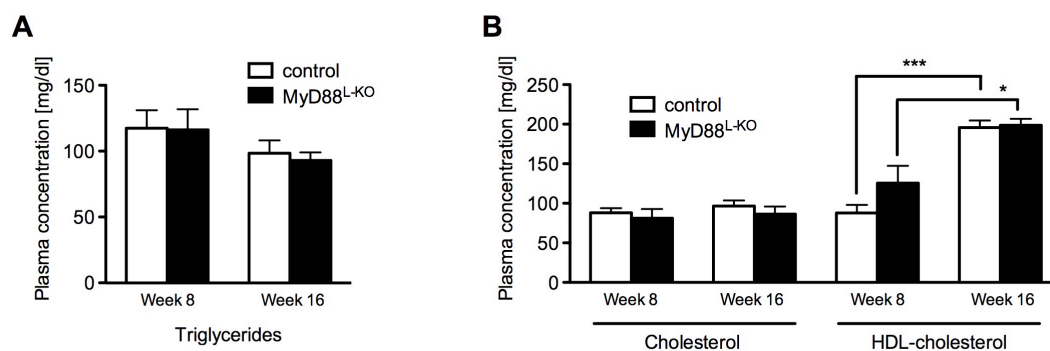


Fig. 26: Unaltered cholesterol and lipid metabolism in MyD88^{L-KO} mice

(A) Plasma triglyceride levels of random fed MyD88^{L-KO} and control mice at week 8 and week 16 (n=9-15/genotype). (B) Random fed blood cholesterol as well as HDL-cholesterol concentrations of 8 and 16 weeks old control and MyD88^{L-KO} mice (n=9-15/genotype). Displayed results represent the mean ± SEM. * p ≤ 0.05; *** p ≤ 0.01 versus controls.

To investigate whether MyD88 signaling in the liver affects lipid concentrations or lipid transport, we analyzed blood plasma levels of TGs, cholesterol and HDL-cholesterol of control and MyD88^{L-KO} mice (Fig. 26). Consistent with the unaltered adiposity observed between both genotypes, plasma levels of TGs, cholesterol and HDL-cholesterol were similar in control and MyD88^{L-KO} mice, although plasma HDL-cholesterol levels were elevated in older control and MyD88^{L-KO} mice compared to younger mice.

Taken together, these results imply hepatic MyD88 signaling as non-essential in maintaining bodyweight or lipid metabolism.

3.2.3 Glucose homeostasis and insulin sensitivity is unaltered in MyD88^{L-KO} mice

The role of TLR signaling, especially through the adaptor protein MyD88, in preventing the development of insulin resistance has been defined in earlier studies in brain, skeletal muscle, WAT and liver (177, 178, 183). However, the role of MyD88 dependent signaling in hepatocytes in maintaining insulin sensitivity is largely undefined. To evaluate the molecular mechanisms linking hepatic MyD88 signaling to glucose homeostasis and insulin sensitivity, we investigated the physiological role of MyD88 in the liver. Therefore, random fed blood glucose levels of control and MyD88^{L-KO} mice were determined. As shown in Figure 27 A, no obvious differences were apparent at week 8 of age as well as at week 16 of age between control and MyD88^{L-KO} mice. In consistency to the unchanged blood glucose levels, random fed circulating insulin concentrations were also unaltered between control and MyD88^{L-KO} mice (Fig. 27 B).

Moreover, glucose homeostasis and insulin sensitivity in control and MyD88^{L-KO} mice were further investigated by GTT and ITT at the age of 12 and 13 weeks, respectively. When challenged with glucose during GTT, MyD88^{L-KO} and control mice exhibit a similar glucose tolerance and a similar

rate of glucose clearance from the blood (Fig. 27 C). In line with unaltered glucose homeostasis, control and MyD88^{L-KO} mice exhibit unaltered insulin sensitivity, when challenged with an intraperitoneal injection of insulin in ITTs (Fig. 27 D).

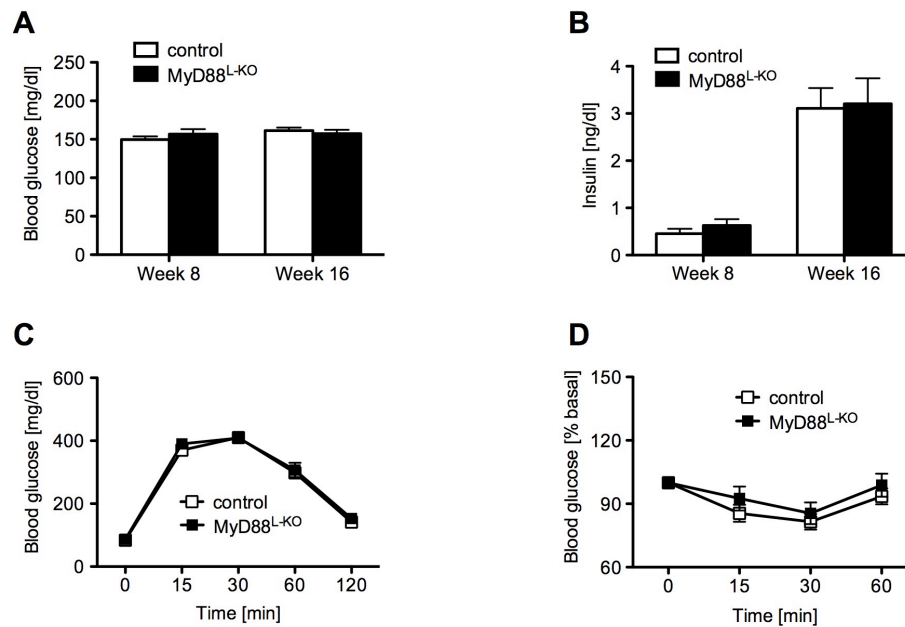


Fig. 27: Unaltered glucose homeostasis and insulin sensitivity in MyD88^{L-KO} mice

(A) Blood glucose levels of random fed MyD88^{L-KO} and control mice at week 8 and week 16 (n=16/genotype). (B) Random fed blood insulin concentrations of 8 and 16 weeks old as determined by ELISA (n=10/genotype). (C) Glucose tolerance test monitored over 120 min of 12 weeks old MyD88^{L-KO} and control mice (n=16/genotype). (D) Insulin tolerance test performed on both groups at the age of 13 weeks (n=16/genotype). The results represent the mean ± SEM.

Taken together, these results indicate that hepatic MyD88 signaling provides no profound effect on glucose homeostasis and insulin sensitivity.

3.2.4 MyD88^{L-KO} mice exhibit reduced DEN-induced hepatocarcinogenesis

Already in 1863, Rudolf Virchow found first indications for the connection between inflammation and cancer, and many studies have supported this assumption over the last decades (184, 185). Additionally, the development of hepatocellular carcinoma (HCC) has been linked with the persistent hepatic inflammation through factors that lead to chronic hepatic injury (106). In experimental studies, the chemical diethylnitrosamine (DEN) is widely used to

induce chronic liver injury, which ultimately leads to the development of HCC (160).

That systemic deletion of MyD88 in mice leads to decreased DEN-induced tumor development was demonstrated previously (118). However, the cell type specific contribution of MyD88 signaling could not be addressed due to the use of conventional KO mice. Thus, we investigated the role of hepatic MyD88 signaling in the development of chemically induced HCC formation. Hence, we treated control and MyD88^{L-KO} mice with the HCC inducer DEN at day 15 after birth and analyzed the DEN-induced HCC development in control and MyD88^{L-KO} mice after 8 months of age.

The alanine transaminase (ALT) and aspartate transaminase (AST) are enzymes, which are predominantly found in liver. Upon tissue damage, the activity as well as protein concentration of these enzymes increases within the liver. The blood serum concentrations are sensitive to toxic liver injury, because only elevated levels of ALT and AST leads to the translocation into the bloodstream (186, 187). Therefore, we examined the blood serum levels of ALT and AST in MyD88^{L-KO} and control mice, either untreated as well as DEN-treated. Although ALT levels were significantly increased after DEN administration in both genotypes, no significant difference was detected between MyD88^{L-KO} and control mice (Fig. 28 A). This was consistent with higher AST levels in the blood of DEN treated MyD88^{L-KO} and control mice, with no alterations between both genotypes (Fig. 28 B). The De-Ritis-Quotient (AST/ALT) (188) gives additional information about liver damage, since hepatic injury leads to stronger elevation of AST compared to ALT concentrations, resulting in a higher De-Ritis-Quotient. While a significantly elevated De-Ritis-Quotient was observed in control mice after DEN injection compared to untreated control mice, the MyD88^{L-KO} mice show only a slightly increased De-Ritis-Quotient (Fig. 28 C). However, this elevation did not reach statistical significance. Together, these results indicate a compromised potential of DEN to induce hepatic injury in MyD88^{L-KO} mice compared to control mice and thereby leading to reduced DEN-induced liver damage.

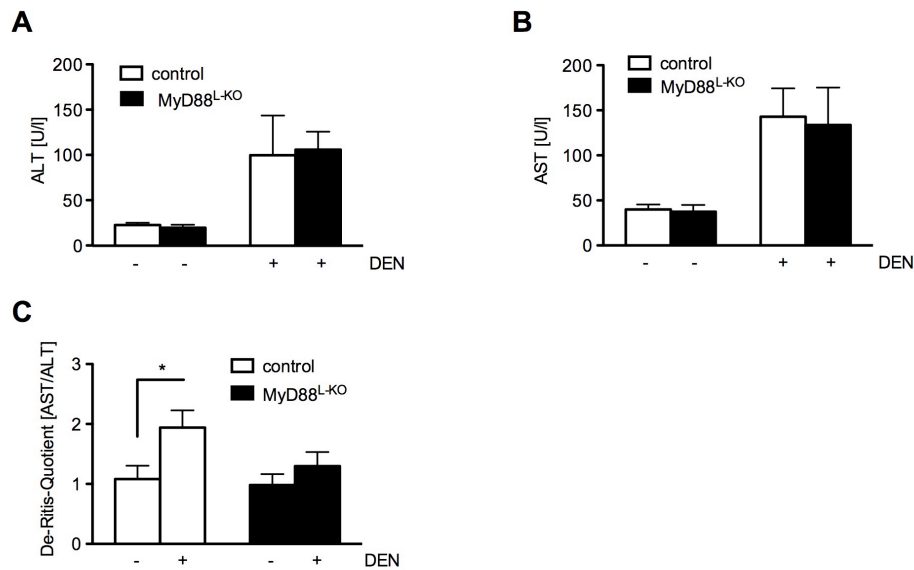


Fig. 28: Reduced DEN-induced liver damage in MyD88^{L-KO} mice

(A-B) Measured (A) ALT and (B) AST levels in sera of untreated and with 25 mg/kg DEN treated MyD88^{L-KO} and control mice at 12-16 weeks of age (n=7-12/genotype). (C) Calculated De-Ritis-Quotient of (A) and (B). The De-Ritis-Quotient is calculated by dividing AST through ALT. Displayed values are means \pm SEM. * $p \leq 0.05$ versus controls.

Strikingly, DEN-induced tumor formation in livers of MyD88^{L-KO} and control mice (Fig. 29) revealed an overall reduced number of hepatocellular carcinomas in MyD88^{L-KO} mice compared to control mice (Fig. 29 C). Additionally, the reduction in number of tumor formation was also accompanied with significantly decreased HCC sizes (Fig. 29 D), implying a prominent role of hepatic MyD88 signaling in regulating DEN-induced HCC formation.

To investigate whether proliferation in the liver is affected in the absence of hepatic MyD88 and thus leads to decreased HCC development, the proliferative status in tumor livers of both genotypes was determined. Ki-67 protein is strongly associated with cell proliferation and therefore a prominent cellular marker for proliferation (189). To examine Ki-67 abundance in tumorigenesis, we performed Ki-67 stainings of DEN treated livers of control and MyD88^{L-KO} mice (Fig. 29 F). However, no genotype-dependent differences of proliferative cells in tumor foci of the liver were observed between control and MyD88^{L-KO} mice (Fig. 29 G).

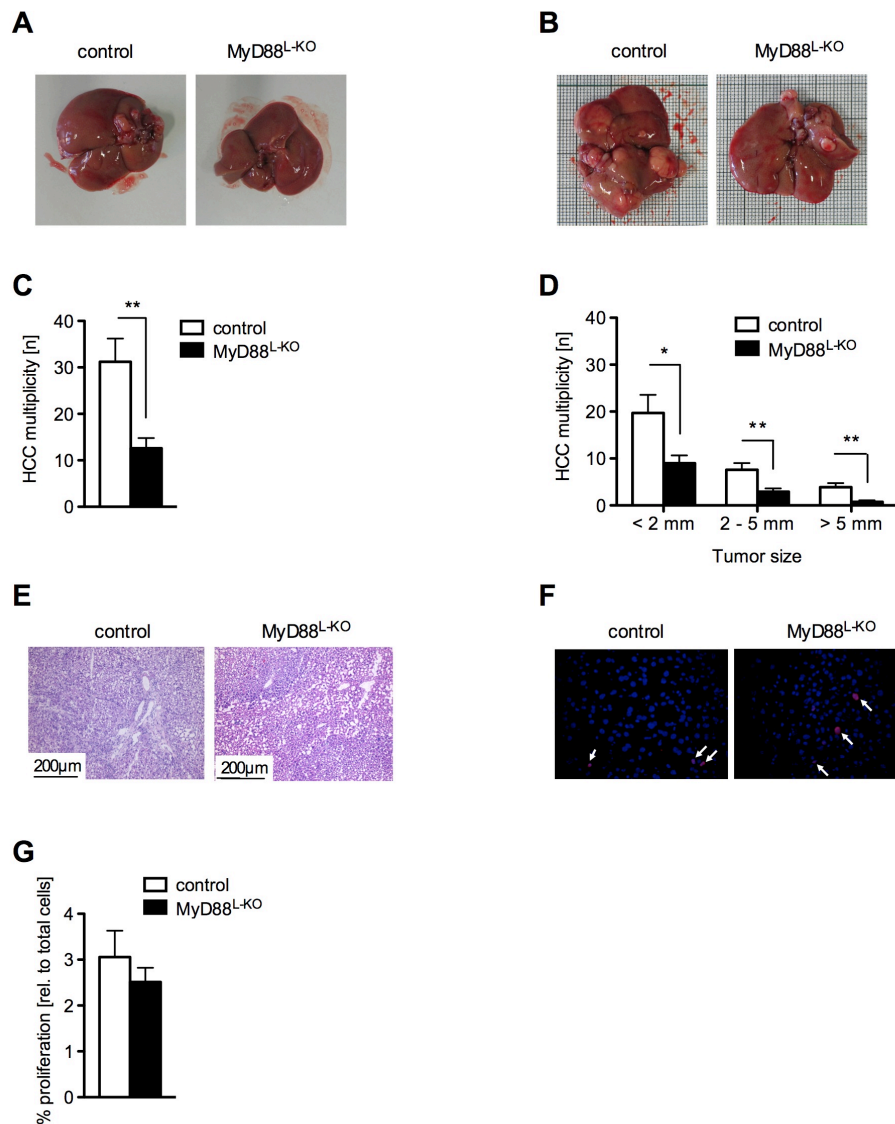


Fig. 29: Lower DEN-induced HCC incidence in MyD88^{L-KO} mice

(A-B) Representative livers of either (A) untreated or (B) 25 mg/kg DEN treated 8 months old MyD88^{L-KO} and control mice. **(C)** Quantification of macroscopic tumor multiplicity, determined by visual inspection in DEN-injected 8 month old control and MyD88^{L-KO} mice (n=10-12/genotype). **(D)** Enumeration of tumor number < 2 mm, 2-5mm and > 5 mm from (C), as determined by visual inspection (n=10-12/genotype). **(E-F)** Cryostat sections of livers from DEN treated MyD88^{L-KO} and control mice stained with (E) H&E for tumor morphology and (F) with Ki-67 (red) to determine proliferative cells as well as DAPI (blue) for total cell number of MyD88^{L-KO} and control mice. **(G)** Quantification of (F) Ki-67 positive cells relative to total cell number (n=4/genotype). Data represent means \pm SEM. * $p \leq 0.05$; ** $p \leq 0.01$ versus controls.

Overall, these findings indicate that the loss of hepatic MyD88 signaling leads to reduced DEN-induced liver damage and to a lower HCC incidence coupled with reduced DEN-induced tumor size. This reduction of tumor incidence was

not due to decreased proliferation in tumor foci of livers of MyD88^{L-KO} mice compared to control mice.

3.2.5 Reduced expression of macrophage markers in HCC of mice lacking hepatic MyD88 signaling

Inflammation plays a major role in the response to damaged cells. It is characterized by infiltrating immune cells, such as macrophages into damaged tissues, where it elicits an inflammatory response characterized by expression and secretion of the key inflammatory cytokines IL-6, TNF- α and IL-1 β . In the liver, mainly liver resident macrophages (Kupffer cells) are responsible for eliciting this inflammatory response. Upon activation by different stimuli in the blood, which is passed through a network of hepatic sinusoids, the Kupffer cells release numerous cytokines, such as IL-6, TNF- α and IL-1 β as well as certain chemokines, such as monocyte chemo-attractant protein 1 (MCP-1), which initiates the recruitment of additional immune cells to the liver (190, 191).

Since macrophages are the key initiator of hepatic inflammation in response to liver damage, we determined the macrophage content of the liver after DEN-induced HCC. Therefore we analyzed the expression of macrophage markers Integrin- α -M (ITGAM), Integrin- α -X (ITGAX), CD-68, F4/80 and MAC-2 in liver lysates of untreated and DEN-injected mice.

The mRNA expression of Integrin- α -M (ITGAM) and Integrin- α -X (ITGAX), expressed in granulocytes and monocytes (192, 193) was unchanged before and after DEN treatment in control and MyD88^{L-KO} mice. Although, the injection of DEN resulted in increased CD-68 mRNA expression in the livers of both genotypes, the CD-68 mRNA expression was unaltered between control and MyD88^{L-KO} mice (Fig. 30 A). In addition, while hepatic mRNA expression of the key macrophage markers F4/80 and MAC-2 (194, 195) were induced by DEN in control mice, the mRNA expression of F4/80 and

MAC-2 was blunted in livers of DEN MyD88^{L-KO} mice (Fig. 30 B), indicating reduced DEN-induced macrophage migration in livers of mice lacking hepatic MyD88 signaling.

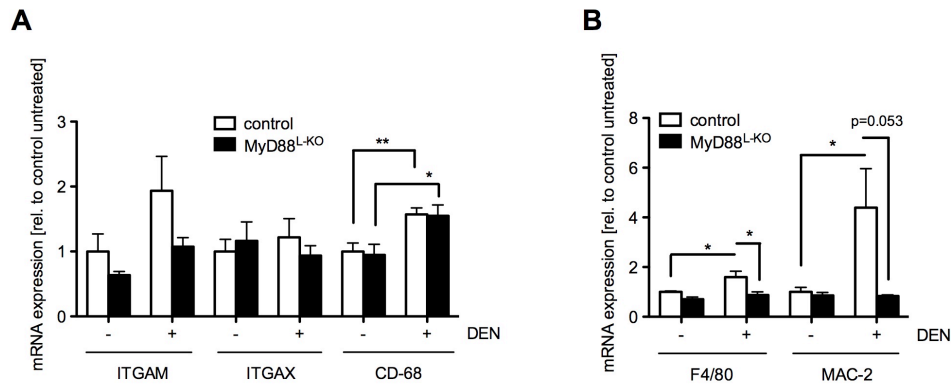


Fig. 30: MyD88^{L-KO} mice show reduced macrophage marker expression in the liver

(A-B) Relative mRNA expression of indicated (A) granulocyte and monocyte markers as well as (B) specific macrophage markers in livers of untreated and DEN treated mice (n=6/genotype). Data were obtained by quantitative RT-PCR of liver lysates. Displayed values are means ± SEM. * p ≤ 0.05; ** p ≤ 0.01 versus controls.

To investigate whether the reduced macrophage marker mRNA expression after DEN treatment in livers of MyD88^{L-KO} mice results from reduced mRNA expression of key chemo-attractants, MCP-1, RANTES, MCP-3, or the macrophage inflammatory proteins (MIP) MIP-1 α and MIP-1 β , we measured mRNA expression of these chemokines in livers of untreated and DEN-injected control and MyD88^{L-KO} mice. While hepatic mRNA expression of MCP-1, RANTES and MCP-3 was unaltered between non-treated and DEN treated control and MyD88^{L-KO} mice, mRNA expression of MIP-1 α and MIP-1 β increased significantly in liver of both genotypes upon DEN treatment. Nevertheless, no genotype-dependent alterations were detectable in MIP-1 α and MIP-1 β mRNA expression between control and MyD88^{L-KO} mice, even in the untreated state (Fig. 31 A and B).

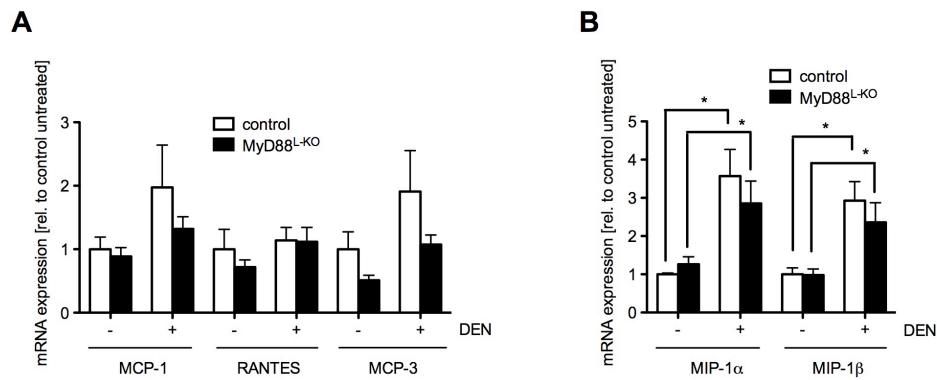


Fig. 31: Unaltered mRNA expression of chemokines between control and MyD88^{L-KO} mice

(A-B) Relative mRNA expression of indicated (A) MCP-1, RANTES and MCP-3 as well as (B) MIP-1 α and MIP-1 β in livers of untreated and DEN treated mice (n=6/genotype), determined by quantitative RT-PCR. Data are means \pm SEM. * $p \leq 0.05$ versus controls.

3.2.6 The mRNA expression of LIF in HCC is mediated by hepatic MyD88

The inflammatory process is characterized by elevated pro-inflammatory cytokine expression, such as IL-6, IL-1 β and leukemia inhibitory factor (LIF). During the development of HCC, not only pro-inflammatory cytokines are expressed, but also anti-inflammatory cytokines, such as IL-10, are increased (196). Several chemokines, e.g. IL-6, LIF and IL-10, induce the activation of STAT-3 by phosphorylation at Tyr 705. Persistently activated STAT-3 increases tumour cell proliferation, survival and invasion by promoting pro-oncogenic inflammatory pathways (197). MyD88 is required for IL-6 induction by necrotic debris and for DEN-induced production of IL-6 *in vivo* (118). To define the role of hepatic MyD88 in this context, we analyzed hepatic expression of the pro-inflammatory cytokines IL-6 and LIF, as well as the anti-inflammatory cytokine IL-10 before and after DEN treatment. Interestingly, mRNA expression of IL-6 in the liver was neither induced by DEN, nor differentially expressed between control and MyD88^{L-KO} mice, indicating a minor role of this cytokine in the development of DEN induced HCC in our study (Fig. 32 A). Strikingly, the mRNA expression of the IL-6 type cytokine LIF was strongly induced in livers of DEN treated control mice, whereas this increased hepatic mRNA expression was significantly blunted in MyD88^{L-KO}

mice. The same was true for the anti-inflammatory cytokine IL-10, which is known to be elevated in HCC (196). Although the mRNA expression was elevated in liver of chemically induced HCC compared to untreated control mice, the hepatic mRNA expression of IL-10 in MyD88^{L-KO} mice was unaltered between untreated and DEN treated livers (Fig. 32 A). To investigate whether this increased mRNA expression of LIF and IL-10 translated in elevated activation of STAT-3 in control mice, we further analyzed the phosphorylation status of STAT-3 at Tyr residue 705 (Fig. 32 B and C).

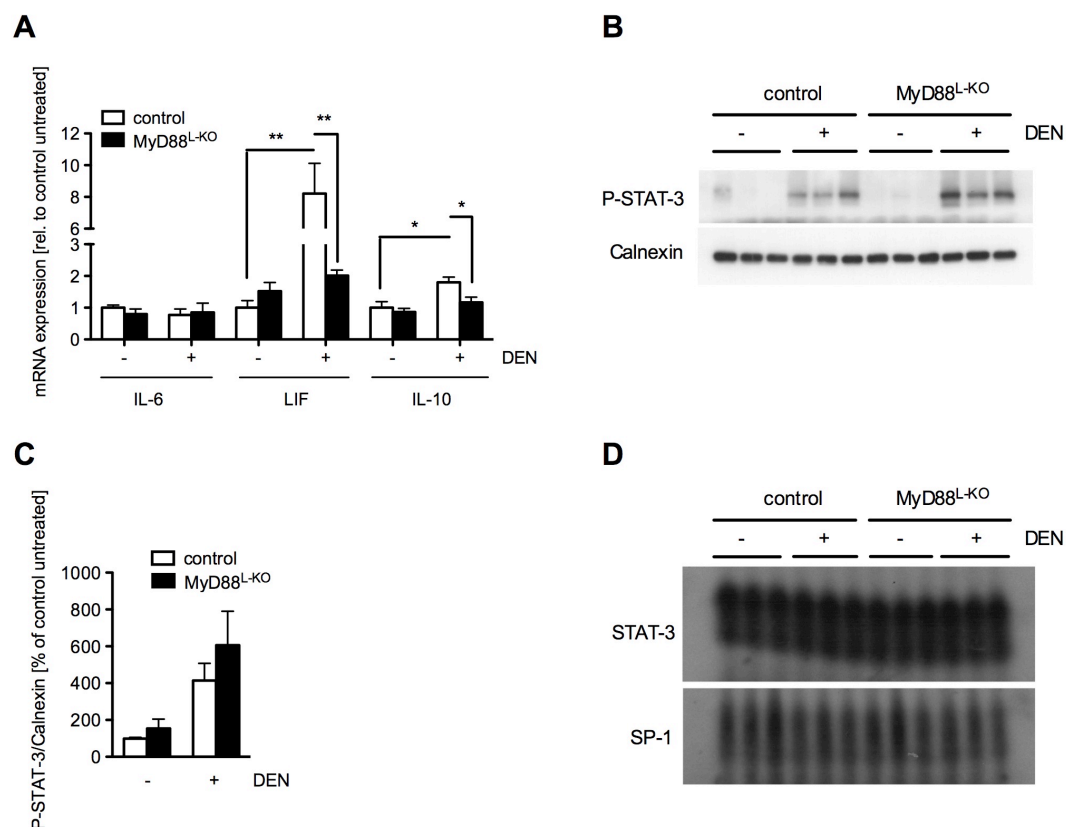


Fig. 32: Elevated mRNA expression of LIF in MyD88^{L-KO} mice compared to control mice

(A) Relative mRNA expression of IL-6, LIF and IL-10 in livers of both genotypes either untreated or DEN treated. The mRNA expression was determined by quantitative RT-PCR (n=6/genotype). **(B)** Western blot analysis of liver lysates from untreated and DEN treated control and MyD88^{L-KO} mice. Protein content was determined by using P-STAT-3 and Calnexin antibodies. **(C)** Quantification of Western blot analysis from (B) to determine the phosphorylation of STAT-3 at Tyr residue 705 relative to Calnexin (n=5-6/genotype). **(D)** EMSA of nuclear protein extracts isolated from livers of control and MyD88^{L-KO} mice either untreated or DEN treated. The DNA-binding capacity of STAT-3 was determined by using radioactively labeled probes of STAT-3 as well as specific protein 1 (SP-1), which served as loading control. Data are means \pm SEM. * $p \leq 0.05$; ** $p \leq 0.01$ versus controls.

Moreover, the DNA-binding capacity of STAT-3 was determined by an electrophoretic mobility shift assay (EMSA) using nuclear extracts from untreated as well as DEN treated control and MyD88^{L-KO} mice. Although LIF and IL-10 mRNA expression as well as the phosphorylation of STAT-3 was clearly elevated in control mice, the DNA-binding capacity of STAT-3 was unaltered between untreated and DEN treated control mice. Additionally, the binding capacity and the phosphorylation of STAT-3 were also unaltered between both genotypes (Fig. 32 D).

Furthermore, we investigated the effects of acute DEN treatment on IL-6 signaling to get insight in early stages of liver damage. Therefore we analyzed hepatic mRNA expression of IL-6 as well as STAT-3 activation of untreated and acute DEN treated control and MyD88^{L-KO} mice (Fig. 33). This analysis revealed no genotype-dependent differences in IL-6 mRNA expression, neither in untreated or 4 h acute DEN-treated control and MyD88^{L-KO} mice (Fig. 33 A). Consistent with the observations in tumor livers, acute DEN treatment lead to increased STAT-3 activation in control and MyD88^{L-KO} mice, although this activation was similar between both genotypes (Fig. 33 B).

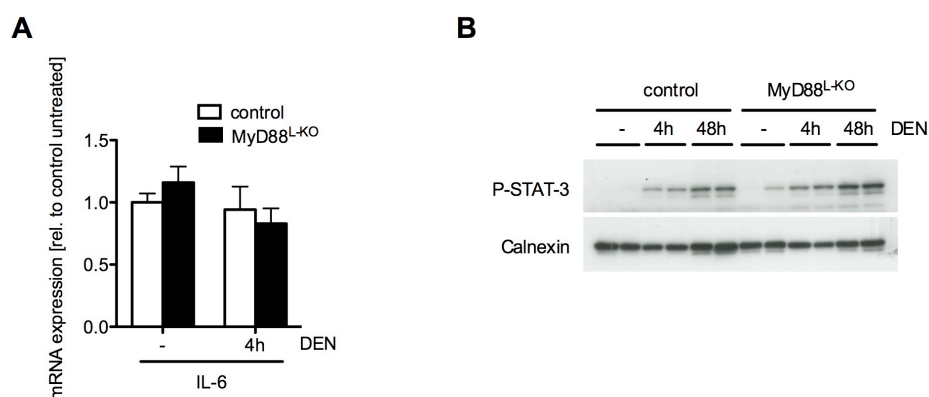


Fig. 33: Unaltered IL-6 signaling in MyD88^{L-KO} mice compared to control mice upon acute DEN treatment

(A) Relative mRNA expression of IL-6 in livers of both genotypes either untreated or 4 h acute DEN-treated. The mRNA expression was determined by quantitative RT-PCR (n=6/genotype). **(B)** Western blot analysis of liver lysates from untreated and 4 h as well as 48 h acute DEN-treated control and MyD88^{L-KO} mice. Protein content was determined by using P-STAT-3 and Calnexin antibodies. Data are means \pm SEM.

Taken together, hepatic MyD88 is important in mediating LIF as well as IL-10 mRNA expression in DEN-induced HCC, since MyD88^{L-KO} mice show no induction of either LIF or IL-10 mRNA expression in DEN-induced HCC, whereas IL-6 mRNA expression in the liver is not dependent on hepatic MyD88. Additionally, the similar IL-6 mRNA expression in both genotypes and treatments could be responsible for unaltered activation and DNA-binding capacity of STAT-3 in these conditions.

3.2.7 Reduced NF- κ B activation in DEN-induced HCC of MyD88^{L-KO} mice

A major link between inflammation and cancer is mediated by NF- κ B transcription factors. While constitutive NF- κ B activation has been observed in tumor tissues (198), hepatocyte specific disruption of IKK β in mice shows hypersusceptibility to DEN-induced hepatocarcinogenesis (141).

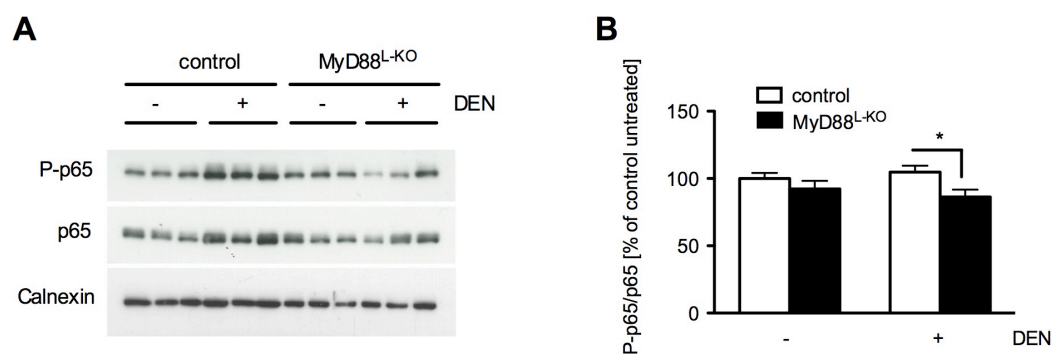


Fig. 34: MyD88^{L-KO} mice exhibit reduced p65 activation upon DEN treatment

(A) Representativ Western blot analysis of liver lysates from untreated as well as DEN treated control and MyD88^{L-KO} mice. Protein content was determined by using P-p65, p65 and Calnexin antibodies. (B) Quantification of Western blot analysis from (A) to determine the phosphorylated status of p65 relative to unphosphorylated p65 (n=6/genotype). Data are means \pm SEM. ** $p \leq 0.01$ versus controls.

Since IKK β is an activator of NF- κ B in response to pro-inflammatory stimuli as well as TLR signaling, we were interested in the activation status of hepatic NF- κ B in DEN-induced HCC of control and MyD88^{L-KO} mice. Therefore we determined the phosphorylation of p65, a part of the NF- κ B complex, at Ser residue 536. Hepatic p65 was neither activated in DEN treated livers of control mice nor in livers of MyD88^{L-KO} mice compared to untreated mice.

Nevertheless, significant decreased activation of hepatic p65 was observed in DEN-induced HCC of MyD88^{L-KO} mice compared to control mice (Fig. 34 A and B), indicating a hypersusceptibility to DEN-induced hepatocarcinogenesis of MyD88^{L-KO} mice.

It was previously shown that reduced NF- κ B activation due to hepatocyte specific IKK β -deficiency not only increases DEN-induced liver cancer, but also leads to elevated JNK activation. Conventional ablation of JNK in IKK β -deficient mice reverses the increased susceptibility to HCC upon DEN-treatment (141).

3.2.8 MyD88^{L-KO} mice exhibit reduced hepatic JNK activation in DEN-induced HCC

The TLR signaling cascade is known to activate JNK as well as other MAPKs, such as ERK and p38. They are major components of pathways controlling differentiation, proliferation and apoptosis, and transduce signaling upon stimulation of cytokines, growth factors, and stress signals (123). Deregulation of MAPKs in various types of tumors, including HCC are also described (124). Whereas elevated levels of active ERK and JNK1 were found in hepatocellular carcinoma (126, 140, 141), p38 exhibits an important role in suppressing HCC tumorigenesis (135). Since TLR signaling leads to the activation of MAPKs by TAK1 (199), we were interested in the role of TLR mediated MAPK signaling in DEN-induced HCC. To investigate the role of hepatic MyD88 in activation of MAPKs during HCC development, we analyzed the phosphorylation status of JNK, ERK1/2 and p38 by Western blot analysis. Nevertheless, phosphorylation of ERK1/2 at Thr 202 and Tyr 204 as well as phosphorylation of p38 at Thr 180 and Tyr 182 were completely unaltered between treatment and genotypes, indicating a minor role of active ERK1/2 and p38 in DEN-induced HCC (Fig. 35 A and E). However, partly activated MAPK signaling was induced in liver of control mice after DEN treatment. In contrast to ERK1/2 and p38 activation, the phosphorylation of hepatic JNK at

Thr 183 and Tyr 185 was significantly increased in DEN treated control mice compared to untreated control mice. However, this activation was significantly blunted in MyD88^{L-KO} mice, indicating an important role of hepatic MyD88 in driving activation of JNK (Fig. 35 C).

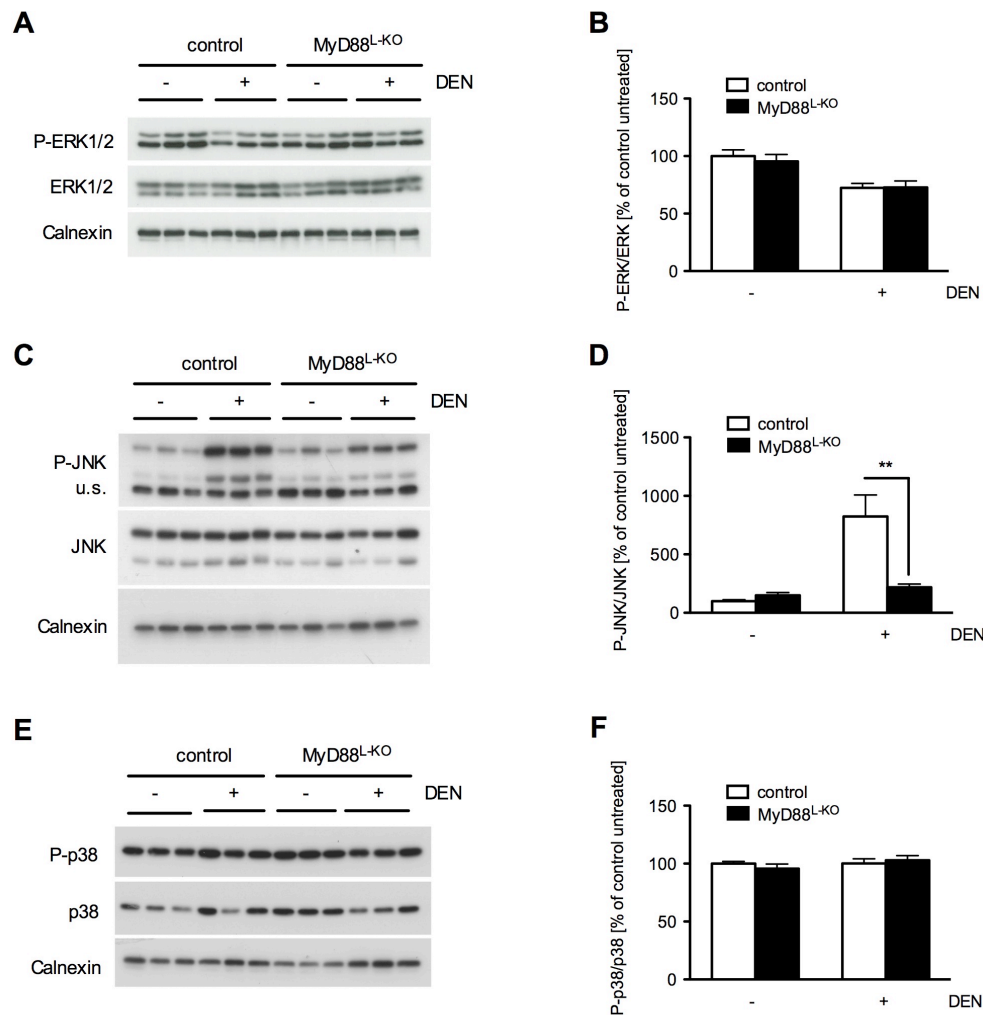


Fig. 35: Reduced JNK activation in HCC of MyD88^{L-KO} mice compared to control mice

(A), (C) and (E) Representative Western blots of livers from both genotypes as well as untreated and DEN treated mice. Protein content was determined by using indicated antibodies. (B), (D) and (F) Quantification of Western blot analysis from (A), (C) and (E) to determine the phosphorylated status of ERK1/2, JNK and p38 relative to unphosphorylated ERK1/2, JNK and p38 α , respectively (n=6/genotype). Data represent means \pm SEM. ** p \leq 0.01 versus controls.

To investigate whether MAPK signaling contributes to the early stages of HCC development, we determined the phosphorylation status of JNK, ERK1/2 and p38 of untreated and 4 h acute DEN treated animals by Western blot analysis (Fig. 36). Consistent with the observed unaltered phosphorylation of ERK1/2 and p38 in DEN-induced HCC, these phosphorylations were also unaltered between treatment and genotypes, indicating a minor role of active ERK1/2 and p38 in the early stages of HCC development (Fig. 36 A and B). In contrast to the observed reduction of active JNK in DEN-induced HCC, the phosphorylation of JNK was similarly elevated in 4 h acute DEN treated animals compared to untreated animals of both genotypes (Fig. 36 C), indicating a MyD88 independent JNK activation at the early phase of tumor development.

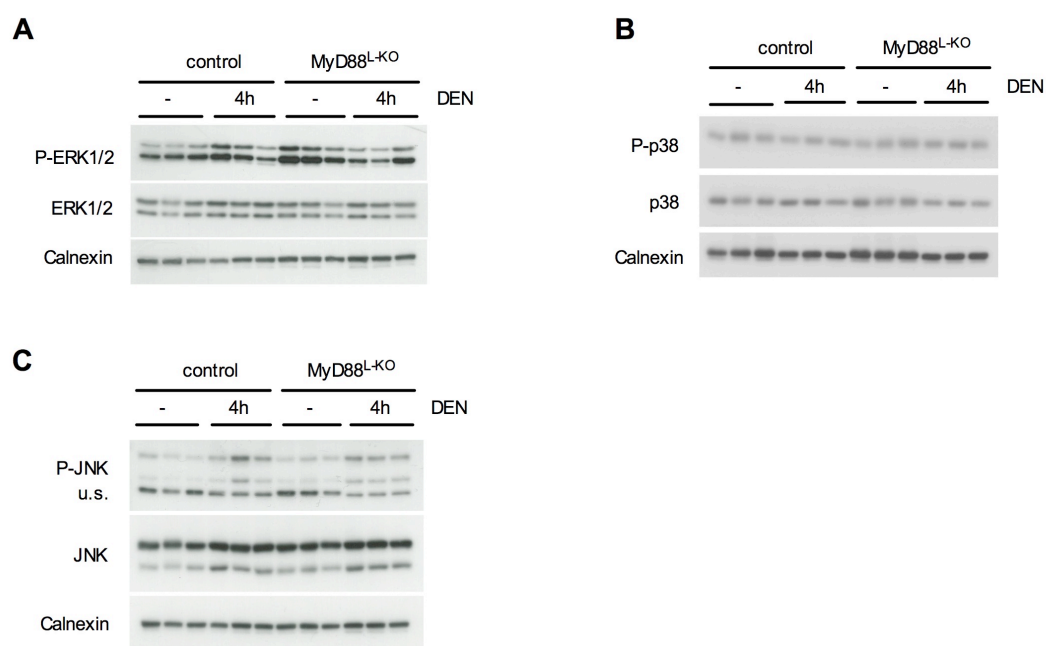


Fig. 36: Unaltered MAPK signaling in MyD88^{L-KO} mice upon acute DEN treatment

(A-C) Western blot analysis of liver lysates from both genotypes (untreated and 4 h acute DEN treated mice). Protein content was determined by using indicated antibodies. Data represent means \pm SEM. ** $p \leq 0.01$ versus controls.

The activation of JNK has been implicated in both, the promotion as well as inhibition of cell death, depending on the stimulus and cell type (200). It was shown that cellular stress leads to JNK activation mediated by tumor necrosis factor receptor 1 (TNFR1), which is the main receptor that induces TNF-induced cellular events such as cell proliferation, differentiation and

apoptosis (201, 202). Additionally, DNA damage-inducible transcript 3 (Ddit3 also known as CHOP) is essential for sensitizing hepatoma cells to TRAIL-induced apoptosis (203) and is known to be activated by the MAPK signaling cascade. Other apoptotic related genes, such as B-cell lymphoma 2 (Bcl-2), Bcl-2-like protein 11 (Bim) and Bcl-2-associated X protein (Bax), are known to be transcriptionally regulated by p38 signaling and play an important role in tumor development (204, 205). Since the loss of sensitivity to apoptosis is a hallmark of cancer, we analyzed the mRNA expression of the pro-apoptotic mediators TNF- α , TNFR1, CHOP, Bcl-2 and Bim in untreated as well as DEN-treated livers of control and MyD88^{L-KO} mice. Interestingly, while mRNA expression of TNF- α in the liver was unaltered in both genotypes and conditions, hepatic TNFR1 and CHOP mRNA expression was significantly increased in DEN-treated control mice compared to untreated control mice. Although untreated MyD88^{L-KO} mice show unaltered mRNA expression of TNFR1 and CHOP compared to untreated control mice, the DEN-induced increase in mRNA expression was blunted in MyD88^{L-KO} mice compared to controls (Fig. 37 A). Consistent with unaltered p38 activation, the hepatic mRNA expression of Bcl-2, Bim and Bax was neither unaltered in untreated control and MyD88^{L-KO} mice, nor induced by DEN in both genotypes (Fig. 37 B).

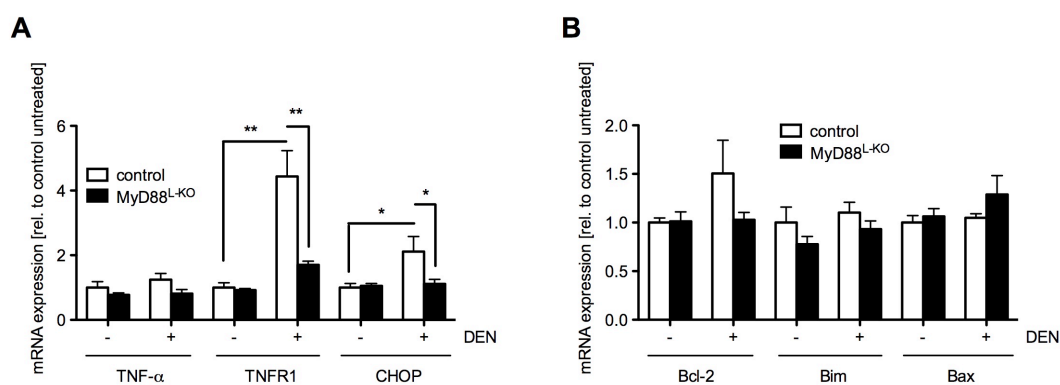


Fig. 37: MyD88^{L-KO} mice exhibit decreased pro-apoptotic marker expression

(A-B) Relative mRNA expression of indicated genes in livers of control and MyD88^{L-KO} mice, determined by quantitative RT-PCR (n=6/genotype). Quantitative RT-PCR was performed on mRNA isolated from livers of untreated as well as DEN treated mice. Data are means \pm SEM. * p \leq 0.05; ** p \leq 0.01 versus controls.

Taken together, these data indicate that hepatic MyD88 signaling is essential for the activation of JNK in DEN-induced HCC, whereas ERK1/2 and p38 activation is MyD88 independent in tumor livers. Additionally, the decreased activation of JNK is possibly due to reduced mRNA expression of TNFR, which presumably translates into impaired induction of CHOP mRNA expression. Since ERK1/2 and p38 activation is unaltered between both genotypes, the reduction of CHOP mRNA expression upon DEN treatment in MyD88^{L-KO} mice does not reach significance when compared to control mice. However, during the early phase of HCC development upon 4 h acute DEN treatment, JNK activation was similar between MyD88^{L-KO} and control mice.

4. Discussion

Over the last decades, chronic inflammation has been linked to the development of various diseases, such as obesity-associated insulin resistance and cancer. However, the underlying mechanisms through which chronic inflammation induces these disorders have not been fully elucidated yet and just begin to emerge. It has been reported earlier that under conditions of obesity, the expression of the pro-inflammatory cytokine TNF- α in adipose tissue is increased, thereby leading to the development of insulin resistance, whereas neutralisation of TNF- α in these mice leads to improved insulin sensitivity (60). Additional work has revealed, that obesity represents a state of chronic, low-grade inflammation, characterized by elevated plasma concentrations of inflammation-associated factors, such as TNF- α , Interleukin-6 (IL-6) and Interleukin-1 β (IL-1 β), which in turn may contribute to the development of insulin resistance (65-68). These cytokines are released from inflamed tissue during the course of obesity, such as WAT and liver. On the other hand, increased number of immune cells in neoplastic tissue might be an indicator for the connection between inflammation and cancer (103).

The Toll-like receptor (TLR) signaling pathway, a classic signaling cascade in innate immunity, as well as the TLR signaling target proteins, NF- κ B and JNK, are crucial regulators for the production of cytokines and are associated with tumor promotion and the development of obesity-associated insulin resistance (118, 140, 149). However, the role of hepatocyte specific TLR signaling in inflammatory-associated diseases, such as obesity-associated insulin resistance and hepatocellular carcinoma, were not elucidated.

In this study, the conditional gene targeting has been applied to hepatocyte specific disruption of either the key receptor of mediating IL-6 signaling or TLR signaling to examine the effect of inflammatory mediators in the liver on the development of obesity-associated insulin resistance and chemically induced hepatocellular carcinoma, respectively. To this end, IL-6R α ^{FL/FL} mice were

crossed with ALFP-Cre mice and offspring carrying the homozygous loxP-flanked allele and the Cre transgene were used to determine the effect of hepatic IL-6 signaling on glucose homeostasis. In order to specifically inactivate TLR signaling in hepatocytes, mice carrying a conditional allele for the essential adaptor molecule MyD88 were crossed to ALFP-Cre mice and phenotypically characterized for the development of insulin resistance and HCC pathogenesis.

4.1 The ALFP-Cre transgene mediates specific inactivation of the loxP-flanked IL-6R α or MyD88 alleles in hepatocytes

The Cre-loxP system is a site-specific recombinase system, used to manipulate genomic DNA sequences in mammals and other species by inversion, excision or translocation of loxP-modified DNA sequences (206, 207). The tissue specific, Cre-mediated recombination is performed using a cell-specific promoter driving the Cre expression. Since expression of the Cre recombinase under control of the albumin promoter/ α -fetoprotein enhancer (ALFP), is restricted to hepatocytes (165), mice harboring the transgenic ALFP-Cre allele were used in this study to delete either IL-6R α or MyD88 selectively in hepatocytes.

The function of IL-6 in the development of obesity-induced insulin resistance is controversially discussed (77). In order to address the specific role of inflammatory signaling downstream of the IL-6R α in hepatocytes on insulin action and glucose homeostasis *in vivo*, the IL-6R α was specifically ablated in hepatocytes. For this, mice bearing the loxP-flanked IL-6R α allele were crossed with mice harboring the transgenic ALFP-Cre allele to obtain hepatocyte specific disruption of the IL-6R α . We verified the selective and efficient deletion of the IL-6R α allele in hepatocytes of IL-6R α ^{L-KO} mice on the genomic DNA and mRNA levels. Strikingly, IL-6R α deficiency in hepatocytes did not affect liver weight, histomorphological liver structure as well as circulating sIL-6R α levels.

On the other hand, to investigate the role of TLR signaling specifically in the liver, we created mice lacking hepatic MyD88 by crossing MyD88^{FL/FL} and ALFP-Cre mice. Specific ablation of MyD88 in hepatocytes of MyD88^{L-KO} mice was verified on mRNA and protein levels. These results indicate that the ALFP-Cre transgene excise loxP-flanked MyD88 specifically and efficiently in hepatocytes, without affecting liver weight and liver morphology.

Taken together, the IL-6R α ^{L-KO} mice as well as MyD88^{L-KO} mice were successfully generated to study the hepatic role of either pathway in the development of obesity-associated diseases.

4.2 Hepatocyte specific disruption of the IL-6R α impairs glucose homeostasis and insulin sensitivity

Currently, the role of IL-6 signaling in energy homeostasis, obesity and insulin resistance is controversially debated. While systemic lack of IL-6 signaling leads to development of mature onset obesity (167), mice lacking hepatic IL-6 signaling exhibit no alterations in energy homeostasis and body weight gain. Moreover, the circulating leptin levels were comparable between control and IL-6R α ^{L-KO} groups of mice, which is accompanied with equal amount of food being consumed in both, IL-6R α ^{L-KO} and control mice. Although these data indicate that hepatic IL-6 signaling is not essential for maintaining energy homeostasis, the loss of hepatic IL-6 signaling impairs glucose homeostasis as IL-6R α ^{L-KO} mice showed impaired glucose clearance during glucose tolerance tests. These experiments are in line with observations that IL-6 treatment increases glucose tolerance in rats (84).

Hepatic insulin resistance leads to the impaired suppression of hepatic glucose production under feeding conditions and thus exhibit a crucial impact on the impairment of whole body glucose metabolism (208). IL-6 signaling plays an important role in the development of hepatic insulin resistance during obesity (80, 209). To investigate the role of hepatic IL-6 signaling in the

development of insulin resistance in control and IL-6R α ^{L-KO} mice, euglycemic-hyperinsulinemic clamp studies were performed and insulin-mediated phosphorylation of AKT in the liver was assessed. During euglycemic-hyperinsulinemic clamp, insulin's ability to mediate AKT activation was blunted in IL-6R α ^{L-KO} mice compared to control mice, revealing the development of hepatic insulin resistance in these mice. This indicates that hepatic IL-6 signaling is essential for the maintenance of hepatic insulin sensitivity. However, the suppression of hepatic glucose production was unchanged between both genotypes, presumably due to the fact, that hepatic glucose output does not only represent glucose production, but also hepatic glucose usage, such as glycogenolysis and gluconeogenesis. Since glucose cycling between glucose and G6P are important mechanisms in regulating glucose homeostasis, we determined the levels of two prominent enzymes, the G6Pase and the GK, that exhibit key roles in regulation of these processes (55, 57). Interestingly, IL-6 is able to downregulate G6Pase expression and thereby reducing hepatic glucose output (85). Here, we confirm the inhibitory action of IL-6 on insulin-mediated suppression of G6Pase. Although, hepatic G6Pase mRNA expression in IL-6R α ^{L-KO} mice is largely suppressed during hyperinsulinemic-euglycemic clamps compared to the fasted state, G6Pase mRNA and protein expression are significantly increased at the steady state phase of IL-6R α ^{L-KO} mice compared to control mice. In contrast, insulin's ability to increase mRNA expression of the G6Pase counteracting glucokinase was significantly enhanced in IL-6R α ^{L-KO} mice compared to control mice, thus promoting glycogen synthesis. This in turn, explains the minor net effect on total hepatic glucose output in IL-6R α ^{L-KO} mice. Taken together, the study provides *in vivo* evidence for partly counteracting effects of IL-6 in hepatic glucose metabolism.

Other key insulin sensitive tissues, such as skeletal muscle and WAT, are susceptible to the development of local insulin resistance in presence of increased caloric intake, thus leading to decreased stimulation of glucose disposal and ultimately resulting in the development of impaired glucose homeostasis (170). IL-6 action increases muscle insulin sensitivity (210) and

IL-6 levels are elevated during exercise (211), a situation in which glucose uptake is crucial for energy supply of skeletal muscle. The consequence of blunted hepatic IL-6 signaling was assessed on muscle insulin sensitivity. To gain insight in the insulin responsiveness in skeletal muscle and WAT, the insulin stimulated glucose uptake was determined during hyperinsulinemic-euglycemic clamp study. The results revealed a significantly reduced glucose uptake in skeletal muscle and WAT of IL-6R α ^{L-KO} mice compared to control mice. Moreover, the efficiency of insulin to stimulate AKT phosphorylation in skeletal muscle was significantly reduced in IL-6R α ^{L-KO} mice compared to control mice, implying the development of systemic insulin resistance in IL-6R α ^{L-KO} mice compared to control mice. Consistent with these findings, insulin's ability to lower blood glucose levels during insulin tolerance tests was significantly reduced in IL-6R α ^{L-KO} mice compared to control mice.

Earlier observations of increased systemic insulin sensitivity and improved glucose tolerance upon IL-6 injection in mice, (84) as well as our findings, support the notion that IL-6 signaling is essential in protecting from the development of obesity-associated insulin resistance.

4.3 Crosstalk between hepatocytes and Kupffer cells through hepatic IL-6 signaling controls the inflammatory tone

We demonstrate that during euglycemic-hyperinsulinemic clamp studies, IL-6 expression is increased in liver, skeletal muscle and WAT, resulting in increased circulating IL-6 concentrations. Additionally, increased expression of TNF- α and IL-10 was also observed in liver and skeletal muscle, whereas only selectively elevated levels of circulating IL-6 and TNF- α were observed in both genotypes. Consistent with the observations of elevated IL-6 and TNF- α levels in circulation, downstream signaling events mediated by IL-6 and TNF- α , such as phosphorylation of I κ B α and STAT-3, were increased in liver and muscle under euglycemic-hyperinsulinemic clamp conditions. Thus, euglycemic-hyperinsulinemic clamp conditions promote an elevated

pro-inflammatory tone and thereby indicate an important contribution of IL-6 in maintaining glucose homeostasis during euglycemic-hyperinsulinemic clamp studies (83, 212).

Although IL-6 seems to act as both pro-inflammatory as well as anti-inflammatory cytokine (213), our study reveals an overall clear anti-inflammatory role for IL-6 signaling in the liver. Consistent findings demonstrated that IL-6 acts as negative feedback regulator of inflammatory signaling pathways in macrophages. On the one hand, the stimulation of macrophages with IL-6 leads to the production of IL-1 receptor antagonists (IL-1R α) as well as soluble TNF receptor p55 (TNFRp55), thereby inhibiting the inflammatory response (214). On the other hand, IL-6 deficient macrophages were shown to have an increased inflammatory response upon lipopolysaccharide stimulation, indicated by elevated expression of TNF- α (172), suggesting that IL-6 can function rather as anti- than pro-inflammatory cytokine to limit the inflammatory tone.

However, in our study, ablation of hepatic IL-6 signaling promotes an activation of inflammatory cytokine expression in liver-resident macrophages (Kupffer cells), indicating an IL-6 dependent crosstalk of hepatocytes to the neighboring Kupffer cells to limit inflammation. The Kupffer cell activation in the IL-6R α ^{L-KO} mice not only induces a hepatic inflammatory response, but also induces increased expression of IL-6, TNF- α and IL-10 in skeletal muscle and WAT, presumably as a consequence of increased Kupffer cell derived TNF- α .

In addition to the role of hepatic IL-6 action in limiting local and systemic inflammation, this study also revealed the functional significance of Kupffer cell activation, which leads to increased TNF- α expression in the IL-6R α ^{L-KO} mice, resulting in impaired glucose homeostasis. Ablation of Kupffer cells or neutralization of TNF- α action in IL-6R α ^{L-KO} mice restored the impaired glucose tolerance in IL-6R α ^{L-KO} mice to normal.

However, whether the development of insulin resistance in IL-6R α ^{L-KO} mice is a consequence of systemic increased IL-6 concentrations leading to the subsequent activation of IL-6 signaling in other tissues than the liver cannot be excluded in this study. Nevertheless, unaltered STAT-3 phosphorylation in skeletal muscle of IL-6R α ^{L-KO} mice indicates a negligible effect of increased IL-6 action in skeletal muscle in the development of insulin resistance.

Besides the elevated chronic systemic inflammation, which leads to the development of insulin resistance, our experiments also indicate that activation of proinflammatory signaling can simultaneously impair β -cell function. This is consistent with the notion that inflammatory cytokines, especially TNF- α , are able to inhibit insulin release from the β -cells (215, 216).

Given these complex effects of IL-6 signaling on hepatic metabolism and the initiation of a systemic inflammatory response upon inhibition of IL-6 signaling, caution should be warranted to potential diabetogenic side effects of newly evolving therapies aiming to interfere with IL-6 signaling to treat chronic inflammatory diseases, such as rheumatoid arthritis (217, 218).

4.5 The role of hepatic MyD88 in energy homeostasis

Recent data indicate that innate immune response pathways are involved in the development of obesity-associated insulin resistance (173). Although the molecular mechanisms, underlying the development of obesity-associated insulin resistance, are still not elucidated, recent observations suggest an unexpected role for MyD88 in preventing diabetes (177). In this study, the authors show that mice carrying MyD88 deficiency on a high fat diet (HFD) had increased circulating levels of insulin, leptin and cholesterol, as well as liver dysfunction. In our study, we could clearly demonstrate that mice lacking MyD88 exclusively in hepatocytes exhibit no alterations in energy homeostasis and body weight gain when fed a normal chow diet (NCD).

Additionally, lipid metabolism, glucose tolerance and insulin sensitivity were unchanged between MyD88^{L-KO} and control mice, indicating that hepatic MyD88^{L-KO} is not essential for maintaining both energy homeostasis and glucose homeostasis on NCD. Interestingly, it was previously shown that mice lacking systemic TLR4, which mainly transduce signaling via MyD88, were protected from FFA-induced insulin resistance upon 8 hour lipid infusion (113, 219). Additional data reveal that MyD88 dependent signaling in the CNS is a key regulator of diet-induced leptin and insulin resistance *in vivo*, since MyD88^{ΔCNS} mice are protected from HFD-induced weight gain and from the induction of leptin resistance by acute central application of palmitate (178). Therefore, an approach of investigating energy homeostasis with MyD88^{L-KO} mice fed a HFD would be interesting.

4.6 MyD88 dependent signaling in the liver promotes chemically induced HCC

DEN-induced hepatocarcinogenesis has given new insights into the development of liver cancer in humans. The MyD88 adaptor molecule of the TLR signaling cascade plays an essential role in TLR-mediated development of insulin resistance and liver carcinogenesis. Consistent with the observations of decreased DEN-induced tumor development in mice lacking MyD88 (118), our study reveals an important role of hepatocytes in this phenotype, since mice lacking hepatic MyD88 signaling exhibit a similarly decreased susceptibility to the development of chemically induced HCC formation, although other cells, e.g. Kupffer cells, are not affected in our model. Necrotic debris released by DEN-injured hepatocytes not only activates Kupffer cells, but also triggers immune cell infiltration in a MyD88 dependent manner. To this end, MyD88^{L-KO} mice exhibit reduced hepatic infiltration upon DEN challenge. Which mechanism accounts for the reduced immune cell attraction in MyD88^{L-KO} mice is not clear, since the chemokines analyzed in this study appeared to be unaltered between the genotypes. Identification of factors, leading to the reduced hepatic infiltration upon DEN

challenge in MyD88^{L-KO} mice, is important and will be performed in the near future. Moreover, while MyD88^{L-KO} mice exhibit reduced markers of liver injury, the hepatotoxic effect of DEN is decreased, which in turn could reduce immune cell attraction.

However, the induction of liver injury in MyD88^{L-KO} mice was not IL-6 dependent as shown previously (118), since IL-6 levels were unchanged between control and MyD88^{L-KO} mice. Our data rather suggest an important role of the IL-6 class cytokine leukemia inhibitory factor (LIF). Whereas DEN-induced HCC development leads to activation of LIF expression in control animals, the MyD88^{L-KO} mice show significantly decreased induction of this cytokine. Consistent with our findings, another study implies elevated LIF as HCC inducer (220). In this study, the authors show that miR-637 acted as a tumor-suppressor by the inhibition of LIF expression and thereby disruption of STAT-3 activation. While this might explain the phenotype in the latter model, this notion could not be applied to MyD88^{L-KO} mice, since we did not observe an elevated DNA-binding capacity of STAT-3 due to increased LIF mRNA expression in control mice. Nevertheless, activation of STAT-3 was induced in HCC and upon acute DEN treatment. Possible reasons for the observations of unaltered DNA-binding capacity of STAT-3 in HCC could be the unaltered IL-6 mRNA expression, which is a really strong STAT-3 activator and thus attenuate the increased LIF expression. Additionally, the determination of hepatic LIF at the protein level is essential in this context.

Other mechanisms involved in decreased tumor formation in MyD88^{L-KO} mice might be the impairment of NF- κ B and MAPK signaling. The NF- κ B and MAPK signaling pathways are connected and often deregulated in various types of tumors, including HCC (124). While ablation of NF- κ B and p38 leads to hypersusceptibility to DEN-induced hepatocarcinogenesis by elevated JNK activation, the deletion of JNK in this context reverses the increased susceptibility to HCC upon DEN treatment (141). Additionally, previous studies indicate that the activation of MAPKs upon liver damage is mediated by MyD88 dependent TLR signaling (221, 222). Since the observations of

reduced p65 activation and simultaneously decreased JNK activation in hepatocytes of DEN-induced HCC in MyD88^{L-KO} mice, we could demonstrate that activation of NF- κ B and JNK signaling in the liver is dependent on hepatic MyD88 signaling after liver injury. Additionally, our study reveals a minor role of hepatic MyD88 in activating p38 and ERK upon DEN treatment. We also confirmed the relation of active JNK to the development of HCC (141), since reduced JNK activation goes along with decreased HCC in MyD88^{L-KO} mice. However, the activation of JNK in early stages of tumor development occurred independent of MyD88 since acute DEN treatments for 4 h revealed JNK activation in MyD88^{L-KO} mice similarly as control mice. So it seems, that elevation of JNK at the early phase of tumor development has no impact on MyD88 related reduction of tumor development, but at later stages of HCC.

It was shown that cellular stress leads to JNK activation mediated by TNFR1. In contrast to previous studies, where liver injury upon DEN treatment was dependent on MyD88 signaling but not through TNFR1 (118), we observe a strong induction of TNFR1 upon DEN treatment, whereas accumulation of TNF- α mRNA was unaltered. Furthermore, the induction of TNFR mRNA expression was dependent on hepatic MyD88 signaling, since MyD88^{L-KO} mice show blunted TNFR1 mRNA expression in DEN-induced HCC. To define whether the reduction of JNK activation in HCC is due to higher sensitivity to TNF-induced apoptosis, needs more investigations.

The molecular and cellular interactions in MyD88 dependent HCC development are still unclear. However, future studies will reveal whether the reduction in JNK signaling is responsible for the reduced tumor load. For this, we will overactivate JNK with a conditional transgene specifically in MyD88 deficient hepatocytes.

5. Summary

Over the last decade, obesity has been recognized as a chronic low inflammatory state that predisposes for the development of diseases, such as obesity-associated insulin resistance and cancer. The chronic low grade inflammation under obese conditions manifests not only as increase of inflammatory mediators, such as TNF- α and IL-6 in circulation, but also in elevated free fatty acids in the bloodstream. Though, this inflammatory condition has been shown to impair insulin action and to increase the incidence of cancer development. The liver specific contribution of IL-6 signaling as well as TLR signaling through the essential adaptor molecule MyD88 in these processes remains unclear.

To examine the role of hepatic IL-6 signaling in glucose homeostasis, we have conditionally inactivated the IL-6R α in hepatocytes of mice (IL-6R α ^{L-KO}). While these animals showed no alterations in body weight gain and body fat content, IL-6R α ^{L-KO} mice developed systemic insulin resistance, manifested as attenuated insulin stimulated glucose transport in skeletal muscle and fat during hyperinsulinemic-euglycemic clamps. Insulin resistance in these mice developed in the presence of increased circulating levels of IL-6 and TNF- α that directly translated in enhanced activation of inflammatory signaling in liver and skeletal muscle, thereby impairing insulin action. Neutralization of TNF- α or ablation of Kupffer cells restored glucose tolerance in IL-6R α ^{L-KO} mice to normal, indicating that increased circulating TNF- α , derived from the Kupffer cells, impairs insulin action systemically. Thus, our results reveal an unexpected role for hepatic IL-6 signaling to limit hepatic inflammation and to protect from local and systemic insulin resistance.

Moreover, TLR-mediated signaling was examined in the development of insulin resistance and HCC, using mice with hepatocyte-specific MyD88 deficiency (MyD88^{L-KO} mice). While glucose homeostasis was largely unaltered, these mice exhibited decreased liver damage, reduced hepatic

macrophage infiltration and a strong reduction in chemically induced hepatocellular carcinoma development. Interestingly, tumor livers of MyD88^{L-KO} mice exhibit reduced JNK activation that could potentially account for the reduced liver tumorigenesis in these animals.

Taken together, this study highlights the hepatic role of inflammatory IL-6 and TLR-induced signaling in the development of obesity-associated insulin resistance and hepatocellular carcinogenesis.

6. Zusammenfassung

In den letzten zehn Jahren wurde Adipositas als chronischer Entzündungszustand anerkannt, der den Körper für die Entstehung von Krankheiten, wie Adipositas-assoziierte Insulinresistenz und Krebs, anfällig macht. Dieser chronische Entzündungszustand äussert sich nicht nur durch die Erhöhung von inflammatorischen Zytokinen, wie z.B. TNF- α und IL-6, sondern auch von freien Fettsäuren im Blut. Frühere Studien haben gezeigt, dass dieser Zustand zur Beeinträchtigung der Insulinwirkung und Erhöhung der Krebsprävalenz führt.

Zur Untersuchung der Rolle des IL-6 Signaltransduktionsweges auf den Glukosehaushalt wurde das IL-6R α Gen in Hepatozyten von Mäusen (IL-6R α ^{L-KO}) konditional inaktiviert. Während diese Mäuse sich nicht in ihrer Gewichtszunahme und ihrem Körperfett unterschieden, entwickelten die IL-6R α ^{L-KO} Mäuse eine systemische Insulinresistenz, welche sich in Euglykämischen-Hyperinsulinämischen Clamp-Studien in einem gestörten Glukosetransport in die Skelettmuskulatur und ins Fettgewebe manifestierten. Diese resultierte aufgrund von erhöhter Konzentration der zirkulierenden Zytokinen IL-6 und TNF- α im Blutspiegel, welche zu einer ansteigenden Immunantwort in der Leber und in der Skelettmuskulatur führte. Die Neutralisation von TNF- α oder die Ablation der Kupffer-Zellen in IL-6R α ^{L-KO} Mäusen führten zu einer Normalisierung der Glukosetoleranz. Dadurch wurde gezeigt, dass die Beeinträchtigung der Insulinwirkung wahrscheinlich durch erhöhte TNF- α Ausschüttung aus Kupffer-Zellen zustande kommt. So zeigen unsere Ergebnisse eine unerwartete Rolle des leberspezifischen IL-6 Signaltransduktionweges in der Verhinderung lokaler und systemischer Insulinresistenz, durch die Limitierung der leberspezifischen Inflammation.

Darüber hinaus wurde die Rolle der TLR-vermittelten Signaltransduktion in der Entwicklung von Insulinresistenz und hepatozellulären Karzinomen, mit Hilfe von Mäusen denen Hepatozyten spezifisches MyD88 fehlt (MyD88^{L-KO}),

untersucht. Während die Glukose Homeostase hauptsächlich unverändert war, zeigten diese Mäuse verminderten Leberschaden, verminderte Infiltration von Makrophagen in der Leber, so wie eine starke Reduktion von chemisch induzierten hepatozellulären Karzinomen. Interessanterweise war die Aktivierungen von JNK in den Tumor befallenen Lebern der MyD88^{L-KO} Mäusen reduziert, was eventuell zur verminderten Ausbildung der Hepatozellulären Karzinomen in diesen Mäusen verantwortlich ist.

Zusammenfassend kann man sagen, dass diese Studie deutliche Hinweise auf die leberspezifischen Rollen der IL-6 und TLR-vermittelten Signaltransduktion in der Ausbildung von Adipositas-assoziieter Insulinresistenz sowie hepatozellulären Karzinomen liefert.

7. References

1. WHO. 2010. Global status report on noncommunicable diseases 2010.
2. Hubert, H. B., M. Feinleib, P. M. McNamara, and W. P. Castelli. 1983. Obesity as an independent risk factor for cardiovascular disease: a 26-year follow-up of participants in the Framingham Heart Study. *Circulation* 67:968-977.
3. Mokdad, A. H., E. S. Ford, B. A. Bowman, W. H. Dietz, F. Vinicor, V. S. Bales, and J. S. Marks. 2003. Prevalence of obesity, diabetes, and obesity-related health risk factors, 2001. *JAMA* 289:76-79.
4. Semenkovich, C. F. 2006. Insulin resistance and atherosclerosis. *J Clin Invest* 116:1813-1822.
5. Calle, E. E., C. Rodriguez, K. Walker-Thurmond, and M. J. Thun. 2003. Overweight, obesity, and mortality from cancer in a prospectively studied cohort of U.S. adults. *N Engl J Med* 348:1625-1638.
6. Dixon, J. B. The effect of obesity on health outcomes. *Mol Cell Endocrinol* 316:104-108.
7. Withrow, D., and D. A. Alter. The economic burden of obesity worldwide: a systematic review of the direct costs of obesity. *Obes Rev* 12:131-141.
8. Kleiber, M. 1947. Body size and metabolic rate. *Physiol Rev* 27:511-541.
9. Spiegelman, B. M., and J. S. Flier. 2001. Obesity and the regulation of energy balance. *Cell* 104:531-543.
10. Galgani, J., and E. Ravussin. 2008. Energy metabolism, fuel selection and body weight regulation. *Int J Obes (Lond)* 32 Suppl 7:S109-119.
11. Schwartz, M. W. 2006. Central nervous system regulation of food intake. *Obesity (Silver Spring)* 14 Suppl 1:1S-8S.
12. Heyman, M. B., V. R. Young, P. Fuss, R. Tsay, L. Joseph, and S. B. Roberts. 1992. Underfeeding and body weight regulation in normal-weight young men. *Am J Physiol* 263:R250-257.
13. Bernstein, I. L., E. C. Lotter, P. J. Kulkosky, D. Porte, Jr., and S. C. Woods. 1975. Effect of force-feeding upon basal insulin levels of rats. *Proc Soc Exp Biol Med* 150:546-548.
14. Woods, S. C., R. J. Seeley, D. Porte, Jr., and M. W. Schwartz. 1998. Signals that regulate food intake and energy homeostasis. *Science* 280:1378-1383.

15. Edholm, O. G. 1977. Energy balance in man studies carried out by the Division of Human Physiology, National Institute for Medical Research. *J Hum Nutr* 31:413-431.
16. Newnham, J. P., C. E. Pennell, S. J. Lye, J. Rampono, and J. R. Challis. 2009. Early life origins of obesity. *Obstet Gynecol Clin North Am* 36:227-244, xii.
17. Krebs, J. R. 2009. The gourmet ape: evolution and human food preferences. *Am J Clin Nutr* 90:707S-711S.
18. Bellisari, A. 2008. Evolutionary origins of obesity. *Obes Rev* 9:165-180.
19. Kahn, B. B., and J. S. Flier. 2000. Obesity and insulin resistance. *J Clin Invest* 106:481.
20. Benito, M. Tissue-specificity of insulin action and resistance. *Arch Physiol Biochem* 117:96-104.
21. Steiner, D. F., D. Cunningham, L. Spigelman, and B. Aten. 1967. Insulin biosynthesis: evidence for a precursor. *Science* 157:697-700.
22. Wardzala, L. J., and B. Jeanrenaud. 1981. Potential mechanism of insulin action on glucose transport in the isolated rat diaphragm. Apparent translocation of intracellular transport units to the plasma membrane. *J Biol Chem* 256:7090-7093.
23. Birnbaum, M. J. 1992. The insulin-sensitive glucose transporter. *Int Rev Cytol* 137:239-297.
24. Kahn, C. R. 1994. Banting Lecture. Insulin action, diabetogenes, and the cause of type II diabetes. *Diabetes* 43:1066-1084.
25. Pilkis, S. J., and D. K. Granner. 1992. Molecular physiology of the regulation of hepatic gluconeogenesis and glycolysis. *Annu Rev Physiol* 54:885-909.
26. Peterson, J. D., and D. F. Steiner. 1975. The amino acid sequence of the insulin from a primitive vertebrate, the atlantic hagfish (*Myxine glutinosa*). *J Biol Chem* 250:5183-5191.
27. Roth, J. 1973. Peptide hormone binding to receptors: a review of direct studies in vitro. *Metabolism* 22:1059-1073.
28. Kahn, C. R., K. L. Baird, D. B. Jarrett, and J. S. Flier. 1978. Direct demonstration that receptor crosslinking or aggregation is important in insulin action. *Proc Natl Acad Sci U S A* 75:4209-4213.
29. White, M. F., J. N. Livingston, J. M. Backer, V. Lauris, T. J. Dull, A. Ullrich, and C. R. Kahn. 1988. Mutation of the insulin receptor at tyrosine 960 inhibits signal transmission but does not affect its tyrosine kinase activity. *Cell* 54:641-649.

30. White, M. F., S. E. Shoelson, H. Keutmann, and C. R. Kahn. 1988. A cascade of tyrosine autophosphorylation in the beta-subunit activates the phosphotransferase of the insulin receptor. *J Biol Chem* 263:2969-2980.
31. Eck, M. J., S. Dhe-Paganon, T. Trub, R. T. Nolte, and S. E. Shoelson. 1996. Structure of the IRS-1 PTB domain bound to the juxtamembrane region of the insulin receptor. *Cell* 85:695-705.
32. Miralpeix, M., X. J. Sun, J. M. Backer, M. G. Myers, Jr., E. Araki, and M. F. White. 1992. Insulin stimulates tyrosine phosphorylation of multiple high molecular weight substrates in Fao hepatoma cells. *Biochemistry* 31:9031-9039.
33. Burks, D. J., S. Pons, H. Towery, J. Smith-Hall, M. G. Myers, Jr., L. Yenush, and M. F. White. 1997. Heterologous pleckstrin homology domains do not couple IRS-1 to the insulin receptor. *J Biol Chem* 272:27716-27721.
34. Jacobs, A. R., D. LeRoith, and S. I. Taylor. 2001. Insulin receptor substrate-1 pleckstrin homology and phosphotyrosine-binding domains are both involved in plasma membrane targeting. *J Biol Chem* 276:40795-40802.
35. Van Obberghen, E., V. Baron, L. Delahaye, B. Emanuelli, N. Filippa, S. Giorgetti-Peraldi, P. Lebrun, I. Mothe-Satney, P. Peraldi, S. Rocchi, D. Sawka-Verhelle, S. Tartare-Deckert, and J. Giudicelli. 2001. Surfing the insulin signaling web. *Eur J Clin Invest* 31:966-977.
36. Rocchi, S., S. Tartare-Deckert, D. Sawka-Verhelle, A. Gamha, and E. van Obberghen. 1996. Interaction of SH2-containing protein tyrosine phosphatase 2 with the insulin receptor and the insulin-like growth factor-I receptor: studies of the domains involved using the yeast two-hybrid system. *Endocrinology* 137:4944-4952.
37. Myers, M. G., Jr., J. M. Backer, X. J. Sun, S. Shoelson, P. Hu, J. Schlessinger, M. Yoakim, B. Schaffhausen, and M. F. White. 1992. IRS-1 activates phosphatidylinositol 3'-kinase by associating with src homology 2 domains of p85. *Proc Natl Acad Sci U S A* 89:10350-10354.
38. De Fea, K., and R. A. Roth. 1997. Protein kinase C modulation of insulin receptor substrate-1 tyrosine phosphorylation requires serine 612. *Biochemistry* 36:12939-12947.
39. Skolnik, E. Y., A. Batzer, N. Li, C. H. Lee, E. Lowenstein, M. Mohammadi, B. Margolis, and J. Schlessinger. 1993. The function of GRB2 in linking the insulin receptor to Ras signaling pathways. *Science* 260:1953-1955.

40. Terauchi, Y., Y. Tsuji, S. Satoh, H. Minoura, K. Murakami, A. Okuno, K. Inukai, T. Asano, Y. Kaburagi, K. Ueki, H. Nakajima, T. Hanafusa, Y. Matsuzawa, H. Sekihara, Y. Yin, J. C. Barrett, H. Oda, T. Ishikawa, Y. Akanuma, I. Komuro, M. Suzuki, K. Yamamura, T. Kodama, H. Suzuki, S. Koyasu, S. Aizawa, K. Tobe, Y. Fukui, Y. Yazaki, and T. Kadowaki. 1999. Increased insulin sensitivity and hypoglycaemia in mice lacking the p85 alpha subunit of phosphoinositide 3-kinase. *Nat Genet* 21:230-235.
41. Hadari, Y. R., E. Tzahar, O. Nativ, P. Rothenberg, C. T. Roberts, Jr., D. LeRoith, Y. Yarden, and Y. Zick. 1992. Insulin and insulinomimetic agents induce activation of phosphatidylinositol 3'-kinase upon its association with pp185 (IRS-1) in intact rat livers. *J Biol Chem* 267:17483-17486.
42. Ito, T., Y. Sasaki, and J. R. Wands. 1996. Overexpression of human insulin receptor substrate 1 induces cellular transformation with activation of mitogen-activated protein kinases. *Mol Cell Biol* 16:943-951.
43. Whitman, M., C. P. Downes, M. Keeler, T. Keller, and L. Cantley. 1988. Type I phosphatidylinositol kinase makes a novel inositol phospholipid, phosphatidylinositol-3-phosphate. *Nature* 332:644-646.
44. Vanhaesebroeck, B., and D. R. Alessi. 2000. The PI3K-PDK1 connection: more than just a road to PKB. *Biochem J* 346 Pt 3:561-576.
45. Manning, B. D., and L. C. Cantley. 2007. AKT/PKB signaling: navigating downstream. *Cell* 129:1261-1274.
46. Klover, P. J., and R. A. Mooney. 2004. Hepatocytes: critical for glucose homeostasis. *Int J Biochem Cell Biol* 36:753-758.
47. Hirota, K., and A. Fukamizu. Transcriptional regulation of energy metabolism in the liver. *J Recept Signal Transduct Res* 30:403-409.
48. Ramnanan, C. J., D. S. Edgerton, G. Kraft, and A. D. Cherrington. Physiologic action of glucagon on liver glucose metabolism. *Diabetes Obes Metab* 13 Suppl 1:118-125.
49. Bierbrauer, J., and S. Weber-Carstens. [Insulin resistance and protein catabolism in critically ill patients]. *Anesthesiol Intensivmed Notfallmed Schmerzther* 46:268-274; quiz 275.
50. Johnston, D. G., and K. G. Alberti. 1976. Carbohydrate metabolism in liver disease. *Clin Endocrinol Metab* 5:675-702.
51. Braillon, A., J. P. Capron, M. A. Herve, C. Degott, and C. Quenum. 1985. Liver in obesity. *Gut* 26:133-139.

52. Gupta, G., J. A. Cases, L. She, X. H. Ma, X. M. Yang, M. Hu, J. Wu, L. Rossetti, and N. Barzilai. 2000. Ability of insulin to modulate hepatic glucose production in aging rats is impaired by fat accumulation. *Am J Physiol Endocrinol Metab* 278:E985-991.
53. Li, L. O., Y. F. Hu, L. Wang, M. Mitchell, A. Berger, and R. A. Coleman. Early hepatic insulin resistance in mice: a metabolomics analysis. *Mol Endocrinol* 24:657-666.
54. Yoshiuchi, I., R. Shingu, H. Nakajima, T. Hamaguchi, Y. Horikawa, T. Yamasaki, T. Oue, A. Ono, J. I. Miyagawa, M. Namba, T. Hanafusa, and Y. Matsuzawa. 1998. Mutation/polymorphism scanning of glucose-6-phosphatase gene promoter in noninsulin-dependent diabetes mellitus patients. *J Clin Endocrinol Metab* 83:1016-1019.
55. Cournarie, F., D. Azzout-Marniche, M. Foretz, C. Guichard, P. Ferre, and F. Foufelle. 1999. The inhibitory effect of glucose on phosphoenolpyruvate carboxykinase gene expression in cultured hepatocytes is transcriptional and requires glucose metabolism. *FEBS Lett* 460:527-532.
56. Froissart, R., M. Piraud, A. M. Boudjemline, C. Vianey-Saban, F. Petit, A. Hubert-Buron, P. T. Eberschweiler, V. Gajdos, and P. Labrune. Glucose-6-phosphatase deficiency. *Orphanet J Rare Dis* 6:27.
57. Mithieux, G. 1996. Role of glucokinase and glucose-6 phosphatase in the nutritional regulation of endogenous glucose production. *Reprod Nutr Dev* 36:357-362.
58. Gregori, C., I. Guillet-Deniau, J. Girard, J. F. Decaux, and A. L. Pichard. 2006. Insulin regulation of glucokinase gene expression: evidence against a role for sterol regulatory element binding protein 1 in primary hepatocytes. *FEBS Lett* 580:410-414.
59. Pollard-Knight, D., and A. Cornish-Bowden. 1982. Mechanism of liver glucokinase. *Mol Cell Biochem* 44:71-80.
60. Hotamisligil, G. S., N. S. Shargill, and B. M. Spiegelman. 1993. Adipose expression of tumor necrosis factor-alpha: direct role in obesity-linked insulin resistance. *Science* 259:87-91.
61. Kern, P. A., M. Saghizadeh, J. M. Ong, R. J. Bosch, R. Deem, and R. B. Simsolo. 1995. The expression of tumor necrosis factor in human adipose tissue. Regulation by obesity, weight loss, and relationship to lipoprotein lipase. *J Clin Invest* 95:2111-2119.
62. Hotamisligil, G. S., P. Arner, J. F. Caro, R. L. Atkinson, and B. M. Spiegelman. 1995. Increased adipose tissue expression of tumor necrosis factor-alpha in human obesity and insulin resistance. *J Clin Invest* 95:2409-2415.

63. Dandona, P., R. Weinstock, K. Thusu, E. Abdel-Rahman, A. Aljada, and T. Wadden. 1998. Tumor necrosis factor-alpha in sera of obese patients: fall with weight loss. *J Clin Endocrinol Metab* 83:2907-2910.
64. Gonzalez, F., K. Thusu, E. Abdel-Rahman, A. Prabhala, M. Tomani, and P. Dandona. 1999. Elevated serum levels of tumor necrosis factor alpha in normal-weight women with polycystic ovary syndrome. *Metabolism* 48:437-441.
65. Mohamed-Ali, V., S. Goodrick, A. Rawesh, D. R. Katz, J. M. Miles, J. S. Yudkin, S. Klein, and S. W. Coppack. 1997. Subcutaneous adipose tissue releases interleukin-6, but not tumor necrosis factor-alpha, in vivo. *J Clin Endocrinol Metab* 82:4196-4200.
66. Bastard, J. P., M. Maachi, J. T. Van Nhieu, C. Jardel, E. Bruckert, A. Grimaldi, J. J. Robert, J. Capeau, and B. Hainque. 2002. Adipose tissue IL-6 content correlates with resistance to insulin activation of glucose uptake both in vivo and in vitro. *J Clin Endocrinol Metab* 87:2084-2089.
67. Esposito, K., A. Pontillo, F. Giugliano, G. Giugliano, R. Marfella, G. Nicoletti, and D. Giugliano. 2003. Association of low interleukin-10 levels with the metabolic syndrome in obese women. *J Clin Endocrinol Metab* 88:1055-1058.
68. Fain, J. N., A. K. Madan, M. L. Hiler, P. Cheema, and S. W. Bahouth. 2004. Comparison of the release of adipokines by adipose tissue, adipose tissue matrix, and adipocytes from visceral and subcutaneous abdominal adipose tissues of obese humans. *Endocrinology* 145:2273-2282.
69. Xu, H., G. T. Barnes, Q. Yang, G. Tan, D. Yang, C. J. Chou, J. Sole, A. Nichols, J. S. Ross, L. A. Tartaglia, and H. Chen. 2003. Chronic inflammation in fat plays a crucial role in the development of obesity-related insulin resistance. *J Clin Invest* 112:1821-1830.
70. Nishimura, S., I. Manabe, M. Nagasaki, K. Eto, H. Yamashita, M. Ohsugi, M. Otsu, K. Hara, K. Ueki, S. Sugiura, K. Yoshimura, T. Kadowaki, and R. Nagai. 2009. CD8+ effector T cells contribute to macrophage recruitment and adipose tissue inflammation in obesity. *Nat Med* 15:914-920.
71. Cai, D., M. Yuan, D. F. Frantz, P. A. Melendez, L. Hansen, J. Lee, and S. E. Shoelson. 2005. Local and systemic insulin resistance resulting from hepatic activation of IKK-beta and NF-kappaB. *Nat Med* 11:183-190.
72. Plomgaard, P., K. Bouzakri, R. Krogh-Madsen, B. Mittendorfer, J. R. Zierath, and B. K. Pedersen. 2005. Tumor necrosis factor-alpha induces skeletal muscle insulin resistance in healthy human subjects

- via inhibition of Akt substrate 160 phosphorylation. *Diabetes* 54:2939-2945.
73. Gale, R. P., R. S. Sparkes, and D. W. Golde. 1978. Bone marrow origin of hepatic macrophages (Kupffer cells) in humans. *Science* 201:937-938.
 74. Naito, M., G. Hasegawa, and K. Takahashi. 1997. Development, differentiation, and maturation of Kupffer cells. *Microsc Res Tech* 39:350-364.
 75. Hebenstreit, D., J. Horejs-Hoeck, and A. Duschl. 2005. JAK/STAT-dependent gene regulation by cytokines. *Drug News Perspect* 18:243-249.
 76. Avruch, J., A. Khokhlatchev, J. M. Kyriakis, Z. Luo, G. Tzivion, D. Vavvas, and X. F. Zhang. 2001. Ras activation of the Raf kinase: tyrosine kinase recruitment of the MAP kinase cascade. *Recent Prog Horm Res* 56:127-155.
 77. Pedersen, B. K., and M. A. Febbraio. 2007. Point: Interleukin-6 does have a beneficial role in insulin sensitivity and glucose homeostasis. *J Appl Physiol* 102:814-816.
 78. Bastard, J. P., C. Jardel, E. Bruckert, P. Blondy, J. Capeau, M. Laville, H. Vidal, and B. Hainque. 2000. Elevated levels of interleukin 6 are reduced in serum and subcutaneous adipose tissue of obese women after weight loss. *J Clin Endocrinol Metab* 85:3338-3342.
 79. Roytblat, L., M. Rachinsky, A. Fisher, L. Greemberg, Y. Shapira, A. Douvdevani, and S. Gelman. 2000. Raised interleukin-6 levels in obese patients. *Obes Res* 8:673-675.
 80. Senn, J. J., P. J. Klover, I. A. Nowak, and R. A. Mooney. 2002. Interleukin-6 induces cellular insulin resistance in hepatocytes. *Diabetes* 51:3391-3399.
 81. Senn, J. J., P. J. Klover, I. A. Nowak, T. A. Zimmers, L. G. Koniaris, R. W. Furlanetto, and R. A. Mooney. 2003. Suppressor of cytokine signaling-3 (SOCS-3), a potential mediator of interleukin-6-dependent insulin resistance in hepatocytes. *J Biol Chem* 278:13740-13746.
 82. Kim, H. J., T. Higashimori, S. Y. Park, H. Choi, J. Dong, Y. J. Kim, H. L. Noh, Y. R. Cho, G. Cline, Y. B. Kim, and J. K. Kim. 2004. Differential effects of interleukin-6 and -10 on skeletal muscle and liver insulin action in vivo. *Diabetes* 53:1060-1067.
 83. Carey, A. L., G. R. Steinberg, S. L. Macaulay, W. G. Thomas, A. G. Holmes, G. Ramm, O. Prelovsek, C. Hohnen-Behrens, M. J. Watt, D. E. James, B. E. Kemp, B. K. Pedersen, and M. A. Febbraio. 2006. Interleukin-6 increases insulin-stimulated glucose disposal in humans

- and glucose uptake and fatty acid oxidation in vitro via AMP-activated protein kinase. *Diabetes* 55:2688-2697.
84. Holmes, A. G., J. L. Mesa, B. A. Neill, J. Chung, A. L. Carey, G. R. Steinberg, B. E. Kemp, R. J. Southgate, G. I. Lancaster, C. R. Bruce, M. J. Watt, and M. A. Febbraio. 2008. Prolonged interleukin-6 administration enhances glucose tolerance and increases skeletal muscle PPARalpha and UCP2 expression in rats. *J Endocrinol* 198:367-374.
 85. Inoue, H., W. Ogawa, A. Asakawa, Y. Okamoto, A. Nishizawa, M. Matsumoto, K. Teshigawara, Y. Matsuki, E. Watanabe, R. Hiramatsu, K. Notohara, K. Katayose, H. Okamura, C. R. Kahn, T. Noda, K. Takeda, S. Akira, A. Inui, and M. Kasuga. 2006. Role of hepatic STAT3 in brain-insulin action on hepatic glucose production. *Cell Metab* 3:267-275.
 86. Saghizadeh, M., J. M. Ong, W. T. Garvey, R. R. Henry, and P. A. Kern. 1996. The expression of TNF alpha by human muscle. Relationship to insulin resistance. *J Clin Invest* 97:1111-1116.
 87. Lang, C. H., C. Dobrescu, and G. J. Bagby. 1992. Tumor necrosis factor impairs insulin action on peripheral glucose disposal and hepatic glucose output. *Endocrinology* 130:43-52.
 88. Cheung, A. T., D. Ree, J. K. Kolls, J. Fuselier, D. H. Coy, and M. Bryer-Ash. 1998. An in vivo model for elucidation of the mechanism of tumor necrosis factor-alpha (TNF-alpha)-induced insulin resistance: evidence for differential regulation of insulin signaling by TNF-alpha. *Endocrinology* 139:4928-4935.
 89. Aguirre, V., T. Uchida, L. Yenush, R. Davis, and M. F. White. 2000. The c-Jun NH(2)-terminal kinase promotes insulin resistance during association with insulin receptor substrate-1 and phosphorylation of Ser(307). *J Biol Chem* 275:9054.
 90. Arkan, M. C., A. L. Hevener, F. R. Greten, S. Maeda, Z. W. Li, J. M. Long, A. Wynshaw-Boris, G. Poli, J. Olefsky, and M. Karin. 2005. IKK-beta links inflammation to obesity-induced insulin resistance. *Nat Med* 11:198.
 91. Hirosumi, J., G. Tuncman, L. Chang, C. Z. Gorgun, K. T. Uysal, K. Maeda, M. Karin, and G. S. Hotamisligil. 2002. A central role for JNK in obesity and insulin resistance. *Nature* 420:333-336.
 92. Croce, C. M. 2008. Oncogenes and cancer. *N Engl J Med* 358:502-511.
 93. WHO. 2008. Cancer Incidence and Mortality Worldwide in 2008. *GLOBOCAN 2008*.

94. El-Serag, H. B., and K. L. Rudolph. 2007. Hepatocellular carcinoma: epidemiology and molecular carcinogenesis. *Gastroenterology* 132:2557-2576.
95. El-Serag, H. B., J. A. Davila, N. J. Petersen, and K. A. McGlynn. 2003. The continuing increase in the incidence of hepatocellular carcinoma in the United States: an update. *Ann Intern Med* 139:817-823.
96. Thorgeirsson, S. S., and J. W. Grisham. 2002. Molecular pathogenesis of human hepatocellular carcinoma. *Nat Genet* 31:339-346.
97. Wang, X. W., S. P. Hussain, T. I. Huo, C. G. Wu, M. Forgues, L. J. Hofseth, C. Brechot, and C. C. Harris. 2002. Molecular pathogenesis of human hepatocellular carcinoma. *Toxicology* 181-182:43-47.
98. Villanueva, A., P. Newell, D. Y. Chiang, S. L. Friedman, and J. M. Llovet. 2007. Genomics and signaling pathways in hepatocellular carcinoma. *Semin Liver Dis* 27:55-76.
99. Yu, M. W., Y. C. Yang, S. Y. Yang, S. W. Cheng, Y. F. Liaw, S. M. Lin, and C. J. Chen. 2001. Hormonal markers and hepatitis B virus-related hepatocellular carcinoma risk: a nested case-control study among men. *J Natl Cancer Inst* 93:1644-1651.
100. Yoshizawa, H. 2002. Hepatocellular carcinoma associated with hepatitis C virus infection in Japan: projection to other countries in the foreseeable future. *Oncology* 62 Suppl 1:8-17.
101. Donato, F., A. Tagger, U. Gelatti, G. Parrinello, P. Boffetta, A. Albertini, A. Decarli, P. Trevisi, M. L. Ribero, C. Martelli, S. Porru, and G. Nardi. 2002. Alcohol and hepatocellular carcinoma: the effect of lifetime intake and hepatitis virus infections in men and women. *Am J Epidemiol* 155:323-331.
102. El-Serag, H. B., H. Hampel, and F. Javadi. 2006. The association between diabetes and hepatocellular carcinoma: a systematic review of epidemiologic evidence. *Clin Gastroenterol Hepatol* 4:369-380.
103. Virchow, R. 1863-1865. Die krankhaften Geschwülste.
104. Coussens, L. M., and Z. Werb. 2002. Inflammation and cancer. *Nature* 420:860-867.
105. Mantovani, A., P. Allavena, A. Sica, and F. Balkwill. 2008. Cancer-related inflammation. *Nature* 454:436-444.
106. Sanz-Cameno, P., M. Trapero-Marugan, M. Chaparro, E. A. Jones, and R. Moreno-Otero. Angiogenesis: from chronic liver inflammation to hepatocellular carcinoma. *J Oncol* 2010:272170.

107. Bisgaard, H. C., and S. S. Thorgeirsson. 1996. Hepatic regeneration. The role of regeneration in pathogenesis of chronic liver diseases. *Clin Lab Med* 16:325-339.
108. Maeda, S. NF-kappaB, JNK, and TLR Signaling Pathways in Hepatocarcinogenesis. *Gastroenterol Res Pract* 2010:367694.
109. Takeuchi, O., and S. Akira. 2001. Toll-like receptors; their physiological role and signal transduction system. *Int Immunopharmacol* 1:625-635.
110. Seki, E., and D. A. Brenner. 2008. Toll-like receptors and adaptor molecules in liver disease: update. *Hepatology* 48:335.
111. Tsung, A., R. Sahai, H. Tanaka, A. Nakao, M. P. Fink, M. T. Lotze, H. Yang, J. Li, K. J. Tracey, D. A. Geller, and T. R. Billiar. 2005. The nuclear factor HMGB1 mediates hepatic injury after murine liver ischemia-reperfusion. *J Exp Med* 201:1135-1143.
112. Lehnardt, S., E. Schott, T. Trimbuch, D. Laubisch, C. Krueger, G. Wulczyn, R. Nitsch, and J. R. Weber. 2008. A vicious cycle involving release of heat shock protein 60 from injured cells and activation of toll-like receptor 4 mediates neurodegeneration in the CNS. *J Neurosci* 28:2320-2331.
113. Shi, H., M. V. Kokoeva, K. Inouye, I. Tzameli, H. Yin, and J. S. Flier. 2006. TLR4 links innate immunity and fatty acid-induced insulin resistance. *J Clin Invest* 116:3015-3025.
114. Shigeoka, A. A., T. D. Holscher, A. J. King, F. W. Hall, W. B. Kiosses, P. S. Tobias, N. Mackman, and D. B. McKay. 2007. TLR2 is constitutively expressed within the kidney and participates in ischemic renal injury through both MyD88-dependent and -independent pathways. *J Immunol* 178:6252-6258.
115. Yamamoto, M., S. Sato, H. Hemmi, S. Uematsu, K. Hoshino, T. Kaisho, O. Takeuchi, K. Takeda, and S. Akira. 2003. TRAM is specifically involved in the Toll-like receptor 4-mediated MyD88-independent signaling pathway. *Nat Immunol* 4:1144-1150.
116. Yamamoto, M., S. Sato, H. Hemmi, H. Sanjo, S. Uematsu, T. Kaisho, K. Hoshino, O. Takeuchi, M. Kobayashi, T. Fujita, K. Takeda, and S. Akira. 2002. Essential role for TIRAP in activation of the signalling cascade shared by TLR2 and TLR4. *Nature* 420:324-329.
117. Kawai, T., and S. Akira. 2006. TLR signaling. *Cell Death Differ* 13:825.
118. Naugler, W. E., T. Sakurai, S. Kim, S. Maeda, K. Kim, A. M. Elsharkawy, and M. Karin. 2007. Gender disparity in liver cancer due to sex differences in MyD88-dependent IL-6 production. *Science* 317:124.
119. Maeda, S., and M. Omata. 2008. Inflammation and cancer: role of nuclear factor-kappaB activation. *Cancer Sci* 99:836-842.

120. Matsumura, T., T. Degawa, T. Takii, H. Hayashi, T. Okamoto, J. Inoue, and K. Onozaki. 2003. TRAF6-NF-kappaB pathway is essential for interleukin-1-induced TLR2 expression and its functional response to TLR2 ligand in murine hepatocytes. *Immunology* 109:127-136.
121. Su, G. L., R. D. Klein, A. Aminlari, H. Y. Zhang, L. Steinstraesser, W. H. Alarcon, D. G. Remick, and S. C. Wang. 2000. Kupffer cell activation by lipopolysaccharide in rats: role for lipopolysaccharide binding protein and toll-like receptor 4. *Hepatology* 31:932-936.
122. Kawai, T., O. Adachi, T. Ogawa, K. Takeda, and S. Akira. 1999. Unresponsiveness of MyD88-deficient mice to endotoxin. *Immunity* 11:115-122.
123. Pearson, G., F. Robinson, T. Beers Gibson, B. E. Xu, M. Karandikar, K. Berman, and M. H. Cobb. 2001. Mitogen-activated protein (MAP) kinase pathways: regulation and physiological functions. *Endocr Rev* 22:153-183.
124. Wagner, E. F., and A. R. Nebreda. 2009. Signal integration by JNK and p38 MAPK pathways in cancer development. *Nat Rev Cancer* 9:537-549.
125. Widmann, C., S. Gibson, M. B. Jarpe, and G. L. Johnson. 1999. Mitogen-activated protein kinase: conservation of a three-kinase module from yeast to human. *Physiol Rev* 79:143-180.
126. Lee, H. C., B. Tian, J. M. Sedivy, J. R. Wands, and M. Kim. 2006. Loss of Raf kinase inhibitor protein promotes cell proliferation and migration of human hepatoma cells. *Gastroenterology* 131:1208-1217.
127. Han, J., J. D. Lee, L. Bibbs, and R. J. Ulevitch. 1994. A MAP kinase targeted by endotoxin and hyperosmolarity in mammalian cells. *Science* 265:808-811.
128. Jiang, Y., C. Chen, Z. Li, W. Guo, J. A. Gegner, S. Lin, and J. Han. 1996. Characterization of the structure and function of a new mitogen-activated protein kinase (p38beta). *J Biol Chem* 271:17920-17926.
129. Lechner, C., M. A. Zahalka, J. F. Giot, N. P. Moller, and A. Ullrich. 1996. ERK6, a mitogen-activated protein kinase involved in C2C12 myoblast differentiation. *Proc Natl Acad Sci U S A* 93:4355-4359.
130. Mertens, S., M. Craxton, and M. Goedert. 1996. SAP kinase-3, a new member of the family of mammalian stress-activated protein kinases. *FEBS Lett* 383:273-276.
131. Remy, G., A. M. Risco, F. A. Inesta-Vaquera, B. Gonzalez-Teran, G. Sabio, R. J. Davis, and A. Cuenda. Differential activation of p38MAPK isoforms by MKK6 and MKK3. *Cell Signal* 22:660-667.

132. Xia, Z., M. Dickens, J. Raingeaud, R. J. Davis, and M. E. Greenberg. 1995. Opposing effects of ERK and JNK-p38 MAP kinases on apoptosis. *Science* 270:1326-1331.
133. Kummer, J. L., P. K. Rao, and K. A. Heidenreich. 1997. Apoptosis induced by withdrawal of trophic factors is mediated by p38 mitogen-activated protein kinase. *J Biol Chem* 272:20490-20494.
134. Nagata, Y., and K. Todokoro. 1999. Requirement of activation of JNK and p38 for environmental stress-induced erythroid differentiation and apoptosis and of inhibition of ERK for apoptosis. *Blood* 94:853-863.
135. Sakurai, T., G. He, A. Matsuzawa, G. Y. Yu, S. Maeda, G. Hardiman, and M. Karin. 2008. Hepatocyte necrosis induced by oxidative stress and IL-1 alpha release mediate carcinogen-induced compensatory proliferation and liver tumorigenesis. *Cancer Cell* 14:156-165.
136. Derijard, B., M. Hibi, I. H. Wu, T. Barrett, B. Su, T. Deng, M. Karin, and R. J. Davis. 1994. JNK1: a protein kinase stimulated by UV light and Ha-Ras that binds and phosphorylates the c-Jun activation domain. *Cell* 76:1025-1037.
137. Weston, C. R., and R. J. Davis. 2007. The JNK signal transduction pathway. *Curr Opin Cell Biol* 19:142-149.
138. Davis, R. J. 2000. Signal transduction by the JNK group of MAP kinases. *Cell* 103:239-252.
139. Hochedlinger, K., E. F. Wagner, and K. Sabapathy. 2002. Differential effects of JNK1 and JNK2 on signal specific induction of apoptosis. *Oncogene* 21:2441-2445.
140. Hui, L., K. Zatloukal, H. Scheuch, E. Stepniak, and E. F. Wagner. 2008. Proliferation of human HCC cells and chemically induced mouse liver cancers requires JNK1-dependent p21 downregulation. *J Clin Invest* 118:3943-3953.
141. Sakurai, T., S. Maeda, L. Chang, and M. Karin. 2006. Loss of hepatic NF-kappa B activity enhances chemical hepatocarcinogenesis through sustained c-Jun N-terminal kinase 1 activation. *Proc Natl Acad Sci U S A* 103:10544-10551.
142. Eferl, R., R. Ricci, L. Kenner, R. Zenz, J. P. David, M. Rath, and E. F. Wagner. 2003. Liver tumor development. c-Jun antagonizes the proapoptotic activity of p53. *Cell* 112:181-192.
143. Nabel, G. J., and I. M. Verma. 1993. Proposed NF-kappa B/I kappa B family nomenclature. *Genes Dev* 7:2063.
144. Karin, M. 2006. Nuclear factor-kappaB in cancer development and progression. *Nature* 441:431-436.

145. Gilmore, T. D. 2006. Introduction to NF-kappaB: players, pathways, perspectives. *Oncogene* 25:6680-6684.
146. Jacobs, M. D., and S. C. Harrison. 1998. Structure of an IkappaBalpha/NF-kappaB complex. *Cell* 95:749-758.
147. Liu, Z. G., H. Hsu, D. V. Goeddel, and M. Karin. 1996. Dissection of TNF receptor 1 effector functions: JNK activation is not linked to apoptosis while NF-kappaB activation prevents cell death. *Cell* 87:565-576.
148. Beg, A. A., and D. Baltimore. 1996. An essential role for NF-kappaB in preventing TNF-alpha-induced cell death. *Science* 274:782-784.
149. Greten, F. R., L. Eckmann, T. F. Greten, J. M. Park, Z. W. Li, L. J. Egan, M. F. Kagnoff, and M. Karin. 2004. IKKbeta links inflammation and tumorigenesis in a mouse model of colitis-associated cancer. *Cell* 118:285-296.
150. Pikarsky, E., R. M. Porat, I. Stein, R. Abramovitch, S. Amit, S. Kasem, E. Gutkovich-Pyest, S. Urieli-Shoval, E. Galun, and Y. Ben-Neriah. 2004. NF-kappaB functions as a tumour promoter in inflammation-associated cancer. *Nature* 431:461-466.
151. Ehlken, H., V. Kondylis, J. Heinrichsdorff, L. Ochoa-Callejero, T. Roskams, and M. Pasparakis. Hepatocyte IKK2 Protects Mdr2 Mice from Chronic Liver Failure. *PLoS One* 6:e25942.
152. Luedde, T., N. Beraza, V. Kotsikoris, G. van Loo, A. Nenci, R. De Vos, T. Roskams, C. Trautwein, and M. Pasparakis. 2007. Deletion of NEMO/IKKgamma in liver parenchymal cells causes steatohepatitis and hepatocellular carcinoma. *Cancer Cell* 11:119-132.
153. Maeda, S., H. Kamata, J. L. Luo, H. Leffert, and M. Karin. 2005. IKKbeta couples hepatocyte death to cytokine-driven compensatory proliferation that promotes chemical hepatocarcinogenesis. *Cell* 121:977-990.
154. Hogan, B., F. Costantini, and E. Lacey. 1986. Manipulating the mouse embryo: A Laboratory Manual. *Cold Spring Harbor Laboratory Press*.
155. Silver, L. M. 1995. Mouse Genetics: Concepts and Applications. *Oxford University Press*:376 pp pp.
156. Ferre, P., A. Leturque, A. F. Burnol, L. Penicaud, and J. Girard. 1985. A method to quantify glucose utilization in vivo in skeletal muscle and white adipose tissue of the anaesthetized rat. *Biochem J* 228:103-110.
157. Van Rooijen, N., and A. Sanders. 1996. Kupffer cell depletion by liposome-delivered drugs: comparative activity of intracellular clodronate, propamidine, and ethylenediaminetetraacetic acid. *Hepatology* 23:1239-1243.

158. Lernmark, A. 1974. The preparation of, and studies on, free cell suspensions from mouse pancreatic islets. *Diabetologia* 10:431-438.
159. Hanninen, P., A. Soini, N. Meltola, J. Soini, J. Soukka, and E. Soini. 2000. A new microvolume technique for bioaffinity assays using two-photon excitation. *Nat Biotechnol* 18:548-550.
160. Scherer, E., and P. Emmelot. 1975. Kinetics of induction and growth of precancerous liver-cell foci, and liver tumour formation by diethylnitrosamine in the rat. *Eur J Cancer* 11:689-696.
161. Chomczynski, P., and P. K. Qasba. 1984. Alkaline transfer of DNA to plastic membrane. *Biochem Biophys Res Commun* 122:340-344.
162. Mullis, K. B., and F. A. Faloona. 1987. Specific synthesis of DNA in vitro via a polymerase-catalyzed chain reaction. *Methods Enzymol* 155:335-350.
163. Saiki, R. K., D. H. Gelfand, S. Stoffel, S. J. Scharf, R. Higuchi, G. T. Horn, K. B. Mullis, and H. A. Erlich. 1988. Primer-directed enzymatic amplification of DNA with a thermostable DNA polymerase. *Science* 239:487-491.
164. Hellman, L. M., and M. G. Fried. 2007. Electrophoretic mobility shift assay (EMSA) for detecting protein-nucleic acid interactions. *Nat Protoc* 2:1849-1861.
165. Kellendonk, C., C. Opherk, K. Anlag, G. Schutz, and F. Tronche. 2000. Hepatocyte-specific expression of Cre recombinase. *Genesis* 26:151-153.
166. Mackiewicz, A., M. Wiznerowicz, E. Roeb, A. Karczewska, J. Nowak, P. C. Heinrich, and S. Rose-John. 1995. Soluble interleukin 6 receptor is biologically active in vivo. *Cytokine* 7:142-149.
167. Wallenius, V., K. Wallenius, B. Ahren, M. Rudling, H. Carlsten, S. L. Dickson, C. Ohlsson, and J. O. Jansson. 2002. Interleukin-6-deficient mice develop mature-onset obesity. *Nat Med* 8:75-79.
168. Carey, A. L., C. R. Bruce, M. Sacchetti, M. J. Anderson, D. B. Olsen, B. Saltin, J. A. Hawley, and M. A. Febbraio. 2004. Interleukin-6 and tumor necrosis factor-alpha are not increased in patients with Type 2 diabetes: evidence that plasma interleukin-6 is related to fat mass and not insulin responsiveness. *Diabetologia* 47:1029-1037.
169. Lazar, M. A. 2005. How obesity causes diabetes: not a tall tale. *Science* 307:373-375.
170. DeFronzo, R. A., R. Gunnarsson, O. Bjorkman, M. Olsson, and J. Wahren. 1985. Effects of insulin on peripheral and splanchnic glucose metabolism in noninsulin-dependent (type II) diabetes mellitus. *J Clin Invest* 76:149-155.

171. Dejager, L., and C. Libert. 2008. Tumor necrosis factor alpha mediates the lethal hepatotoxic effects of poly(I:C) in D-galactosamine-sensitized mice. *Cytokine* 42:55-61.
172. Xing, Z., J. Gauldie, G. Cox, H. Baumann, M. Jordana, X. F. Lei, and M. K. Achong. 1998. IL-6 is an antiinflammatory cytokine required for controlling local or systemic acute inflammatory responses. *J Clin Invest* 101:311-320.
173. Hotamisligil, G. S., and E. Erbay. 2008. Nutrient sensing and inflammation in metabolic diseases. *Nat Rev Immunol* 8:923-934.
174. Uysal, K. T., S. M. Wiesbrock, M. W. Marino, and G. S. Hotamisligil. 1997. Protection from obesity-induced insulin resistance in mice lacking TNF-alpha function. *Nature* 389:610-614.
175. Yuan, M., N. Konstantopoulos, J. Lee, L. Hansen, Z. W. Li, M. Karin, and S. E. Shoelson. 2001. Reversal of obesity- and diet-induced insulin resistance with salicylates or targeted disruption of Ikkbeta. *Science* 293:1673-1677.
176. Tsukumo, D. M., M. A. Carvalho-Filho, J. B. Carvalheira, P. O. Prada, S. M. Hirabara, A. A. Schenka, E. P. Araújo, J. Vassallo, R. Curi, L. A. Velloso, and M. J. Saad. 2007. Loss-of-function mutation in Toll-like receptor 4 prevents diet-induced obesity and insulin resistance. *Diabetes* 56:1998.
177. Hosoi, T., S. Yokoyama, S. Matsuo, S. Akira, and K. Ozawa. Myeloid differentiation factor 88 (MyD88)-deficiency increases risk of diabetes in mice. *PLoS One* 5.
178. Kleinridders, A., D. Schenten, A. C. Könnner, B. F. Belgardt, J. Mauer, T. Okamura, F. T. Wunderlich, R. Medzhitov, and J. C. Brüning. 2009. MyD88 signaling in the CNS is required for development of fatty acid-induced leptin resistance and diet-induced obesity. *Cell Metab* 10:259.
179. Wellen, K. E., and G. S. Hotamisligil. 2003. Obesity-induced inflammatory changes in adipose tissue. *J Clin Invest* 112:1785-1788.
180. Hollister, L. E., J. E. Overall, and H. L. Snow. 1967. Relationship of obesity to serum triglyceride, cholesterol, and uric acid, and to plasma-glucose levels. *Am J Clin Nutr* 20:777-782.
181. Boden, G. 1998. Free fatty acids (FFA), a link between obesity and insulin resistance. *Front Biosci* 3:d169-175.
182. Dullaart, R. P., W. J. Sluiter, L. D. Dikkeschei, K. Hoogenberg, and A. Van Tol. 1994. Effect of adiposity on plasma lipid transfer protein activities: a possible link between insulin resistance and high density lipoprotein metabolism. *Eur J Clin Invest* 24:188-194.

183. Kim, S. J., Y. Choi, Y. H. Choi, and T. Park. Obesity activates toll-like receptor-mediated proinflammatory signaling cascades in the adipose tissue of mice. *J Nutr Biochem*.
184. Balkwill, F., and A. Mantovani. 2001. Inflammation and cancer: back to Virchow? *Lancet* 357:545.
185. Brigati, C., D. M. Noonan, A. Albini, and R. Benelli. 2002. Tumors and inflammatory infiltrates: friends or foes? *Clin Exp Metastasis* 19:247-258.
186. Amacher, E. D. 1998. Serum Transaminase Elevations as Indicators of Hepatic Injury Following the Administration of Drugs. *Regulatory Toxicology and Pharmacology* 27:130.
187. Schmidt, E., and F. W. Schmidt. 1990. Progress in the enzyme diagnosis of liver disease: reality or illusion? *Clin Biochem* 23:375-382.
188. De Ritis, F., M. Coltorti, and G. Giusti. 2006. An enzymic test for the diagnosis of viral hepatitis: the transaminase serum activities. 1957. *Clin Chim Acta* 369:148-152.
189. Scholzen, T., and J. Gerdes. 2000. The Ki-67 protein: from the known and the unknown. *J Cell Physiol* 182:311-322.
190. Racanelli, V., and B. Rehermann. 2006. The liver as an immunological organ. *Hepatology* 43:S54-62.
191. Tacke, F., T. Luedde, and C. Trautwein. 2009. Inflammatory pathways in liver homeostasis and liver injury. *Clin Rev Allergy Immunol* 36:4-12.
192. Hynes, R. O. 2002. Integrins: bidirectional, allosteric signaling machines. *Cell* 110:673-687.
193. Stewart, M., M. Thiel, and N. Hogg. 1995. Leukocyte integrins. *Curr Opin Cell Biol* 7:690-696.
194. Austyn, J. M., and S. Gordon. 1981. F4/80, a monoclonal antibody directed specifically against the mouse macrophage. *Eur J Immunol* 11:815.
195. Hughes, R. C. 1994. Mac-2: a versatile galactose-binding protein of mammalian tissues. *Glycobiology* 4:5-12.
196. Hsia, C. Y., T. I. Huo, S. Y. Chiang, M. F. Lu, C. L. Sun, J. C. Wu, P. C. Lee, C. W. Chi, W. Y. Lui, and S. D. Lee. 2007. Evaluation of interleukin-6, interleukin-10 and human hepatocyte growth factor as tumor markers for hepatocellular carcinoma. *Eur J Surg Oncol* 33:212.
197. Yu, H., D. Pardoll, and R. Jove. 2009. STATs in cancer inflammation and immunity: a leading role for STAT3. *Nat Rev Cancer* 9:798-809.

198. Tai, D. I., S. L. Tsai, Y. H. Chang, S. N. Huang, T. C. Chen, K. S. Chang, and Y. F. Liaw. 2000. Constitutive activation of nuclear factor kappaB in hepatocellular carcinoma. *Cancer* 89:2274-2281.
199. Sato, S., H. Sanjo, K. Takeda, J. Ninomiya-Tsuji, M. Yamamoto, T. Kawai, K. Matsumoto, O. Takeuchi, and S. Akira. 2005. Essential function for the kinase TAK1 in innate and adaptive immune responses. *Nat Immunol* 6:1087-1095.
200. Chang, L., and M. Karin. 2001. Mammalian MAP kinase signalling cascades. *Nature* 410:37-40.
201. Yang, Q., Y. S. Kim, Y. Lin, J. Lewis, L. Neckers, and Z. G. Liu. 2006. Tumour necrosis factor receptor 1 mediates endoplasmic reticulum stress-induced activation of the MAP kinase JNK. *EMBO Rep* 7:622-627.
202. Baud, V., and M. Karin. 2001. Signal transduction by tumor necrosis factor and its relatives. *Trends Cell Biol* 11:372-377.
203. Moon, D. O., S. Y. Park, Y. H. Choi, J. S. Ahn, and G. Y. Kim. Guggulsterone sensitizes hepatoma cells to TRAIL-induced apoptosis through the induction of CHOP-dependent DR5: Involvement of ROS-dependent ER-stress. *Biochem Pharmacol* 82:1641-1650.
204. Chen, Y. J., W. H. Liu, P. H. Kao, J. J. Wang, and L. S. Chang. Involvement of p38 MAPK- and JNK-modulated expression of Bcl-2 and Bax in *Naja nigricollis* CMS-9-induced apoptosis of human leukemia K562 cells. *Toxicol* 55:1306-1316.
205. Lu, J., B. Quearry, and H. Harada. 2006. p38-MAP kinase activation followed by BIM induction is essential for glucocorticoid-induced apoptosis in lymphoblastic leukemia cells. *FEBS Lett* 580:3539-3544.
206. Sternberg, N., D. Hamilton, and R. Hoess. 1981. Bacteriophage P1 site-specific recombination. II. Recombination between loxP and the bacterial chromosome. *J Mol Biol* 150:487-507.
207. Sauer, B., and N. Henderson. 1988. Site-specific DNA recombination in mammalian cells by the Cre recombinase of bacteriophage P1. *Proc Natl Acad Sci U S A* 85:5166-5170.
208. Ferrannini, E., and L. C. Groop. 1989. Hepatic glucose production in insulin-resistant states. *Diabetes Metab Rev* 5:711-726.
209. Klover, P. J., A. H. Clementi, and R. A. Mooney. 2005. Interleukin-6 depletion selectively improves hepatic insulin action in obesity. *Endocrinology* 146:3417-3427.
210. Geiger, P. C., C. Hancock, D. C. Wright, D. H. Han, and J. O. Holloszy. 2007. IL-6 increases muscle insulin sensitivity only at

- superphysiological levels. *Am J Physiol Endocrinol Metab* 292:E1842-1846.
211. Pedersen, B. K., A. Steensberg, C. Fischer, C. Keller, P. Keller, P. Plomgaard, E. Wolsk-Petersen, and M. Febbraio. 2004. The metabolic role of IL-6 produced during exercise: is IL-6 an exercise factor? *Proc Nutr Soc* 63:263-267.
212. Kim, S., C. Domon-Dell, J. Kang, D. H. Chung, J. N. Freund, and B. M. Evers. 2004. Down-regulation of the tumor suppressor PTEN by the tumor necrosis factor-alpha/nuclear factor-kappaB (NF-kappaB)-inducing kinase/NF-kappaB pathway is linked to a default IkappaB-alpha autoregulatory loop. *J Biol Chem* 279:4291.
213. Scheller, J., A. Chalaris, D. Schmidt-Arras, and S. Rose-John. The pro- and anti-inflammatory properties of the cytokine interleukin-6. *Biochim Biophys Acta* 1813:878-888.
214. Tilg, H., E. Trehu, M. B. Atkins, C. A. Dinarello, and J. W. Mier. 1994. Interleukin-6 (IL-6) as an anti-inflammatory cytokine: induction of circulating IL-1 receptor antagonist and soluble tumor necrosis factor receptor p55. *Blood* 83:113-118.
215. Southern, C., D. Schulster, and I. C. Green. 1990. Inhibition of insulin secretion by interleukin-1 beta and tumour necrosis factor-alpha via an L-arginine-dependent nitric oxide generating mechanism. *FEBS Lett* 276:42-44.
216. Zhang, S., and K. H. Kim. 1995. TNF-alpha inhibits glucose-induced insulin secretion in a pancreatic beta-cell line (INS-1). *FEBS Lett* 377:237-239.
217. Choy, E. H., D. A. Isenberg, T. Garrood, S. Farrow, Y. Ioannou, H. Bird, N. Cheung, B. Williams, B. Hazleman, R. Price, K. Yoshizaki, N. Nishimoto, T. Kishimoto, and G. S. Panayi. 2002. Therapeutic benefit of blocking interleukin-6 activity with an anti-interleukin-6 receptor monoclonal antibody in rheumatoid arthritis: a randomized, double-blind, placebo-controlled, dose-escalation trial. *Arthritis Rheum* 46:3143-3150.
218. Nishimoto, N., K. Yoshizaki, N. Miyasaka, K. Yamamoto, S. Kawai, T. Takeuchi, J. Hashimoto, J. Azuma, and T. Kishimoto. 2004. Treatment of rheumatoid arthritis with humanized anti-interleukin-6 receptor antibody: a multicenter, double-blind, placebo-controlled trial. *Arthritis Rheum* 50:1761-1769.
219. Suganami, T., K. Tanimoto-Koyama, J. Nishida, M. Itoh, X. Yuan, S. Mizuarai, H. Kotani, S. Yamaoka, K. Miyake, S. Aoe, Y. Kamei, and Y. Ogawa. 2007. Role of the Toll-like receptor 4/NF-kappaB pathway in saturated fatty acid-induced inflammatory changes in the interaction

- between adipocytes and macrophages. *Arterioscler Thromb Vasc Biol* 27:84-91.
220. Zhang, J. F., M. L. He, W. M. Fu, H. Wang, L. Z. Chen, X. Zhu, Y. Chen, D. Xie, P. Lai, G. Chen, G. Lu, M. C. Lin, and H. F. Kung. Primate-specific miRNA-637 inhibits tumorigenesis in hepatocellular carcinoma by disrupting stat3 signaling. *Hepatology*.
221. Gorina, R., M. Font-Nieves, L. Marquez-Kisinousky, T. Santalucia, and A. M. Planas. Astrocyte TLR4 activation induces a proinflammatory environment through the interplay between MyD88-dependent NFkappaB signaling, MAPK, and Jak1/Stat1 pathways. *Glia* 59:242-255.
222. Seki, E., H. Tsutsui, Y. Imuro, T. Naka, G. Son, S. Akira, T. Kishimoto, K. Nakanishi, and J. Fujimoto. 2005. Contribution of Toll-like receptor/myeloid differentiation factor 88 signaling to murine liver regeneration. *Hepatology* 41:443-450.

8. Acknowledgements

First I would like to thank Prof. Dr. Jens C. Brüning for giving me the opportunity to work in his lab and providing me with these interesting and exciting projects.

Furthermore I would like to thank Priv. Doz. Dr. F. Thomas Wunderlich for his tremendous support, help and patience during my graduation.

Further gratitudes go to Prof. Dr. Peter Kloppenburg and Dr. Ursula Lichtenberg for agreeing to form my thesis committee.

My graduate studies would not have been the same without the help from my colleagues in the Department of Mouse Genetics and Metabolism. I especially acknowledge my colleagues and friends Dr. Bhagirath Chaurasia and Bruno Klisch for interesting and stimulating discussions and a lot of help. I would also like to thank Dr. Christine Könner for providing time and help during the performance of the hyperinsulinemic-euglycemic clamps studies as well as Brigitte Hampel for all the immunohistochemical stainings. Additional gratitudes go to Dr. Jan Mauer, Justus Ackermann and Dr. Denis Delic for proofreading the manuscript. Many thanks go all my colleagues, especially to the “lab in the back” for stimulating discussions, help with experiments, friendship and the good time (“TGIF!”).

Finally, I am forever indebted to my family, my parents Ute and Günter Ströhle, my brothers Alexander and Heiko, and my loved Erikas for all their love, support, endless patience and encouragement when it was most required.

9. Erklärung

Ich versichere, daß ich die von mir vorgelegte Dissertation selbständig angefertigt, die benutzten Quellen und Hilfsmittel vollständig angegeben und die Stellen der Arbeit einschließlich Tabellen, Karten und Abbildungen, die anderen Werken im Wortlaut oder dem Sinn nach entnommen sind, in jedem Einzelfall als Entlehnung kenntlich gemacht habe; dass diese Dissertation noch keiner anderen Fakultät oder Universität zur Prüfung vorgelegen hat; dass sie – abgesehen von unten angegebenen Teilpublikationen – noch nicht veröffentlicht worden ist sowie, dass ich eine solche Veröffentlichung vor Abschluß des Promotionsverfahren nicht vornehmen werde. Die Bestimmungen dieser Promotionsordnung sind mir bekannt. Die von mir vorgelegte Dissertation ist von Prof. Dr. Jens C. Brüning betreut worden.

Köln, 05. Dezember 2011

Peter Dirk Ströhle

Nachfolgend genannte Teilpublikationen liegen vor:

Wunderlich, F. T.*, **P. Ströhle***, A. C. Könner, S. Gruber, S. Tovar, H. S. Brönneke, L. Juntti-Berggren, L. S. Li, N. van Rooijen, C. Libert, P. O. Berggren, and J. C. Brüning. Interleukin-6 signaling in liver-parenchymal cells suppresses hepatic inflammation and improves systemic insulin action. *Cell Metab* 12:249.

* These authors are contributed equally to this work

10. Curriculum Vitae

Name: Peter Ströhle
Geburtsdaten: 1. Dezember 1980 in Mutlangen
Familienstand: ledig
Adresse: Keltenstrasse 10, 50996 Köln
Konfession: evangelisch
Staatsangehörigkeit: deutsch
E-Mail Adresse: StroehleP@gmx.de

Bildungsweg:

seit März 2008	Promotion in der Abteilung Mausgenetik und Metabolismus im Labor von Prof. Jens C. Brüning im Institut für Genetik der Universität zu Köln
2007-2008	Wissenschaftlicher Mitarbeiter im Labor von Prof. Dr. Diethard Tautz an der Universität zu Köln
Juni 2007	Abschluss Diplomarbeit in der Abteilung Evolution und Entwicklung im Labor von Prof. Dr. Diethard Tautz an der Universität zu Köln Titel: „Mikroarray Technologie: Genexpressionsanalysen zur Identifizierung von Somitogenese relevanten Genen im Zebrafisch (<i>Danio rerio</i>)“
2001-2007	Studium im Fachbereich Biologie auf Diplom an der Universität zu Köln Hauptfach: Genetik Nebenfächer: Biochemie, Organische Chemie
1997-2000	Technisches Gymnasium in Aalen

Publikationen:

- 2010 Wunderlich, F. T.*, **P. Ströhle***, A. C. Könner, S. Gruber, S. Tovar, H. S. Brönneke, L. Juntti-Berggren, L. S. Li, N. van Rooijen, C. Libert, P. O. Berggren, and J. C. Brüning. Interleukin-6 signaling in liver-parenchymal cells suppresses hepatic inflammation and improves systemic insulin action. *Cell Metab* 12:249.
* These authors are contributed equally to this work